UNIVERSIDAD NACIONAL AUTÓNOMA DE MÉXICO

PROGRAMA DE MAESTRÍA Y DOCTORADO EN CIENCIAS MATEMÁTICAS Y DE LA ESPECIALIZACIÓN EN ESTADÍSTICA APLICADA

UN PROBLEMA INVERSO DE FLUIDO DE STOKES PARA LA DETECCIÓN DE ESTENOSIS: UNA APLICACIÓN DE FUNCIONES DE BASE RADIAL DE DIVERGENCIA CERO

TESIS
QUE PARA OPTAR POR EL GRADO DE:
DOCTOR EN CIENCIAS

PRESENTA:
LOUIS DAVID BRETON TENORIO

TUTOR PRINCIPAL:
DR. JESÚS LÓPEZ ESTRADA
FACULTAD DE CIENCIAS, UNAM

MIEMBROS DEL COMITÉ TUTOR
DR. PEDRO GONZÁLEZ CASANOVA HENRÍQUEZ
INSTITUTO DE MATEMÁTICAS, UNAM

DR. ANTONIO CAPELLA KORT
INSTITUTO DE MATEMÁTICAS, UNAM

CIUDAD UNIVERSITARIA, CIUDAD DE MÉXICO, JUNIO 2023.

AN INVERSE STOKES FLUID PROBLEM FOR STENOSIS DETECTION: AN APPLICATION OF DIVERGENCE-FREE RADIAL BASIS FUNCTIONS

Abstract

This work addresses the inverse geometric problem of identifying obstructions in viscous fluid flows using sound wave measurements. We develop a Radial Basis Function (RBF) free divergence hybrid method to simulate and solve the direct and inverse problems. The proposed approach combines theoretical results and numerical simulations and is based on the interaction between a fluid-acoustic wave system. This non-invasive method has the potential to be applied in the early detection of stenosis in coronary arteries, which is essential for preventing heart attacks, and so, avoiding the occurrence of death.

This work is organized as follows: Chapters 1 to 4 are based on the article that is in the process of being published [18]. In Chapter 1, we introduce the formulation of the fluid-sound wave direct problem. Chapter 2 offers theoretical results on the identification of obstructions in fluid flows. In Chapter 3, we demonstrate the viability of the hybrid RBF method through numerical simulations. Finally, in Chapter 4, we solve the inverse problem of identifying obstructions using sound wave measurements, showing the real-world applicability of the theory.

In Chapter 5, we prove some results regarding the continuity of the non-stationary Stokes equation with respect to the domain, using a method similar to that in [62].

Chapters 6 to 8 are dedicated to the hybrid divergence-free radial basis functions (RBF) method developed in this thesis and published in [17]. In these chapters, we discuss the formulation, properties, and advantages of the method, as well as provide a comprehensive understanding of its development and applications.

This study lays the groundwork for future research and applications in the field of obstruction identification in viscous fluid flows and early detection of stenosis in coronary arteries. The proposed methodology has the potential to significantly improve current diagnostic techniques and provide a more efficient and non-invasive approach in clinical practice.

Contents

Resumen

En este trabajo, abordamos el problema geométrico inverso de detectar obstrucciones en flujos de fluidos viscosos utilizando mediciones de ondas acústicas. Desarrollamos un método híbrido de divergencia libre de funciones de base radial (RBF) para simular y resolver el problema directo e inverso. El enfoque propuesto combina resultados teóricos y simulaciones numéricas, y se basa en la interacción entre un sistema de flujo-onda acústica. Este método no invasivo tiene el potencial de ser aplicado en la detección temprana de estenosis en arterias coronarias, lo cual es fundamental para prevenir infartos al miocardio y con ello, evitando la ocurrencia de muertes .

Este trabajo está organizado de la siguiente manera: Los capítulos 1 a 4 se basan en el artículo que esta envia de publica [18]. En el Capítulo 1, introducimos la formulación del problema directo de onda fluido-sonido. El Capítulo 2 ofrece resultados teóricos sobre la identificación de obstrucciones en flujos de fluidos. En el Capítulo 3, demostramos la viabilidad del método híbrido RBF a través de simulaciones numéricas. Finalmente, en el Capítulo 4, resolvemos el problema inverso de identificar obstrucciones utilizando mediciones de ondas sonoras, mostrando la aplicabilidad real de la teoría.

En el Capítulo 5, demostramos algunos resultados sobre la continuidad de la ecuación de Stokes no estacionaria con respecto al dominio, utilizando un método similar al presentado en [62].

Los Capítulos 6 a 8 están dedicados al método híbrido de divergencia libre de funciones de base radial (RBF) desarrollado en esta tesis y publicado en [17]. En estos capítulos, discutimos la formulación, propiedades y ventajas del método, así como proporcionamos una comprensión integral de su desarrollo y aplicaciones.

Este estudio sienta las bases para futuras investigaciones y aplicaciones en el campo de la identificación de obstrucciones en flujos de fluidos viscosos y la detección temprana de enfermedades cardiovasculares. La metodología propuesta tiene el potencial de mejorar significativamente las técnicas actuales de diagnóstico y proporcionar un enfoque más eficiente y no invasivo en la práctica clínica.

Introducción en español

La enfermedad de las arterias coronarias (EAC), también conocida como enfermedad coronaria, es el tipo de enfermedad cardíaca más prevalente. El infarto de miocardio (ataque cardíaco) es una de las principales causas de muerte en muchas naciones del primer mundo, con un aumento en la incidencia en naciones emergentes. En los Estados Unidos, al menos 360,000 muertes ocurren cada año (ver Lewandowoski y Cinquegrani, *Enfermedad del corazón coronario* en [66, Sect.2 Chap.8] y [57] y referencias en ellos).

Esta enfermedad es causada por la formación de placas ateroscleróticas dentro de las paredes de las arterias coronarias debido a la acumulación lenta de colesterol, ácidos grasos, calcio y tejido conectivo fibroso, entre otras sustancias (ver [66, Sect.2 Chap.8] y [31]).

La presencia de estas placas ateroscleróticas causa una obstrucción local (conocida como estenosis) del flujo sanguíneo, que puede tener consecuencias catastróficas, como el infarto de miocardio. Aunque los síntomas de la EAC se hacen más evidentes en etapas posteriores, es extremadamente difícil diagnosticar la enfermedad antes de la aparición de los síntomas iniciales, que generalmente es un infarto de miocardio rápido que a menudo resulta en mortalidad [58].

La estenosis coronaria puede ser detectada mediante cateterización femoral por fluoroscopia o tomografía computarizada multidetectora, particularmente para cuantificar los depósitos de calcio coronario que se correlacionan con lesiones obstructivas significativas [66]. Sin embargo, ambas técnicas son invasivas. Por lo tanto, el desarrollo de una técnica alternativa no invasiva de "auscultación" para la detección temprana de estenosis en los vasos coronarios es de gran importancia.

Está bien establecido que la presencia de una obstrucción en la pared de una arteria coronaria produce una onda acústica (soplo) que se propaga desde la pared del vaso coronario a través de la cavidad torácica hasta la superficie del tórax, donde se puede registrar utilizando sensores especializados ([47], [12]). Esto sienta las bases para un método de "auscultación" no invasivo para la detección temprana de la estenosis de las arterias coronarias que es relativamente fácil de usar, asequible y adecuado para entornos hospitalarios o de consultorios donde el ruido de fondo es inevitable [47].

Desde una perspectiva fisico matematica, el problema de detección temprana de estenosis coronaria mediante procedimientos no invasivos conduce a un problema inverso fluido-estructra con datos externos.

Aunque la modelización y simulación del flujo sanguíneo, problema directo, me-

diante diferentes técnicas, han sido realizadas por muchos grupos con el fin de proporcionar conocimientos sobre el comportamiento del flujo para aplicaciones clínicas [56], [57], existe un creciente interés en conectar esfuerzos computacionales y análisis teórico de manera única. Sin embargo, debido a la complejidad que surge de tal combinación, se encuentra en una etapa temprana incluso para el problema directo, es decir, el problema de la buena formulación en el sentido de Hadamard.

En este trabajo, presentamos un problema inverso geométrico 2D relacionado con la identificación y detección de estenosis en un conducto coronario utilizando "registros" de ondas acústicas. En nuestro enfoque, el problema de detección se refiere a la posición, extensión y reducción de la luz coronaria. En otras palabras, abordamos un problema de obstáculo de frontera inversa a través de "mediciones externas" de mediciones de ondas acústicas locales, que se encuentran fuera (a una distancia adecuada) de la arteria coronaria. En este contexto, los términos "registro" y "mediciones externas" son equivalentes. Esta técnica no es simple debido a su no invasividad y al hecho de que se utiliza a diario en la práctica clínica a través de técnicas de ultrasonido [13, 55] y radiación de ondas acústicas en materiales biológicos [53]. Además, considerar modelos complejos y acoplados con datos específicos del paciente hace que los esfuerzos teóricos y computacionales sean exorbitantes.

Simultáneamente, se modela la transmisión y propagación del sonido a través de los tejidos biológicos circundantes utilizando una ecuación de onda lineal. El dominio acústico se discretiza mediante una cuadrícula cartesiana, con acoplamiento con fluido que ocurre en una pared (superior o inferior) con condiciones de deslizamiento de Navier. Considerando que las condiciones de deslizamiento de Navier describen el fluido en las paredes arteriales (paredes superior e inferior), el término de acoplamiento entre el fluido y la onda corresponde al componente normal del tensor de tensiones de Cauchy. Con esta información, nuestro problema inverso consiste en detectar el obstáculo $\mathcal{O}$ a partir del conocimiento de los datos externos proporcionados por el estado de onda en una subparte de su borde que no está en contacto con el fluido durante un intervalo de tiempo determinado $(0, T)$. En su forma actual, este problema y su geometría asociada pueden considerarse como un problema "de juguete" en 2D; sin embargo, hay algunos aspectos relevantes que destacar:

a) *Condición* $\overline{\mathcal{O}} \cap \partial\Omega \neq \emptyset$. En términos generales, esta condición refleja un problema inverso de obstáculo de frontera para un fluido lineal bidimensional. Aunque existe una amplia literatura sobre problemas inversos de obstáculos

que implican la obstrucción dentro del dominio (es decir, $\overline{\mathcal{O}} \subset\subset \partial\Omega$) con diferentes técnicas [23, 7, 11, 21, 22, 3], hasta donde sabemos, no se ha informado un análisis inicial para el caso en el que $\overline{\mathcal{O}} \cap \partial\Omega \neq \emptyset$.

b) *Condiciones de borde y término de transmisión.* Siguiendo un marco teórico reciente para fluidos de Navier-Stokes con condiciones de deslizamiento de Navier [10, 1], demostramos la existencia y unicidad de una solución débil para fluidos de Stokes considerando condiciones de borde mixtas; ver (1.2) a continuación. El término de transmisión sigue las ideas formuladas en [48], y por lo tanto la información proporcionada por el tensor de tensiones de Cauchy se encuentra en una condición de borde para una ecuación de onda.

c) *Mediciones externas para el problema inverso.* Nuestro enfoque aborda el problema inverso de obstáculo de frontera fluido-estructura (estructura rígida) a partir de mediciones externas proporcionadas por datos locales de ondas de sonido. Cabe señalar que se ha realizado un estudio computacional de un problema directo para un modelo fluido-acústico diferente en [59]. Sin embargo, nuestro modelo tiene una estructura diferente, que se basa en condiciones de deslizamiento de Navier y el acoplamiento de onda acústica con el fluido a través del tensor de tensiones de Cauchy. En cuanto a las observaciones externas, el artículo reciente [44] utiliza el método de soluciones fundamentales con regularización de Tikhonov para resolver la identificación de obstáculos sumergidos en un fluido estacionario de Oseen (con condiciones de borde de Dirichlet), y cuyas mediciones externas se basan en la velocidad del fluido, la fuerza de tracción o el gradiente de presión.

1 An Introduction to the Stokes Boundary Obstacle Problem

1.1 Introduction

Coronary artery disease (CAD), also known as coronary heart disease, is the most prevalent type of heart disease. Myocardial infarction (heart attack) is a leading cause of death in many first-world nations, with a rising incidence in emerging nations. In the United States, at least 360,000 deaths occur each year (see Lewandowoski and Cinquegrani, *Coronary Heart Disease* in [66, Sect.2 Chap.8] and [57] and references therein).

This disease is caused by the formation of atherosclerotic plaques within the coronary artery walls due to the slow accumulation of cholesterol, fatty acids, calcium, and fibrous connective tissue, among other substances (see [66, Sect.2 Chap.8] and [31]).

The presence of these atherosclerotic plaques causes local obstruction (known as stenosis) of the blood flow, which may have catastrophic consequences such as myocardial infarction. Although CAD symptoms become more evident in later stages, it is extremely difficult to diagnose the disease before the appearance of initial symptoms, which is typically a sudden myocardial infarction that often results in mortality [58].

Coronary stenosis can be detected by fluoroscopy femoral catheterization or multidetector computed tomography scanning, particularly to quantify coronary calcium deposits that correlate with significant obstructive lesions [66]. However, both techniques are invasive. Consequently, the development of an alternative non-invasive "auscultation" technique for the early detection of stenosis in coronary vessels is of great importance.

It is well established that the presence of an obstruction on the wall of a coronary artery generates turbulent flow downstream, which in turn generates an acoustic wave, commonly known as a murmur. This murmur propagates from the artery's wall, traversing the thoracic cavity, and reaches the chest's surface. Here, it can

be captured by utilizing specialized sensors ([47], [12]). This lays the foundation for a noninvasive "auscultation" method for the early detection of coronary artery stenosis that is relatively simple to use, affordable, and suitable for hospital or office settings where background noise is unavoidable [47].

From a mathematical perspective, the early detection problem of coronary stenosis by non-invasive procedures leads to an inverse fluid-structure problem with external data.

Although the modeling and simulation of blood flow, direct problem, through different techniques, have been carried out by many groups in order to provide knowledge of flow behavior for clinical applications [56], [57], there is a growing interest in connecting computational efforts and theoretical analysis in a unique way. However, due to the complexity arising from such a combination, it is in an early stage even for the direct problem, i.e., the well-posedness problem in the sense of Hadamard.

In this work, we present a 2D geometrical inverse problem concerning the identifiability and detection of stenosis in a coronary duct by using "records" from acoustic waves. In our setting, the detection problem refers to position, extension, and coronary lumen reduction. In other words, we address an inverse boundary obstacle problem through "external measurements" of local acoustic waves measurements, which are located outside (at a suitable distance) from the coronary artery. In this context, the terms "record" and "external measurements" are equivalent. This technique is not simple due to its non-invasiveness and the fact that it is used daily in clinical practice through ultrasound techniques [13, 55] and acoustic wave radiation in biological materials [53]. Moreover, considering complex and coupled models with patient-specific data makes both theoretical and computational efforts exorbitant.

For these reasons, in this work, we consider a simple rectangular geometry Ω to model the blood flow as a viscous Stokes fluid in 2D with both Dirichlet and Navier-slip conditions on the arterial walls. Hereafter, these kinds of boundary conditions are called mixed boundary conditions. The domain has an obstacle $\mathcal{O}$ representing stenosis, and such that $\overline{\mathcal{O}}$ intersects the fluid domain at only one part of the boundary, i.e., $\overline{\mathcal{O}} \cap \partial\Omega \neq \emptyset$. The Dirichlet boundary conditions are applied to the velocity flow at the inlet and exit, while Navier-slip boundary conditions are used for the top and bottom walls.

Simultaneously, the transmission and propagation of sound through surrounding biological tissues are modeled using a linear wave equation. The acoustic domain is discretized using a Cartesian grid, with fluid coupling occurring at a wall (top or

bottom) with Navier slip conditions. Considering that the Navier slip conditions describe the fluid at arterial walls (top and bottom walls), the coupling term between the fluid and the wave corresponds to the normal component of the Cauchy stress tensor. With this information, our inverse problem consists of detecting the obstacle $\mathcal{O}$ from the knowledge of external data provided by the wave state on a subpart of its boundary not in contact with the fluid during a certain time interval $(0, T)$. In its current form, this problem and its associated geometry can be considered as a 2D toy problem; however, there are some relevant aspects to highlight:

a) *Condition* $\overline{\mathcal{O}} \cap \partial\Omega \neq \emptyset$. In general terms, this condition reflects an inverse boundary obstacle problem for a two-dimensional linear fluid. Although there is extensive literature on inverse obstacle problems involving obstruction inside the domain (i.e., $\overline{\mathcal{O}} \subset\subset \partial\Omega$) with different techniques [23, 7, 11, 21, 22, 3], to the best of our knowledge, no initial analysis has been reported for the case where $\overline{\mathcal{O}} \cap \partial\Omega \neq \emptyset$.

b) *Boundary conditions and transmission term.* Following a recent theoretical framework for Navier-Stokes fluids with Navier slip boundary conditions [10, 1], we demonstrate the existence and uniqueness of a weak solution for Stokes fluids considering mixed boundary conditions; see (1.2) below. The transmission term follows the ideas formulated in [48], and thus, the information provided by the Cauchy stress tensor lies in a boundary condition for a wave equation.

c) *External measurements for the inverse problem.* Our approach addresses the inverse fluid-structure (rigid structure) boundary obstacle problem using external measurements provided by local sound wave data. It should be noted that a computational study of a direct problem for a different fluid-acoustic model was conducted in [59]. However, our model has a different structure, relying on Navier slip conditions and the coupling of acoustic wave with the fluid through the Cauchy stress tensor. Regarding external observations, the recent article [44] uses the method of fundamental solutions with Tikhonov regularization to solve the identification of submerged obstacles in a stationary Oseen fluid (with Dirichlet boundary conditions), with external measurements based on fluid velocity, traction force, or pressure gradient.

1.2 The problem setting

We define the spatial domain of fluid flow by $\Omega := (0, L) \times (0, D)$, where $L > 0$ can be understood as the length of the blood vessel and $D > 0$ its diameter. Assume that $\partial\Omega$ is divided into four parts $\Gamma_{inlet}, \Gamma_{wall}^{up}, \Gamma_{wall}^{down}$ and Γ_{out} of a non-vanishing measure such that $\Gamma_{inlet} \bigcap \Gamma_{wall}^{up} \bigcap \Gamma_{wall}^{down} \bigcap \Gamma_{out} = \emptyset$. Throughout this research work, we adopt the convention that a boldface character denotes a vector or a tensor. Furthermore, we consider an obstacle $\mathcal{O} \subset \overline{\Omega}$ with non-empty interior such that $\Omega_{\mathcal{O}} := \Omega \backslash \overline{\mathcal{O}}$ only has one connected component, which is split into four parts $\Gamma_{inlet}, \Gamma_{wall}^{\mathcal{O},up}, \Gamma_{wall}^{\mathcal{O},down}$, Γ_{out} and the boundary $\partial\mathcal{O}$ of $\mathcal{O}$ satisfies (see Figure 1.1):

$$\begin{cases} \partial\mathcal{O} \cap \Gamma_{inlet} & = \emptyset, \\ \partial\mathcal{O} \cap \Gamma_{out} & = \emptyset, \\ \partial\mathcal{O} \cap \Gamma_{wall}^{up} & \neq \emptyset, \end{cases} \quad \text{or} \quad \begin{cases} \partial\mathcal{O} \cap \Gamma_{inlet} & = \emptyset, \\ \partial\mathcal{O} \cap \Gamma_{out} & = \emptyset, \\ \partial\mathcal{O} \cap \Gamma_{wall}^{down} & \neq \emptyset. \end{cases} \tag{1.1}$$

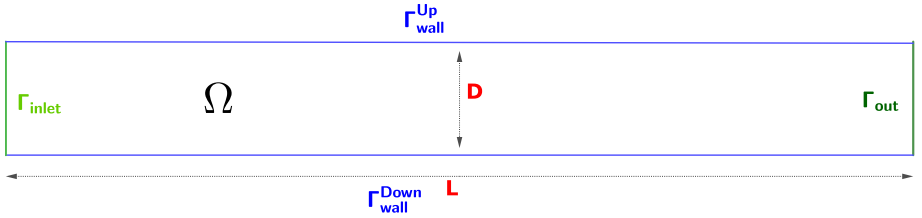

(a)

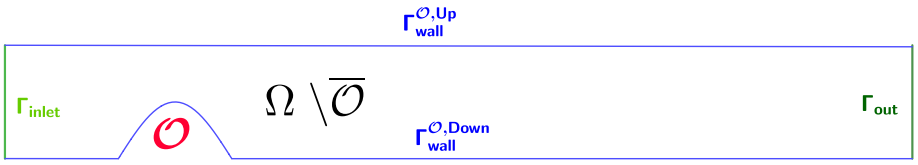

(b)

Figure 1.1: Geometric representation of the domain: a) Ω , b) $\Omega_{\mathcal{O}} := \Omega \backslash \overline{\mathcal{O}}$.

The velocity vector $\boldsymbol{u}$ and the scalar pressure p of the fluid in the presence of the obstacle $\mathcal{O}$ are modeled by the Stokes system with mixed boundary conditions:

$$\begin{cases} \boldsymbol{u}_t - \operatorname{div}(\sigma(\boldsymbol{u}, p)) = 0 & \text{in } \Omega_{\mathcal{O}} \times (0, T), \\ \operatorname{div}(\boldsymbol{u}) = 0 & \text{in } \Omega_{\mathcal{O}} \times (0, T), \\ \boldsymbol{u} = \boldsymbol{g_{in}} & \text{on } \Gamma_{inlet} \times (0, T), \\ \boldsymbol{u} = \boldsymbol{g_{out}} & \text{on } \Gamma_{out} \times (0, T), \\ \boldsymbol{u} \cdot \boldsymbol{n} = 0,\ [\sigma(\boldsymbol{u}, p)\boldsymbol{n}]_{tg} = 0 & \text{on } \Gamma^{\mathcal{O}}_{wall} \times (0, T), \\ \boldsymbol{u}(\cdot, 0) = \boldsymbol{u}_0(\cdot) & \text{in } \Omega_{\mathcal{O}}, \end{cases} \tag{1.2}$$

Given that $\boldsymbol{n}$ is the unit outward normal vector of $\partial\Omega_{\mathcal{O}}$, and $\boldsymbol{g_{in}}$ and $\boldsymbol{g_{out}}$ are defined as nontrivial Dirichlet data. Additionally, $\sigma(\boldsymbol{u}, p)$ is identified as the Cauchy stress tensor, that is, $\sigma(\boldsymbol{u}, p) = 2\boldsymbol{D}(\boldsymbol{u}) - Ip = 2\mu\frac{\nabla+\nabla^t}{2}\boldsymbol{u} - pI$. Here, I represents the identity matrix of size 2×2, while $\mu > 0$ is the kinetic viscosity coefficient. The subscript tg marks the tangential component of the relevant vector field, defined as $\boldsymbol{v}_{tg} := \boldsymbol{v} - (\boldsymbol{v} \cdot \boldsymbol{n})\boldsymbol{n}$, as given in [54].

Concurrently, the acoustic wave propagation in the arterial wall and nearby tissue is depicted through a linear wave equation within a bounded domain $S := (0, L) \times (D, H)$ as follows:

$$\begin{cases} w_{tt} - c^2\Delta w = 0 & \text{in } S \times (0, T), \\ w = (\sigma(\boldsymbol{u}, p)\boldsymbol{\nu}) \cdot \boldsymbol{\nu} & \text{on } ([0, L] \times \{D\}) \times (0, T), \\ \frac{\partial w}{\partial t} + c\frac{\partial w}{\partial n} = 0 & \text{on } (\partial S \setminus ([0, L] \times \{D\})) \times (0, T), \\ w_t(\cdot, 0) = w(\cdot, 0) = 0 & \text{in } S, \end{cases} \tag{1.3}$$

In this context, $\boldsymbol{\nu} := (0, 1)^t$, $\frac{\partial}{\partial n}$ stands for the normal partial derivative operator and c denotes the assigned wave speed. From a mechanical perspective, $H > 0$ is interpreted as the gap between the blood vessel and the chest surface, where the acoustic wave will be detected, as illustrated in Figure 1.2. Meanwhile, the term $(\sigma(\boldsymbol{u}, p)\boldsymbol{\nu}) \cdot \boldsymbol{\nu}$ physically symbolizes the normal stress imposed by the fluid on the top wall of the domain $\Omega_{\mathcal{O}}$. It is worth highlighting that the expression $(\sigma(\boldsymbol{u}, p)\boldsymbol{\nu}) \cdot \boldsymbol{\nu}$ represents the coupling term in an explicit form, that is, once the solution to (1.2) has been determined, such a boundary condition of the wave equation (1.3) is directly obtained. Keep in mind that the second boundary condition aligns with the Higton absorbing boundary condition of order 1, as per [36, 43]. It is widely recognized that the application of absorbing boundary conditions is a strategy to minimize the required spatial domain when numerically resolving partial differential equations that accept traveling waves. The well-posedness of the initial boundary value problem associated with the absorbing boundary conditions,

coupled to the wave equation, has been debated in multiple studies, for instance, [63, 14, 45].

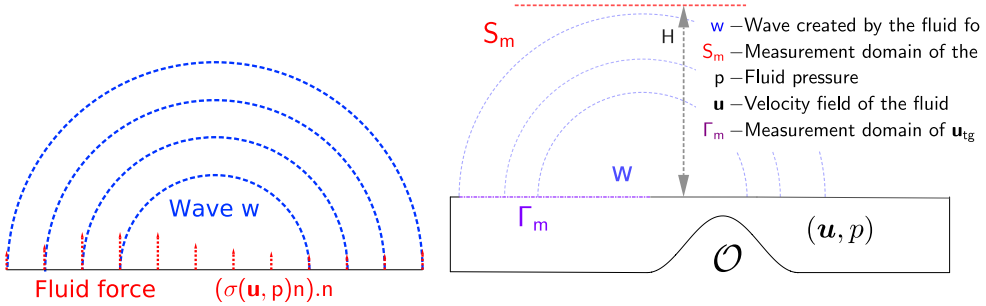

Figure 1.2: Geometric representation of the wave w.

As mentioned, there are no papers dealing with the effective reconstruction of an obstacle in contact with a subset of $\partial\Omega$, and using some type of external measurement for unsteady Stokes fluids with mixed boundary conditions. The aim of this work consists in determining an obstacle $\mathcal{O} \subset \overline{\Omega}$ (time-independent and satisfying (1.1)) using external measurements from the acoustic wave w (see (1.3)) in the set $S_m \times (0, T_0)$, where $S_m := [k_1, k_2] \times \{H\} \subset \partial S$ with $0 < k_1 < k_2 < L$, and $T_0 < T$. Our idea consists in uncoupling the system (1.2)–(1.3) and analysing the inverse obstacle problem throughout two inverse sub-problems, namely: one inverse problem for the wave equation related to recovering a boundary datum from $w|_{S_m \times (0,T_0)}$ and, another one connecting the recovered boundary datum for the wave equation with partial information of the Cauchy tensor given by the Stokes fluid; see Theorem 2.3.4. To consider a wave domain S independent of the obstruction $\mathcal{O}$, we impose the geometrical condition $\partial\mathcal{O} \bigcap \overline{\Gamma_{wall}^{up}} = \emptyset$, as well as a priori knowledge of one of the configurations given in (1.1).

2 The stokes equation with mixed boundary conditions

In this chapter, we present a detailed proof of the existence and uniqueness of weak solutions for the two-dimensional Stokes system with mixed boundary conditions. Specifically, we consider the Stokes system with a combination of Dirichlet and Navier-slip boundary conditions. While the paper [15] mentioned these mixed boundary conditions, it did not provide a rigorous proof. Therefore, to ensure completeness, we rely on recent research works [1, 2, 10] that deal with both the unsteady and steady Stokes system with Navier boundary conditions. These types of problems are commonly known as Zaremba's problems in the literature. For simplicity, we assume the viscosity to be $\mu = 1$.

We recall that $C^{n,\alpha}$ refers to a space of functions whose derivatives up to order 'm' exist and are α-Hölder continuous. Until further notice, we assume that $\Omega \subset \mathbb{R}^2$ is a bounded curvilinear polygone of class $C^{1,1}$ in the sense of [40, Definition 1.4.5.1]. We assume that there is $M \in \mathbb{N}$ such that:

$$\Gamma = \partial\Omega = \bigcup_{j=1}^{2M} \overline{\Gamma_j} \quad ,$$

were each Γ_j is a curve of class $C^{k,1}$, Γ_{j+1} follows Γ_j according to the positive orientation and we have that $\Gamma_j \subset \Gamma$, $\Gamma_j \bigcap \Gamma_{j+1} = \emptyset$. We define $\Gamma_D, \Gamma_N \subset \Gamma$ as:

$$\Gamma_D = \bigcup_{j=2}^{M} \Gamma_{(2j)} \text{ and } \Gamma_N = \bigcup_{j=1}^{M} \Gamma_{(2j-1)} \quad .$$

As mentioned before, we denote by $\boldsymbol{v}_{tg}$ as the tangential component of $\boldsymbol{v}$, i.e., $\boldsymbol{v}_{tg} = \boldsymbol{v} - (\boldsymbol{v}\cdot\boldsymbol{n})\boldsymbol{n}$. Moreover, we consider the following spaces equipped with their

usual respective norms (for instance see [10]) :

$$\begin{aligned}
\boldsymbol{V}(\Omega) &= \{\boldsymbol{u} \in \boldsymbol{H}^1(\Omega) :\ \mathrm{div}(\boldsymbol{u}) = 0, \boldsymbol{u}|_{\Gamma_D} = 0, \boldsymbol{u}\cdot\boldsymbol{n} = 0 \text{ on } \partial\Omega\},\\
\boldsymbol{H}_{0,\Gamma_D}(\Omega) &= \{\boldsymbol{u} \in \boldsymbol{H}^{\mathbf{1}}(\Omega) :\ \boldsymbol{u}|_{\Gamma_D} = 0\},\\
\boldsymbol{H}(\mathrm{div},\Omega) &= \{\boldsymbol{u} \in \boldsymbol{L}^2(\Omega) :\ \mathrm{div}(\boldsymbol{u}) \in \boldsymbol{L}^2(\Omega)\},\\
\boldsymbol{H}_0(\mathrm{div},\Omega) &= \{\boldsymbol{u} \in \boldsymbol{L}^2(\Omega) :\ \mathrm{div}(\boldsymbol{u}) \in \boldsymbol{L}^2(\Omega), \boldsymbol{u}\cdot\boldsymbol{n} = 0 \text{ on } \partial\Omega\},\\
\boldsymbol{E}(\Omega) &= \{\boldsymbol{u} \in \boldsymbol{H}^1(\Omega) :\ \Delta\boldsymbol{u} \in \boldsymbol{H}_0(\mathrm{div},\Omega)'\},\\
L^2_0(\Omega) &= \{p \in L^2(\Omega) :\ \int_\Omega p\,dx = 0\}
\end{aligned}$$

The main novelty compared to [10] is our treatment of the mixed boundary condition. To handle this rigorously, we make use of the Lions-Magenes space [50, Chp 11] [40, Section 1.5.2] defined as follows:

$$\boldsymbol{H}^{1/2}_{00}(\Gamma_i) = \left\{\boldsymbol{u} \in \boldsymbol{H}^{1/2}(\Gamma_i) :\ d(x,\partial\Gamma_i)^{-1/2}\boldsymbol{u} \in \boldsymbol{L}^2(\Gamma_i)\right\}\ ,$$

equipped with the norm: $\|\boldsymbol{u}\|^2_{\boldsymbol{H}^{1/2}_{00}(\Gamma_i)} = \|\boldsymbol{u}\|^2_{\boldsymbol{H}^{\mathbf{1/2}}(\Gamma_i)} + \left\|d^{-1/2}\boldsymbol{u}\right\|^2_{\boldsymbol{L}^2(\Gamma_i)}$, where $d(x,\partial\Gamma_i)$ is the geodesic distance from x to $\partial\Gamma_i$. Following this definition we set:

$$\boldsymbol{H}^{1/2}_{00}(\Gamma_D) = \prod_{j=2}^{M} \boldsymbol{H}^{1/2}_{00}(\Gamma_{(2j)}) \text{ and } \boldsymbol{H}^{1/2}_{00}(\Gamma_N) = \prod_{j=1}^{M} \boldsymbol{H}^{1/2}_{00}(\Gamma_{(2j-1)})$$

In other to avoid heavy notation, for this section, we will denote:

$\langle\cdot,\cdot\rangle_{\Gamma_i}$ as the dual pairing between $\boldsymbol{H}^{1/2}_{00}(\Gamma_i)'$ and $\boldsymbol{H}^{1/2}_{00}(\Gamma_i)$,
$\langle\cdot,\cdot\rangle_{\partial\Omega}$ as the dual pairing between $\boldsymbol{H}^{-1/2}(\partial\Omega)$ and $\boldsymbol{H}^{1/2}(\partial\Omega)$,
$\langle\cdot,\cdot\rangle_{\Omega}$ as the dual pairing between $\boldsymbol{H}_0(\mathrm{div},\Omega)'$ and $\boldsymbol{H}_0(\mathrm{div},\Omega)$.

To continue with the upcoming sections, we will rely on the following Green identity, which will be proven in Section 2.4.

Theorem 2.0.1. *Let Ω be a bounded open subset of $\mathbb{R}^2$ whose boundary is a curvilinear polygon of class at least C^1. Let $\gamma_j(\boldsymbol{u})$ denote the following trace mapping:*

$$\gamma_j(\boldsymbol{u}) : \boldsymbol{u} \to \boldsymbol{u}|_{\Gamma_j} \quad .$$

Furthermore assume that $\gamma_j(\boldsymbol{u}) \in \boldsymbol{H}^{1/2}_{00}(\Gamma_j)$ for all $j \in \{1,..,2M\}$. Then we have the following Green identity:

$$-\langle \Delta \boldsymbol{u}, \boldsymbol{\varphi} \rangle_{\Omega} = \int_{\Omega} 2\boldsymbol{D}(\boldsymbol{u}) : \boldsymbol{D}(\boldsymbol{\varphi})\, dx - \sum_{j=1}^{2M} \langle 2[\boldsymbol{D}(\boldsymbol{u})\boldsymbol{n}]_{tg}, \gamma_j(\boldsymbol{\varphi}) \rangle_{\Gamma_j} \tag{2.1}$$

for all $\boldsymbol{u} \in \boldsymbol{E}(\Omega)$ *and* $\varphi \in \{\boldsymbol{u} \in \boldsymbol{H}^1(\Omega) | \mathrm{div}(\boldsymbol{u}) = 0\}$

Remark 2.0.2. In Theorem 2.0.1 the spaces $\boldsymbol{H}_{00}^{1/2}$ are necessary to decompose the dual pairing $\langle \cdot, \cdot \rangle_{\partial\Omega}$ into the sum of the dual pairing. This is due to the lack of regularity of the tangential component of the Cauchy stress tensor $[\boldsymbol{D}(\boldsymbol{u})\boldsymbol{n}]_{tg}$ when $\boldsymbol{u} \in \boldsymbol{E}(\Omega)$.

2.1 Steady Stokes system with mixed boundary condition

While our primary focus is to establish the existence and uniqueness of the evolutionary Stokes flow with mixed boundary conditions, it is crucial to begin by proving the stationary case. Therefore, the objective of this subsection is to demonstrate the existence and uniqueness of a weak solution for the steady Stokes system with mixed boundary conditions.

$$\begin{cases} -\mathrm{div}(\sigma(\boldsymbol{u}, p)) = \boldsymbol{f} & \text{in } \Omega, \\ \mathrm{div}(\boldsymbol{u}) = 0 & \text{in } \Omega, \\ \boldsymbol{u} \cdot \boldsymbol{n} = 0 & \text{in } \partial\Omega, \\ \boldsymbol{u} = \boldsymbol{g} & \text{on } \Gamma_D, \\ [2\boldsymbol{D}(\boldsymbol{u})\boldsymbol{n}]_{tg} = \boldsymbol{h} & \text{on } \Gamma_N. \end{cases} \tag{2.2}$$

The main result of this section is the following theorem.

Theorem 2.1.1. *Let* $\boldsymbol{f} \in \boldsymbol{H}_0(\mathrm{div}, \Omega)'$, $\boldsymbol{h} \in (\boldsymbol{H}_{00}^{1/2}(\Gamma_N))'$ *and* $\boldsymbol{g} \in \boldsymbol{H}_{00}^{1/2}(\Gamma_D)$ *such that:*

$$\boldsymbol{g} \cdot \boldsymbol{n} = 0 \text{ and } \langle \boldsymbol{h}, \boldsymbol{n} \rangle_{\Gamma_N} = 0. \tag{2.3}$$

Then the problem of finding $(\boldsymbol{u}, p) \in \boldsymbol{H}^1(\Omega) \times L_0^2(\Omega)$ *satisfying* (2.2) *in the distribution sense has a unique solution. Furthermore, we have the following estimate:*

$$\|\boldsymbol{u}\|_{\boldsymbol{H}^1(\Omega)} + \|p\|_{L^2(\Omega)} \leq C \left(\|\boldsymbol{f}\|_{\boldsymbol{H}_0(\mathrm{div},\Omega)'} + \|\boldsymbol{g}\|_{\boldsymbol{H}_{00}^{1/2}(\Gamma_D)} + \|\boldsymbol{h}\|_{(\boldsymbol{H}_{00}^{1/2}(\Gamma_N))'} \right). \tag{2.4}$$

Before presenting the proof of Theorem 2.1.1, we need to establish some preliminary results. In particular, we recall the De Rham theorem 2.1.2 [9, Theorem 2.1] which has significant implications for the Stokes problem. It excels at handling all distributions, unlike the Stokes problem, which tackles more specific ones. Notably, if $\boldsymbol{f}$ belongs to $H^{-1}(\Omega)$ and satisfies equation (2.5), Girault and Raviart's [35] simplified the theorem's proof.

Theorem 2.1.2. *Let Ω be an open subset of $\mathbb{R}^d$ and let $\boldsymbol{f}$ be a distribution in $\mathcal{D}'(\Omega)$ that satisfies:*

$$\forall \boldsymbol{\varphi} \in \boldsymbol{\mathcal{D}}_\sigma(\Omega), \quad \langle \boldsymbol{f}, \boldsymbol{\varphi} \rangle_{\boldsymbol{\mathcal{D}}'(\Omega)\times\boldsymbol{\mathcal{D}}(\Omega)} = 0 \ . \tag{2.5}$$

where $\boldsymbol{\mathcal{D}}_\sigma(\Omega) = \{\boldsymbol{\varphi} \in \mathcal{D}(\Omega) | div(\boldsymbol{\varphi}) = 0\}$. Then there exists a distribution p in $\boldsymbol{\mathcal{D}}'(\Omega)$ such that:

$$\boldsymbol{f} = \nabla p$$

The next Proposition establishes an equivalence between two formulations of a problem involving the Stokes equations.

Proposition 2.1.3. *Assume $\boldsymbol{g} = 0$ in (2.2). Let $\boldsymbol{f} \in \boldsymbol{H}_0(\mathrm{div}, \Omega)'$, $\boldsymbol{h} \in (\boldsymbol{H}_{00}^{1/2}(\Gamma_N))'$ such that:*

$$\langle \boldsymbol{h}, \boldsymbol{n} \rangle_{\Gamma_N} = 0. \tag{2.6}$$

Then, the problem of finding a pair $(\boldsymbol{u}, p) \in \boldsymbol{H}^1(\Omega) \times L^2(\Omega)$ satisfying (2.2) in the distribution sense is equivalent to the following:

$$\begin{cases} \text{Find } \boldsymbol{u} \in \boldsymbol{V}(\Omega) \text{ such that} \\ \forall \boldsymbol{v} \in \boldsymbol{V}(\Omega), \ 2\int_\Omega \boldsymbol{D}(\boldsymbol{u}) : \boldsymbol{D}(\boldsymbol{v})\, dx = \langle \boldsymbol{f}, \boldsymbol{v} \rangle_\Omega + \langle \boldsymbol{h}, \boldsymbol{v} \rangle_{\Gamma_N} . \end{cases} \tag{2.7}$$

Proof. Let $(\boldsymbol{u}, p) \in \boldsymbol{H}^1(\Omega) \times L^2(\Omega)$ be a solution of (2.2), and let $\boldsymbol{v} \in \boldsymbol{V}(\Omega)$. Integrating by part with the help of [10, Lemma 2.4], we obtain:

$$\int_\Omega 2\boldsymbol{D}(\boldsymbol{u}) : \boldsymbol{D}(\boldsymbol{v})\, dx = \langle \boldsymbol{f}, \boldsymbol{v} \rangle_\Omega + \langle 2\boldsymbol{D}(\boldsymbol{u})\boldsymbol{n}, \boldsymbol{v} \rangle_{\partial\Omega} \ . \tag{2.8}$$

Given that $\boldsymbol{v}|_{\Gamma_D} = 0$, we can conclude from Theorem 2.4.2 that $\boldsymbol{v}|_{\Gamma_N} \in \boldsymbol{H}_{00}^{1/2}(\Gamma_N)$. Therefore, utilizing Theorem 2.0.1, we can proceed with the following decomposition:

$$\begin{aligned}\int_{\partial\Omega} 2\boldsymbol{D}(\boldsymbol{u})\boldsymbol{n}\cdot\boldsymbol{v}\,dS &= \int_{\Gamma_D} 2\boldsymbol{D}(\boldsymbol{u})\boldsymbol{n}\cdot\boldsymbol{v}\,dS + \int_{\Gamma_N} 2\boldsymbol{D}(\boldsymbol{u})\boldsymbol{n}\cdot\boldsymbol{v}\,dS \\ &= \int_{\Gamma_N} \left[(2\boldsymbol{D}(\boldsymbol{u})\boldsymbol{n})\cdot\boldsymbol{n}\right]\boldsymbol{n}\cdot\boldsymbol{v}\,dS + \int_{\Gamma_N} [2\boldsymbol{D}(\boldsymbol{u})\boldsymbol{n}]_{tg}\cdot\boldsymbol{v}\,dS \\ &= \int_{\Gamma_N} [2\boldsymbol{D}(\boldsymbol{u})\boldsymbol{n}]_{tg}\cdot\boldsymbol{v}\,dS = \int_{\Gamma_N} \boldsymbol{h}\cdot\boldsymbol{v}\,dS\ ,\end{aligned} \tag{2.9}$$

where the integrals are to be understood as a dual pairing. Therefore, from equations (2.8) and (2.9) we have the following:

$$\int_\Omega 2\boldsymbol{D}(\boldsymbol{u}) : \boldsymbol{D}(\boldsymbol{v})\,dx = \langle \boldsymbol{f}, \boldsymbol{v}\rangle_\Omega + \langle 2\boldsymbol{D}(\boldsymbol{u})\boldsymbol{n}, \boldsymbol{v}\rangle_{\Gamma_N}\ . \tag{2.10}$$

Conversely, let $\boldsymbol{u} \in \boldsymbol{V}(\Omega)$ solution of (2.7), and let $\boldsymbol{\varphi} \in \boldsymbol{\mathcal{D}}_\sigma(\Omega) = \{\boldsymbol{\varphi} \in \boldsymbol{\mathcal{D}}(\Omega) | \mathrm{div}(\boldsymbol{\varphi}) = 0\}$, and notice that we have that (see [10]):

$$2\int_\Omega \boldsymbol{D}(\boldsymbol{u}) : \boldsymbol{D}(\boldsymbol{\varphi})\,dx = \int_\Omega \nabla\boldsymbol{u} : \nabla\boldsymbol{\varphi}\,dx\ .$$

As a consequence, we have:

$$\forall \boldsymbol{\varphi} \in \boldsymbol{\mathcal{D}}_\sigma(\Omega), \quad \langle -\Delta\boldsymbol{u} - \boldsymbol{f}, \boldsymbol{\varphi}\rangle_{\boldsymbol{\mathcal{D}}(\Omega)'\times\boldsymbol{\mathcal{D}}(\Omega)} = 0\ .$$

Therefore by De Rham theorem 2.1.2, there exists a distribution $p \in \mathcal{D}(\Omega)'$ defined uniquely up to an additive constant such that:

$$-\Delta\boldsymbol{u} + \nabla p = \boldsymbol{f}\ . \tag{2.11}$$

Note that since $\boldsymbol{H}_0(\mathrm{div}, \Omega)'$ is embedded in $\boldsymbol{H}^{-1}(\Omega)$ we can say that $p \in L^2(\Omega)$ (see [9, Proposition 2.10]). Let $\boldsymbol{v} \in \boldsymbol{V}(\Omega)$, using (2.10) and (2.11) we obtain the following:

$$\langle [2\boldsymbol{D}(\boldsymbol{u})\boldsymbol{n}]_{tg} - \boldsymbol{h}, \boldsymbol{v}\rangle_{\Gamma_N} = 0 \tag{2.12}$$

Now let $\boldsymbol{\alpha} \in \boldsymbol{H}_{00}^{1/2}(\Gamma_N)$ and let $\widetilde{\boldsymbol{\alpha}}$ be its extension by zero to $\partial\Omega$, it follows from Theorem 2.4.3 that $\widetilde{\boldsymbol{\alpha}} \in \boldsymbol{H}^{1/2}(\partial\Omega)$. Therefore, there exists $\boldsymbol{\varphi} \in \boldsymbol{H}^1(\Omega)$ such that:

$$\begin{cases} \mathrm{div}(\boldsymbol{\varphi}) = 0 & \text{in } \Omega\ , \\ \boldsymbol{\varphi} = \widetilde{\boldsymbol{\alpha}}_{tg} & \text{on } \Gamma\ . \end{cases}$$

It is clear that $\boldsymbol{\varphi} \in \boldsymbol{V}(\Omega)$, therefore, using the compatibility condition (2.6) and the equation (2.12), we have:

$$\begin{aligned}\langle [2\boldsymbol{D}(\boldsymbol{u})\boldsymbol{n}]_{tg} - \boldsymbol{h}, \boldsymbol{\alpha}\rangle_{\Gamma_N} &= \langle [2\boldsymbol{D}(\boldsymbol{u})\boldsymbol{n}]_{tg} - \boldsymbol{h}, \boldsymbol{\alpha}_{tg}\rangle_{\Gamma_N} \\ &= \langle [2\boldsymbol{D}(\boldsymbol{u})\boldsymbol{n}]_{tg} - \boldsymbol{h}, \boldsymbol{\varphi}\rangle_{\Gamma_N} \\ &= 0 \ .\end{aligned}$$

We can conclude that $[2\boldsymbol{D}(\boldsymbol{u})\boldsymbol{n}]_{tg} = \boldsymbol{h}$ on Γ_N. □

To prove the existence of a weak solution, we will employ a Korn-type inequality. This inequality can be derived by utilizing the Poincaré inequality, which holds in $H^1_{0,\Gamma_D}(\Omega)$, and the Korn inequality. The details of this proof can be found in [5, Theorem 5.3.4].

Proposition 2.1.4. *Let Ω be a Lipschitz bounded domain. Then there exists a constant $C > 0$ depending only on Ω such that*

$$\|\boldsymbol{u}\|^2_{\boldsymbol{H}^1(\Omega)} \leq C\|\boldsymbol{D}(\boldsymbol{u})\|^2_{L^2(\Omega)} \quad \forall \boldsymbol{u} \in \boldsymbol{H}_{0,\Gamma_D}(\Omega). \tag{2.13}$$

Proposition 2.1.5. *Suppose that $\boldsymbol{g} = \boldsymbol{0}$, and let $\boldsymbol{f} \in \boldsymbol{H}_0(\mathrm{div}, \Omega)'$, $\boldsymbol{h} \in (\boldsymbol{H}^{1/2}_{00}(\Gamma_N))'$. Then the problem of finding $(\boldsymbol{u}, p) \in \boldsymbol{H}^1(\Omega) \times L^2_0(\Omega)$ that satisfies (2.2) in the distribution sense has a unique solution. Furthermore, we have the following estimate:*

$$\|\boldsymbol{u}\|_{\boldsymbol{H}^1(\Omega)} + \|p\|_{L^2_0(\Omega)} \leq C\left(\|\boldsymbol{f}\|_{\boldsymbol{H}_0(\mathrm{div},\Omega)'} + \|\boldsymbol{h}\|_{(\boldsymbol{H}^{1/2}_{00}(\Gamma_N))'}\right) \ . \tag{2.14}$$

Proof. Using the proposition 2.1.3, we only have to prove the existence and uniqueness of the following variational problem:

$$\begin{cases}\text{Find } \boldsymbol{u} \in \boldsymbol{V}(\Omega) \text{ such that} \\ \forall \boldsymbol{v} \in \boldsymbol{V}(\Omega),\ \int_\Omega 2\boldsymbol{D}(\boldsymbol{u}) : \boldsymbol{D}(\boldsymbol{v})\, dx = \langle \boldsymbol{f}, \boldsymbol{v}\rangle_\Omega + \langle \boldsymbol{h}, \boldsymbol{v}\rangle_{\Gamma_N} \ .\end{cases}$$

We set:

$$\begin{aligned}a(\boldsymbol{u}, \boldsymbol{v}) &= 2\int_\Omega \boldsymbol{D}(\boldsymbol{u}) : \boldsymbol{D}(\boldsymbol{v})\, dx \ , \\ L(\boldsymbol{v}) &= \langle \boldsymbol{f}, \boldsymbol{v}\rangle_\Omega + \langle \boldsymbol{h}, \boldsymbol{v}\rangle_{\Gamma_N}\end{aligned}$$

Notice that the bi-linear form $a(.\,,.)$ is continuous in $\boldsymbol{V}(\Omega)$ since:

$$\left|\int_\Omega \boldsymbol{2D}(\boldsymbol{u}) : \boldsymbol{D}(\boldsymbol{v})\, dx\right| = \left|\int_\Omega \nabla \boldsymbol{u} : \nabla \boldsymbol{v}\, dx\right| \leq \|\nabla \boldsymbol{u}\|_{L^2(\Omega)} \|\nabla \boldsymbol{v}\|_{L^2(\Omega)} \ .$$

Using proposition 2.1.4 and the fact that $\boldsymbol{V}(\Omega) \subset \boldsymbol{H}_{0,\Gamma}(\Omega)$ we also obtain the coercivity of the bilinear form $a(.,.)$ on $\boldsymbol{V}(\Omega)$. Now since:

$$\begin{aligned} \langle \boldsymbol{f}, \boldsymbol{v} \rangle_{\Omega} &\leq \|\boldsymbol{f}\|_{\boldsymbol{H}_0(\mathrm{div},\Omega)'} \|\boldsymbol{v}\|_{\boldsymbol{H}_0(\mathrm{div},\Omega)} \\ &\leq \|\boldsymbol{f}\|_{\boldsymbol{H}_0(\mathrm{div},\Omega)'} \|\boldsymbol{v}\|_{\boldsymbol{H}^1(\Omega)} \end{aligned} \tag{2.15}$$

Using the fact that $\boldsymbol{v}|_{\Gamma_D} = 0$ from theorem 2.4.2 we know that the mapping $\boldsymbol{v}|_{\Gamma_N}$: $\boldsymbol{V}(\Omega) \to \boldsymbol{H}_{00}^{1/2}(\Gamma_N)$ is continuous. Thus there exist a constant $C_0 > 0$ such that:

$$\langle \boldsymbol{h}, \boldsymbol{v} \rangle_{\Gamma_N} \leq C_0 \|\boldsymbol{h}\|_{\boldsymbol{H}_{00}^{1/2}(\Gamma_N)'} \|\boldsymbol{v}\|_{\boldsymbol{H}^1(\Omega)} \ , \tag{2.16}$$

Therefore $L : V \to \mathbb{R}$ is continuous, and thus by the Lax-Milgram theorem and the proposition 2.1.3, we can guarantee the existence and uniqueness of $(\boldsymbol{u}, p) \in \boldsymbol{H}^1(\Omega) \times L_0^2(\Omega)$ satisfying (2.2) in the distribution sense.
To obtain a continuity estimate (2.14) notice that, by Proposition 2.1.4 and inequalities (2.15),(2.16) there exists a constant $C_1 > 0$ such that:

$$\|\boldsymbol{u}\|_{\boldsymbol{H}^1(\Omega)} \leq C_1 \left(\|\boldsymbol{f}\|_{\boldsymbol{H}_0(\mathrm{div},\Omega)'} + \|\boldsymbol{h}\|_{(\boldsymbol{H}_{00}^{1/2}(\Gamma_N))'} \right) \ . \tag{2.17}$$

Now, from (2.11) we have:

$$\begin{aligned} \|\nabla p\|_{\boldsymbol{H}^{-1}(\Omega)} &\leq \|\boldsymbol{f}\|_{\boldsymbol{H}^{-1}(\Omega)} + \|\Delta \boldsymbol{u}\|_{\boldsymbol{H}^{-1}(\Omega)} \\ &\leq C_1 \|\boldsymbol{f}\|_{\boldsymbol{H}_0(\mathrm{div},\Omega)'} + C_2 \|\boldsymbol{u}\|_{\boldsymbol{H}^1(\Omega)} \ . \end{aligned}$$

As a result, we can infer from [9, Proposition 2.10] that:

$$\|p\|_{L_0^2(\Omega)} \leq C_3 \left(\|\boldsymbol{f}\|_{\boldsymbol{H}_0(\mathrm{div},\Omega)'} + \|\boldsymbol{u}\|_{\boldsymbol{H}^1(\Omega)} \right) \ . \tag{2.18}$$

Using (2.17) and (2.18) we obtain the desired estimate. □

Now, we are ready to demonstrate the primary outcome of this subsection, Theorem 2.1.1.

Proof of theorem 2.1.1. Let $\widetilde{\boldsymbol{g}}$ be the extension by zero to $\partial\Omega$ of $\boldsymbol{g}$. According to Theorem 2.4.3, it follows that $\widetilde{\boldsymbol{g}} \in \boldsymbol{H}^{1/2}(\partial\Omega)$ and there exists a constant $C > 0$ such that:

$$\|\widetilde{\boldsymbol{g}}\|_{\boldsymbol{H}^{1/2}(\partial\Omega)} \leq C \|\boldsymbol{g}\|_{\boldsymbol{H}_{00}^{1/2}(\Gamma_D)} \tag{2.19}$$

Using the compatibility condition (2.3), let $(\boldsymbol{w},\pi) \in \boldsymbol{H}^1(\Omega)\times L^2_0(\Omega)$ be the solution of:

$$\begin{cases} -\operatorname{div}(\sigma(\boldsymbol{w},\pi)) = 0 & \text{in } \Omega, \\ \operatorname{div}(\boldsymbol{w}) = 0 & \text{in } \Omega, \\ \boldsymbol{w} = \widetilde{\boldsymbol{g}} & \text{on } \partial\Omega. \end{cases} \tag{2.20}$$

Therefore, using the classical estimate and inequality (2.19) there is a constant $C_0 > 0$ such that:

$$\|\boldsymbol{w}\|_{\boldsymbol{H}^1(\Omega)} + \|\pi\|_{L^2(\Omega)} \leq C_0 \|\boldsymbol{g}\|_{\boldsymbol{H}^{1/2}_{00}(\Gamma_D)} .$$

Now notice that $\boldsymbol{w} \in \boldsymbol{E}(\Omega)$ since $\pi \in L^2(\Omega)$ therefore $[2\boldsymbol{D}(\boldsymbol{w})\boldsymbol{n}]_{tg}|_{\Gamma_N} \in \boldsymbol{H}^{1/2}_{00}(\Gamma_N)'$ due to Theorem 2.4.4. Thus we obtain the following inequality:

$$\begin{aligned} \|[2\boldsymbol{D}(\boldsymbol{w})\boldsymbol{n}]_{tg}\|_{(\boldsymbol{H}^{1/2}_{00}(\Gamma_N))'} &\leq C_1 \|\boldsymbol{w}\|_{E(\Omega)} \\ &\leq C_2 \left(\|\boldsymbol{w}\|_{\boldsymbol{H}^1(\Omega)} + \|\pi\|_{L^2(\Omega)} \right) \\ &\leq C_3 \|\boldsymbol{g}\|_{\boldsymbol{H}^{1/2}_{00}(\Gamma_D)} . \end{aligned} \tag{2.21}$$

Now since $\boldsymbol{h} - [2\boldsymbol{D}(\boldsymbol{w})\boldsymbol{n}]_{tg} \in (\boldsymbol{H}^{1/2}_{00}(\Gamma_N))'$, using theorem 2.1.5, we denote $(\widetilde{\boldsymbol{u}}, \widetilde{\pi}) \in \boldsymbol{H}^1(\Omega) \times L^2_0(\Omega)$ to be a solution of

$$\begin{cases} -\operatorname{div}(\sigma(\widetilde{\boldsymbol{u}}, \widetilde{\pi})) = \boldsymbol{f} & \text{in} \quad \Omega, \\ \operatorname{div}(\widetilde{\boldsymbol{u}}) = 0 & \text{in} \quad \Omega, \\ \widetilde{\boldsymbol{u}} \cdot \boldsymbol{n} = 0 & \text{in} \quad \partial\Omega, \\ \widetilde{\boldsymbol{u}} = 0 & \text{in} \quad \Gamma_D, \\ [2\boldsymbol{D}(\widetilde{\boldsymbol{u}})\boldsymbol{n}]_{tg} = \boldsymbol{h} - [2\boldsymbol{D}(\boldsymbol{w})\boldsymbol{n}]_{tg} & \text{in} \quad \Gamma_N. \end{cases} \tag{2.22}$$

Defining $\boldsymbol{u} = \widetilde{\boldsymbol{u}} + \boldsymbol{w}$, $\pi = \widetilde{\pi} + \pi$, we obtain the desired existence and uniqueness result. Using the estimation (2.14) and the equation (2.21) and the triangle inequality, we obtain the desired estimates. □

2.2 Unsteady Stokes system with mixed boundary conditions

The aim of this section is to establish the existence and uniqueness of a weak solution for the unsteady Stokes system with mixed boundary conditions:

$$\begin{cases} \boldsymbol{u}_t - \operatorname{div}(\sigma(\boldsymbol{u},p)) = \boldsymbol{f} & \text{in} \quad \Omega \times (0,T), \\ \operatorname{div}(\boldsymbol{u}) = 0 & \text{in} \quad \Omega \times (0,T), \\ \boldsymbol{u}\cdot\boldsymbol{n} = 0 & \text{on} \quad \partial\Omega \times (0,T), \\ \boldsymbol{u} = \boldsymbol{g} & \text{on} \quad \Gamma_D \times (0,T), \\ [2\boldsymbol{D}(\boldsymbol{u})\boldsymbol{n}]_{tg} = \boldsymbol{h} & \text{on} \quad \Gamma_N \times (0,T), \\ \boldsymbol{u}(0,x) = \boldsymbol{u}_0(x) & \text{in} \quad \Omega\ . \end{cases} \tag{2.23}$$

Since we are handling the non-stationary case, we need an additional space:

$$\boldsymbol{H} = \{\boldsymbol{u} \in \boldsymbol{L}^2(\Omega) :\ \operatorname{div}(\boldsymbol{u}) = 0, \boldsymbol{u}\cdot\boldsymbol{n} = 0 \text{ on } \partial\Omega\}.$$

The main result of this section is presented in the following theorem.

Theorem 2.2.1. *Let* $\boldsymbol{f} \in L^2(0,T;\boldsymbol{H}_0(\operatorname{div},\Omega)')$, $\boldsymbol{h} \in L^2(0,T;(\boldsymbol{H}_{00}^{1/2}(\Gamma_N))')$, $\boldsymbol{g} \in L^2(0,T;\boldsymbol{H}_{00}^{1/2}(\Gamma_D))$ *and* $\boldsymbol{u_0} \in \boldsymbol{H}$ *such that:*

$$\boldsymbol{g}(t)\cdot\boldsymbol{n} = 0 \text{ and } \langle \boldsymbol{h}(t), \boldsymbol{n}\rangle_{\Gamma_N} = 0 \quad \forall t \in (0,T)\ . \tag{2.24}$$

Then the problem of finding $(\boldsymbol{u},p) \in L^2(0,T;\boldsymbol{V}(\Omega)) \cap C([0,T],\boldsymbol{H}) \times L^2(0,T;L_0^2(\Omega))$ *that satisfies* (2.23) *in the distribution sense has a unique solution.*

Remark 2.2.2. Notice that if we define $\boldsymbol{V}_0(\Omega) = \{\boldsymbol{u} \in H_0^1(\Omega)\ :\ \operatorname{div}(\boldsymbol{u}) = 0\}$, it is clear that $\boldsymbol{V}_0(\Omega) \subset \boldsymbol{V}(\Omega) \subset \boldsymbol{H}$ and we know by [61] that $\boldsymbol{V}_0(\Omega)$ is dense in $\boldsymbol{H}$ therefore $\boldsymbol{V}(\Omega)$ is dense in $\boldsymbol{H}$.

Before presenting the proof of theorem 2.1.1, some preliminary results are needed. The following result [19, Theorem 10.9] which prove can be found in [50, Chap 3, Theorem 4.1] provides a powerful tool to establish the existence and uniqueness of weak solutions for parabolic problems in a highly general setting.

Theorem 2.2.3 (J.-L. Lions)**.** *Let* H *be a Hilbert space with a scalar product denoted as* $(\ ,\ )$ *and a norm denoted as* $|\ |$. *We identify the dual space* $H^\star$ *with* H. *Let* V *be another Hilbert space, equipped with the norm* $\|\ \|$. *We assume that* V *is a densely and continuously injected subspace of* H, *i.e.,*

$$V \subset H \subset V^\star.$$

Fix a $T > 0$. For almost every $t \in [0,T]$, we are given a bilinear form $a(t;u,v) : V \times V \to \mathbb{R}$ that satisfies:

1. *For every $u, v \in V$, the function $t \mapsto a(t;u,v)$ is measurable.*
2. *$|a(t;u,v)| \leq M\|u\|\|v\|$ for almost every $t \in [0,T]$, for all $u, v \in V$.*
3. *$a(t;v,v) \geq \alpha\|v\|^2 - C|v|^2$ for almost every $t \in [0,T]$, for all $v \in V$.*

Here, $\alpha > 0$, M, and C are constants. Given $f \in L^2(0,T;V^\star)$ and $u_0 \in H$, there exists a unique function u satisfying

$$u \in L^2(0,T;V) \cap C([0,T];H), \quad \frac{du}{dt} \in L^2(0,T;V^\star)$$

$$\left\langle \frac{du}{dt}(t), v \right\rangle + a(t;u(t),v) = \langle f(t), v\rangle \quad \text{for a.e } t \in (0,T), \quad \forall v \in V,$$

and

$$u(0) = u_0.$$

The following proposition characterizes the distributional solution of (2.23) in terms of weak solutions.

Proposition 2.2.4. *Suppose that $\boldsymbol{g} = 0$, and let $\boldsymbol{f} \in L^2\left(0,T;\boldsymbol{H}_0(\mathrm{div},\Omega)'\right)$, $\boldsymbol{h} \in L^2(0,T;(\boldsymbol{H}_{00}^{1/2}(\Gamma_N))')$ and $\boldsymbol{u_0} \in \boldsymbol{H}$ such that:*

$$\langle \boldsymbol{h}(t), \boldsymbol{n}\rangle_{\Gamma_N} = 0 \quad \forall t \in (0,T)\ .$$

Then the problem of finding $\boldsymbol{u} \in L^2(0,T;\boldsymbol{V}(\Omega)) \bigcap C([0,T],\boldsymbol{H})$ and $p \in L^2(0,T;L_0^2(\Omega))$ satisfying (2.23) in the distribution sense is equivalent to:

$$\begin{cases} \text{Find } u \in L^2(0,T;\boldsymbol{V}(\Omega)) \cap C([0,T],\boldsymbol{H}) \text{ such that } \forall \boldsymbol{v} \in \boldsymbol{V}(\Omega), \\ \frac{d}{dt}\int_\Omega \boldsymbol{u}\cdot\boldsymbol{v}\,dx + \int_\Omega 2\boldsymbol{D}(\boldsymbol{u}) : \boldsymbol{D}(\boldsymbol{v})\,dx = \langle \boldsymbol{f}, \boldsymbol{v}\rangle_\Omega + \langle \boldsymbol{h}, \boldsymbol{v}\rangle_{\Gamma_N} \\ \text{in the distributional sense on } (0,T), \text{ and} \\ \boldsymbol{u}(0) = \boldsymbol{u_0}. \end{cases} \tag{2.25}$$

Proof. Let $\boldsymbol{u} \in L^2(0,T;\boldsymbol{V}(\Omega)) \cap C([0,T],\boldsymbol{H})$ and $p \in L^2(0,T;L_0^2(\Omega))$ be a solution of (2.23), and let $\boldsymbol{v} \in \boldsymbol{V}(\Omega)$, integrating by part as in Proposition 2.1.3 we obtain:

$$\frac{d}{dt}\int_\Omega \boldsymbol{u}.\boldsymbol{v}\,dx + \int_\Omega 2\boldsymbol{D}(\boldsymbol{u}) : \boldsymbol{D}(\boldsymbol{v})\,dx = \langle \boldsymbol{f}, \boldsymbol{v}\rangle_\Omega + \langle \boldsymbol{h}, \boldsymbol{v}\rangle_{\Gamma_N}\ . \tag{2.26}$$

Conversely, let $\boldsymbol{u} \in L^2(0,T;\boldsymbol{V}(\Omega)) \cap C([0,T],\boldsymbol{H})$ be a solution of (2.25). Let $\boldsymbol{\varphi} \in \boldsymbol{\mathcal{D}}_\sigma(\Omega) = \{\boldsymbol{\varphi} \in \boldsymbol{\mathcal{D}}(\Omega) \,:\, \mathrm{div}(\boldsymbol{\varphi}) = 0\}$, and notice that we have the following identity:

$$\int_\Omega \frac{d\boldsymbol{u}}{dt}(t) \cdot \boldsymbol{\varphi}\, dx + \int_\Omega \nabla(\boldsymbol{u}(t)) : \nabla(\boldsymbol{\varphi})\, dx = \langle \boldsymbol{f}(t), \boldsymbol{\varphi} \rangle_\Omega \ .$$

As a consequence, we have:

$$\forall \boldsymbol{\varphi} \in \boldsymbol{\mathcal{D}}_\sigma(\Omega), \quad \left\langle \frac{d\boldsymbol{u}}{dt}(t) - \Delta \boldsymbol{u}(t) - \boldsymbol{f}(t), \boldsymbol{\varphi} \right\rangle_{\boldsymbol{\mathcal{D}}(\Omega)' \times \boldsymbol{\mathcal{D}}(\Omega)} = 0 \ .$$

Therefore, thanks to De Rham Theorem [9, Theorem 2.1], there exists a distribution $p(t) \in \mathcal{D}(\Omega)'$ defined uniquely up to an additive constant such that:

$$\frac{d\boldsymbol{u}}{dt}(t) - \Delta \boldsymbol{u}(t) + \nabla p(t) = \boldsymbol{f}(t) \ . \tag{2.27}$$

Note that since $L^2(0,T;\boldsymbol{H}_0(\mathrm{div},\Omega)')$ is embedded in $L^2(0,T;\boldsymbol{H}^{-1}(\Omega))$(i.e. $\boldsymbol{H}_0(\mathrm{div},\Omega)' \hookrightarrow \boldsymbol{H}^{-1}(\Omega)$), we have $p \in L^2(0,T;L^2_0(\Omega))$.

Now let $\boldsymbol{v} \in \boldsymbol{V}(\Omega)$, using equations (2.26),(2.27), and the same argument as in proposition 2.1.3 we obtain:

$$\langle [2\boldsymbol{D}(\boldsymbol{u}(t))\boldsymbol{n}]_{tg} - \boldsymbol{h}(t), \boldsymbol{v} \rangle_{\Gamma_N} = 0 \ .$$

By assumption $\boldsymbol{u}(0) = \boldsymbol{u}_0$ and $\boldsymbol{u} \in L^2(0,T;\boldsymbol{V}(\Omega)) \cap C([0,T],\boldsymbol{H})$. This completes the proof of Proposition 2.2.4. □

The main objective is to prove the existence of the solution as defined in equation (2.25). To accomplish this, we will make use of Theorem 2.2.3 and the following lemma:

Lemma 2.2.5. *Suppose that* $\boldsymbol{g} = 0$, *and let* $\boldsymbol{f} \in L^2(0,T;\boldsymbol{H}_0(\mathrm{div},\Omega)')$, $\boldsymbol{h} \in L^2(0,T;(\boldsymbol{H}^{1/2}_{00}(\Gamma_N))')$, $\boldsymbol{u_0} \in \boldsymbol{H}$ *such that:*

$$\langle \boldsymbol{h}(t), \boldsymbol{n} \rangle_{\Gamma_N} = 0 \quad \forall t \in (0,T) \ .$$

Then the problem of finding $(\boldsymbol{u},p) \in L^2(0,T;\boldsymbol{V}(\Omega)) \cap C([0,T],\boldsymbol{H}) \times L^2(0,T;L^2_0(\Omega))$ *satisfying* (2.23) *in the distribution sense has a unique solution.*

Proof. Thanks to proposition 2.2.4 , we only need to prove the existence and uniqueness of the following initial variational problem:

$$\begin{cases} \text{Find } \boldsymbol{u} \in L^2(0,T;\boldsymbol{V}(\Omega)) \cap C([0,T],\boldsymbol{H}) \text{such that} \forall \boldsymbol{v} \in V(\Omega) \\ \frac{d}{dt}\int_\Omega \boldsymbol{u}\cdot\boldsymbol{v}\,dx + \int_\Omega 2\boldsymbol{D}(\boldsymbol{u}) : \boldsymbol{D}(\boldsymbol{v})\,dx = \langle \boldsymbol{f},\boldsymbol{v}\rangle_\Omega + \langle \boldsymbol{h},\boldsymbol{v}\rangle_{\Gamma_N} \\ \text{in the distributional sense on } (0,T), \text{ and} \\ \boldsymbol{u}(0) = \boldsymbol{u_0}. \end{cases}$$

We commence our approach by invoking 2.2.3. Notably, we observe that $\boldsymbol{V}(\Omega) \subset \boldsymbol{H}$ and that $\boldsymbol{V}(\Omega)$ is dense in $\boldsymbol{H}$ with continuous injection. In Proposition 2.1.5, we have already established that the bilinear form $a(u,v) = 2\int_\Omega \boldsymbol{D}(\boldsymbol{u}) : \boldsymbol{D}(\boldsymbol{v})\,dx$ is both continuous and coercive over $\boldsymbol{V}(\Omega)$. Moreover, consider the functional $L(t;v) = \langle \boldsymbol{f}(t),\boldsymbol{v}\rangle_\Omega + \langle \boldsymbol{h}(t),\boldsymbol{v}\rangle_{\Gamma_N}$, which is a continuous linear function belonging to $L^2(0,T;\boldsymbol{V}(\Omega)')$.

Hence, by employing Theorem 2.2.3 and Proposition 2.2.4, we conclude that there exists a unique solution $(\boldsymbol{u},p) \in L^2(0,T;\boldsymbol{V}(\Omega)) \cap C([0,T],\boldsymbol{H}) \times L^2(0,T;L^2_0(\Omega))$ to equation (2.25). Additionally, we note that $\frac{du}{dt} \in L^2(0,T;\boldsymbol{V}(\Omega)')$.

□

Now we are in a position to prove the main result of this subsection, theorem 2.2.1.

Proof of theorem 2.2.1. Let $\boldsymbol{w} \in L^2(0,T;\boldsymbol{V}(\Omega)) \bigcap C([0,T],\boldsymbol{H}))$, and $\pi \in L^2(0,T;L^2_0(\Omega))$ be the unique solution, as guaranteed by the compatibility condition of $\boldsymbol{g}$ in equation (2.24).

$$\begin{cases} u_t - \operatorname{div}(\sigma(\boldsymbol{w},\pi)) = 0 & \text{in } \Omega\times(0,T), \\ \operatorname{div}(\boldsymbol{w}) = 0 & \text{in } \Omega\times(0,T), \\ \boldsymbol{w} = \boldsymbol{g} & \text{on } \Gamma_D\times(0,T), \\ \boldsymbol{w} = 0 & \text{on } \Gamma_N\times(0,T), \\ \boldsymbol{u}(0,x) = 0 & \text{in } \Omega\ . \end{cases}$$

Using an analogous argumentation as in theorem 2.1.1 we have that $\boldsymbol{h} - [2\boldsymbol{D}(\boldsymbol{w})\boldsymbol{n}]_{tg}|_{\Gamma_N}$ belong to $L^2(0,T;\boldsymbol{H}^{1/2}_{00}(\Gamma_N)')$.

From lemma 2.2.5, let $\widetilde{\boldsymbol{u}} \in L^2(0,T;\boldsymbol{V}(\Omega)) \bigcap C([0,T],\boldsymbol{H})$ and $\widetilde{\pi} \in L^2(0,T;L^2_0(\Omega))$

be the unique solution to:

$$\begin{cases} \widetilde{\boldsymbol{u}}_t - \operatorname{div}(\sigma(\widetilde{\boldsymbol{u}}, \widetilde{\pi})) = 0 & \text{in } \Omega \times (0,T), \\ \operatorname{div}(\widetilde{\boldsymbol{u}}) = 0 & \text{in } \Omega \times (0,T), \\ \widetilde{\boldsymbol{u}} \cdot \boldsymbol{n} = \boldsymbol{0} & \text{on } \partial\Omega \times (0,T), \\ \widetilde{\boldsymbol{u}} = 0 & \text{on } \Gamma_D \times (0,T), \\ [2\boldsymbol{D}(\widetilde{\boldsymbol{u}})\boldsymbol{n}]_{tg} = \boldsymbol{h} - [2\boldsymbol{D}(\boldsymbol{w})\boldsymbol{n}]_{tg} & \text{on } \Gamma_N \times (0,T), \\ \widetilde{\boldsymbol{u}}(0,x) = \boldsymbol{u}_0 & \text{in } \Omega\ . \end{cases}$$

Defining $\boldsymbol{u} = \widetilde{\boldsymbol{u}} + \boldsymbol{w}$, $p = \widetilde{\pi} + \pi$, we obtain the desired existence and uniqueness result.

□

Remark 2.2.6. As far as we know the regular solution with mixed boundary conditions, as in (2.23), for general Lipschitz domains is an open problem. However, some results for the polygonal case and for similar boundary conditions are available in [20] using potential theory. The generalization of these results to our particular case is out of the scope of this research work and will be subject to further investigation.

2.3 Theoretical results to the identification problem

In this section, we prove the identifiability of the obstacle $\mathcal{O}$ associated with the Stokes system with mixed boundary conditions (1.2). To account for the obstacle's position in contact with part of the boundary $\partial\Omega$ (as described in (1.1)), we first define the admissible deformation of the domain. Then, we present the proof of our main result, Theorem 2.3.4. Our proof builds on the arguments presented in [7], where the authors proved the identification of immersed obstacles from boundary data for the Navier–Stokes system with Dirichlet boundary conditions. However, our proof includes novel contributions, such as considering the unique geometrical configuration where the obstacle intersects the flow boundary, and mixed boundary conditions instead of Dirichlet boundary conditions.

Definition 2.3.1. Let $\Omega \subset \mathbb{R}^2$ be a simple connected and bounded curvilinear polygon of class $C^{1,1}$, $\partial\Omega = \Gamma_{inlet} \cup \Gamma_{wall} \cup \Gamma_{out}$. A domain $\Omega_{\mathcal{O}}$ is called an admissible deformation of Ω if and only if:

i) $\Omega_{\mathcal{O}} \subset \Omega$ is simple a connected and bounded curvilinear polygon of class $C^{1,1}$.

ii) $\partial\Omega_{\mathcal{O}} := \Gamma_{inlet} \cup \Gamma^{\mathcal{O}}_{wall} \cup \Gamma_{out}$ and $\Gamma_{wall} \cap \Gamma^{\mathcal{O}}_{wall}$ are non–empty relatively open sets of Γ_{wall}.

iii) There exist a relative open set $W \subset \Omega$ satisfying $\Omega \backslash \overline{\Omega_{\mathcal{O}}} \subset W$, there exists a diffeomorphism $\psi : \overline{\Omega} \to \overline{\Omega}$ such that $\psi(\Omega) = \Omega_{\mathcal{O}}$ and $\psi = I$ in $\Omega \backslash \overline{W}$ (see Figure 2.1).

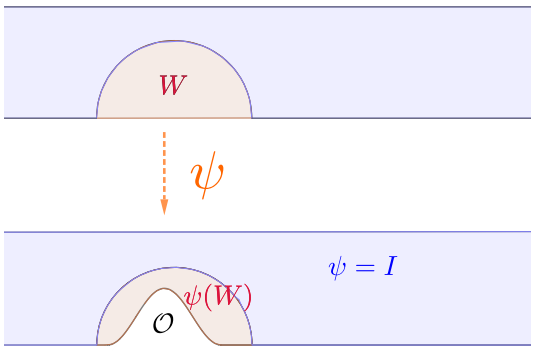

Figure 2.1: Diffeomorphism example

Remark 2.3.2. From definition 2.3.1, given an admissible deformation $\Omega_{\mathcal{O}}$, an admissible obstruction can be define as $\mathcal{O} = \Omega \backslash \overline{\Omega_{\mathcal{O}}}$.

The following theorem is due to Fabre and Lebeau in [27]. It is worth noting that this result is independent of the boundary conditions, thus, it can be applied specifically to Navier-slip boundary conditions.

Theorem 2.3.3. *Let $\Omega \subset \mathbb{R}^N$ be a connected open set, $N \geq 2$ and $T > 0$. Let $a \in L^{\infty}_{loc}(\Omega \times (0,T))^N$ and $c \in C([0,T]; L^r_{loc}(\Omega, \mathbb{R}^{N\times N}))$ be a matrix-value function with $r > N$. If $(\boldsymbol{v}, p) \in L^2(0,T; H^1_{loc}(\Omega)) \times L^2_{loc}(\Omega \times (0,T))$ is a solution of:*

$$\begin{cases} \boldsymbol{v}_t - \Delta \boldsymbol{v} + (a.\nabla)\boldsymbol{v} + c\boldsymbol{v} + \nabla p = 0 & in \quad \Omega \times (0,T), \\ \operatorname{div}(\boldsymbol{v}) = 0 & in \quad \Omega \times (0,T), \end{cases} \tag{2.28}$$

with $\boldsymbol{v} = 0$ in $\omega_0 \times (0,T)$, where ω_0 is and open set of Ω. Then $\boldsymbol{v} = 0$ in $\Omega \times (0,T)$ and p is a constant.

Using the above theorem, we have the following corollary, which is essential for the next identification theorem. We note that this result can also be found in [7, Corollary 2.4] and a similar one in [16]. Since no proof is provided in [7], we present a short proof.

Corollary 2.3.1. *Let $\Omega \subset \mathbb{R}^N$ be a connected open Lipschitz domain, $N \geq 2$ and $T > 0$. If $(\boldsymbol{u}, p) \in L^2(0,T; H^1(\Omega)^N) \times L^2(\Omega \times (0,T))$ is a solution of:*

$$\begin{cases} \boldsymbol{u}_t - \operatorname{div}(\sigma(\boldsymbol{u}, p)) = 0 & \text{in} \quad \Omega \times (0,T), \\ \operatorname{div}(\boldsymbol{u}) = 0 & \text{in} \quad \Omega \times (0,T), \end{cases} \tag{2.29}$$

satisfying $\boldsymbol{u} = \sigma(\boldsymbol{u}, p)\boldsymbol{n} = 0$ on $\Gamma \times (0,T)$ where $\Gamma \subset \partial\Omega$ is relatively open non-empty subsets, then

$$\boldsymbol{u} = 0 \quad \text{in} \quad \Omega \times (0,T) \ .$$

Proof. Let $\boldsymbol{x_0} \in \Gamma$ and $r > 0$ such that $\boldsymbol{B}(\boldsymbol{x_0}, r) \cap \partial\Omega \subset \Gamma$. Let $B = \boldsymbol{B}(\boldsymbol{x_0}, r) \cap \Omega^c$ and $\widetilde{\Omega} = \Omega \cup B$, we define the extension by 0 of $\boldsymbol{u}$ and p in $\widetilde{\Omega}$ by:

$$\widetilde{\boldsymbol{u}} \ (\text{resp } \widetilde{p}) = \begin{cases} \boldsymbol{u} \ (\text{resp } p) & \text{in } \Omega \times (0,T), \\ 0 & \text{in } B \times (0,T). \end{cases}$$

Our goal now is to prove that $(\widetilde{\boldsymbol{u}}, \widetilde{p})$ is solution of (2.29) in $\widetilde{\Omega}$, for this let $\boldsymbol{\varphi} \in \boldsymbol{D}(\widetilde{\Omega})$ and notice that:

$$\langle \sigma(\widetilde{\boldsymbol{u}}, \widetilde{p})\boldsymbol{n}, \boldsymbol{\varphi} \rangle_{\boldsymbol{H}^{-1/2}(\partial B) \times \boldsymbol{H}^{1/2}(\partial B)} = \langle \sigma(\widetilde{\boldsymbol{u}}, \widetilde{p})\boldsymbol{n}, \boldsymbol{\varphi} \rangle_{\boldsymbol{H}^{-1/2}(\Gamma) \times \boldsymbol{H}^{1/2}(\Gamma)} = 0$$

Therefore using integration by parts, it follows that:

$$\langle (\widetilde{\boldsymbol{u}}_t - \operatorname{div}(\sigma(\widetilde{\boldsymbol{u}}, \widetilde{p}))) \, \chi_B, \boldsymbol{\varphi} \rangle_{\boldsymbol{D'}(\widetilde{\Omega}) \times \boldsymbol{D}(\widetilde{\Omega})} = 0$$

In a similar way, we can also deduce that:

$$\langle (\widetilde{\boldsymbol{u}}_t - \operatorname{div}(\sigma(\widetilde{\boldsymbol{u}}, \widetilde{p}))) \, \chi_\Omega, \boldsymbol{\varphi} \rangle_{\boldsymbol{D'}(\widetilde{\Omega}) \times \boldsymbol{D}(\widetilde{\Omega})} = 0.$$

Therefore, we obtain:

$$\langle \widetilde{\boldsymbol{u}}_t - \operatorname{div}(\sigma(\widetilde{\boldsymbol{u}}, \widetilde{p})), \boldsymbol{\varphi} \rangle_{\boldsymbol{D'}(\widetilde{\Omega}) \times \boldsymbol{D}(\widetilde{\Omega})} = 0.$$

Using Theorem 2.3.3 for $(\widetilde{\boldsymbol{u}}, \widetilde{p})$ we obtain the desired result. □

Theorem 2.3.4. *Let $\Omega_0, \Omega_1 \subset \mathbb{R}^N$ be two admissible deformation of Ω according to the definition 2.3.1 such that $\Omega_0 \cap \Omega_1$ is a curvilinear polygons of class $C^{1,1}$ domain with a finite number of disjoint connected components. Let $(\boldsymbol{u}_j, p_j) \in L^2(0,T; H^1(\Omega_j)^N) \times L^2(0,T; L^2(\Omega_j))$ be the solution of:*

$$\begin{cases} \frac{\partial \boldsymbol{u}_j}{\partial t} - \operatorname{div}(\sigma(\boldsymbol{u}_j, p_j)) = 0 & \text{in} \quad \Omega_j \times (0,T), \\ \operatorname{div}(\boldsymbol{u}_j) = 0 & \text{in} \quad \Omega_j \times (0,T), \\ \boldsymbol{u}_j = \boldsymbol{g} & \text{on} \quad \Gamma_{inlet} \cup \Gamma_{out} \times (0,T), \qquad j = 0, 1 \\ \boldsymbol{u}_j \cdot \boldsymbol{n} = 0, \ (\sigma(\boldsymbol{u}_j, p)\boldsymbol{n})_{tg} = 0 & \text{on} \quad \Gamma^j_{wall} \times (0,T), \\ \boldsymbol{u}(\cdot, 0) = 0 & \text{in} \quad \Omega_j. \end{cases} \tag{2.30}$$

Assume that $\boldsymbol{g} \neq 0 \in H_{00}^{1/2}(\Gamma_{inlet} \cup \Gamma_{out})$ *and that* $\Gamma_m \subset \Gamma_{wall}^0 \cap \Gamma_{wall}^1$ *is a non-zero measure set satisfying* $\Gamma_m \subset \partial(\Omega_0 \cap \Omega_1)$*, such that:*

$$(\sigma(\boldsymbol{u}_0, p_0)\boldsymbol{n}) \cdot \boldsymbol{n} = (\sigma(\boldsymbol{u}_1, p_1)\boldsymbol{n}) \cdot \boldsymbol{n} \quad \textit{and} \quad \boldsymbol{u}_0 \cdot \boldsymbol{\tau} = \boldsymbol{u}_1 \cdot \boldsymbol{\tau} \quad \textit{on } \Gamma_m \times (0,T),$$

where $\boldsymbol{n}$ *is external unit normal and* $\boldsymbol{\tau}$ *is tangent unit vector of* Γ_m*. Then* $\Omega_0 \equiv \Omega_1$*.*

Proof of theorem 2.3.4. First within the context of Theorem 2.2.1 by defining $\Gamma_D = \Gamma_{inlet} \cup \Gamma_{out}$ and $\Gamma_N = \Gamma_{wall}^j$ we can guarantee the existences and uniqueness of the solutions $\boldsymbol{u_0}, \boldsymbol{u_1}$ to the equations (2.30). Setting $\boldsymbol{u} = \boldsymbol{u}_0 - \boldsymbol{u}_1$ and $p = p_0 - p_1$, we obtain:

$$\begin{cases} \frac{\partial \boldsymbol{u}}{\partial t} - \operatorname{div}(\sigma(\boldsymbol{u}, p)) = 0 & \text{in} \quad \Omega_0 \cap \Omega_1 \times (0,T), \\ \operatorname{div}(\boldsymbol{u}) = 0 & \text{in} \quad \Omega_0 \cap \Omega_1 \times (0,T), \\ \boldsymbol{u} = 0 & \text{on} \quad \Gamma_D \times (0,T), \\ \boldsymbol{u} \cdot \boldsymbol{n} = 0, \ (\sigma(\boldsymbol{u}, p)\boldsymbol{n})_{tg} = 0 & \text{on} \quad \Gamma_m \times (0,T), \\ \boldsymbol{u}(.,0) = 0 & \text{on} \quad \Omega_0 \cap \Omega_1. \end{cases} \tag{2.31}$$

Since $\sigma(\boldsymbol{u}, p)\boldsymbol{n} = 0$, $\boldsymbol{u} = 0$ on $\Gamma_m \times (0,T)$ and $\Gamma_m \subset \partial(\Omega_0 \cap \Omega_1)$, it follows from corollary 2.3.1 applied to each connected component of $\Omega_0 \cap \Omega_1$ that :

$$\boldsymbol{u}_0 = \boldsymbol{u}_1 \text{ in } (\Omega_0 \cap \Omega_1) \times (0,T). \tag{2.32}$$

Now lets assume that $\Omega_0 \backslash \overline{\Omega_1}$ is a non-empty open subset of Ω_0. Thus, we have the following:

$$\frac{\partial \boldsymbol{u}_0}{\partial t} - \operatorname{div}(\sigma(\boldsymbol{u}_0, p_0)\boldsymbol{n}) = 0 \quad \textit{in} \quad (\Omega_0 \backslash \overline{\Omega_1}) \times (0,T) \ . \tag{2.33}$$

Given that $\Omega_0 = (\Omega_0 \backslash \overline{\Omega_1}) \cup (\Omega_0 \cap \overline{\Omega_1})$ we have:

$$\frac{d}{dt}\int_{(\Omega_0 \backslash \overline{\Omega_1})} |\boldsymbol{u}_0(x,t)|^2 dx = \frac{d}{dt}\int_{\Omega_0} |\boldsymbol{u}_0(x,t)|^2 dx - \frac{d}{dt}\int_{\Omega_0 \cap \Omega_1} |\boldsymbol{u}_0(x,t)|^2 dx. \tag{2.34}$$

From the assumption that $\Omega_0 \cap \Omega_1$ is smooth, we can perform the following integration by parts:

$$\begin{aligned} \frac{d}{dt}\int_{\Omega_0 \cap \Omega_1} |\boldsymbol{u}_0(x,t)|^2 dx = &- \int_{\Omega_0 \cap \Omega_1} |\boldsymbol{D}(\boldsymbol{u}_0)|^2 dx + \int_{\partial(\Omega_0 \cap \Omega_1)} 2\boldsymbol{D}(\boldsymbol{u}_0)\boldsymbol{n} \cdot \boldsymbol{u_0}\, dS \\ &+ \int_{\partial(\Omega_0 \cap \Omega_1)} p_0 \boldsymbol{u}_0 \cdot \boldsymbol{n} dS \ . \end{aligned} \tag{2.35}$$

Observing that for any two admissible deformations, we have the following (as depicted in Figure 2.2):

$$\partial\left(\Omega_0 \cap \Omega_1\right) = \Gamma_D \cup \left[\Gamma^0_{wall} \cap \partial(\Omega_0 \cap \Omega_1)\right] \cup \left[\Gamma^1_{wall} \cap \partial(\Omega_0 \cap \Omega_1)\right].$$

And notice that from equation (2.32) we have that:

$$\begin{cases} [\boldsymbol{D}(\boldsymbol{u}_0)\boldsymbol{n}]_{tg} = [\boldsymbol{D}(\boldsymbol{u}_1)\boldsymbol{n}]_{tg} = 0 \quad \text{on } [\Gamma^0_{wall} \cap \partial(\Omega_0 \cap \Omega_1)] \cup [\Gamma^1_{wall} \cap \partial(\Omega_0 \cap \Omega_1)] \\ \boldsymbol{u}_0 \cdot \boldsymbol{n} = \boldsymbol{u}_1 \cdot \boldsymbol{n} = 0 \end{cases}$$

Therefore, from equation (2.35) it follows that:

$$\frac{d}{dt}\int_{\Omega_0\cap\Omega_1} |\boldsymbol{u}_0(x,t)|^2 dx = -\int_{\Omega_0\cap\Omega_1} |\boldsymbol{D}(\boldsymbol{u}_0)|^2 dx + \int_{\Gamma_D} [\boldsymbol{D}(\boldsymbol{u}_0)\boldsymbol{n}]_{tg} \cdot \boldsymbol{g}\, dS\ . \tag{2.36}$$

Also by assumption, we know that $\boldsymbol{u}_0 \cdot \boldsymbol{n} = [\boldsymbol{D}(\boldsymbol{u}_0)\boldsymbol{n}]_{tg} = 0$ on Γ^0_{wall}, thus we obtain:

$$\frac{d}{dt}\int_{\Omega_0} |\boldsymbol{u}_0(x,t)|^2 dx = -\int_{\Omega_0} |\boldsymbol{D}(\boldsymbol{u}_0)|^2 dx + \int_{\Gamma_D} [\boldsymbol{D}(\boldsymbol{u}_0)\boldsymbol{n}]_{tg} \cdot \boldsymbol{g}\, dS\ . \tag{2.37}$$

It follows from equations (2.34), (2.36), and (2.37) that:

$$\frac{d}{dt}\int_{(\Omega_0\setminus\overline{\Omega_1})} |\boldsymbol{u}_0(x,t)|^2 dx = -\int_{(\Omega_0\setminus\overline{\Omega_1})} |\boldsymbol{D}(\boldsymbol{u}_0)|^2 dx$$

Therefore

$$E(t) = \int_{\Omega_0\setminus\overline{\Omega_1}} |\boldsymbol{u}_0(x,t)|^2 dx$$

is a decreasing non-negative function. However since $\boldsymbol{u}_0(x,0) = 0$, we have that $\boldsymbol{u}_0|_{\Omega_0\setminus\overline{\Omega_1}} = 0$ for all $t \in (0,T)$. It then follows from theorem 2.3.3 that:

$$\boldsymbol{u}_0 = 0 \ \ in \quad \Omega_0\ .$$

Nevertheless, this is impossible since $\boldsymbol{u}_0 \neq 0$, because $\boldsymbol{g} \neq 0$. Therefore $\Omega_0\setminus\overline{\Omega_1} = \emptyset$, analogously we can deduce that $\Omega_1\setminus\overline{\Omega_0} = \emptyset$ which implies that $\Omega_0 = \Omega_1$. □

As mentioned above, our main purpose is to study and solve the full inverse problem from a numerical point of view. In relation to the direct problem, the smooth dependence of the Cauchy forces for the Stokes system with mixed boundary conditions might be obtained by proving an extension of [7, theorem 5.1]. However, its proof requires a thorough analysis of the holomorphic semigroup associated with the main operator of (1.2), which, as is known, involves mixed boundary

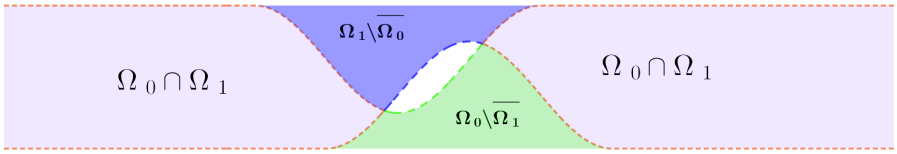

Figure 2.2: Example of domain intersection

conditions. Regarding the inverse wave equation problem, it is necessary to obtain the regularity of the Stokes fluid with mixed boundary conditions, which is an open problem in itself. To deal with hyperbolic inverse problems, a different set of tools has to be used, such as the Hilbert uniqueness method, as can be seen in [49, 67]. Since these topics deserve special attention, we have not attempted to address them in this research work; further work is in progress.

2.4 The $H_{00}^{1/2}$ space

In this section, we recall some useful results about the $H_{00}^{1/2}$ space and also we prove Theorem 2.0.1. Until further notice, we consider a bounded open $\Omega \subset \mathbb{R}^2$ such that $\partial\Omega$ is a curvilinear polygons of class $C^{k,1}$ in the sense of [40, Definition 1.4.5.1]. Furthermore, we assume that there is $M \in \mathbb{N}$ such that:

$$\partial\Omega = \Gamma = \bigcup_{j=1}^{2M} \overline{\Gamma_j} \quad ,$$

were each Γ_j is a curve of class $C^{k,1}$, Γ_{j+1} follows Γ_j according to the positive orientation and we have that $\Gamma_j \subset \partial\Omega$, $\Gamma_j \bigcap \Gamma_{j+1} = \emptyset$. We denote by S_j the vertex which is the end point of $\bar{\Gamma}_j$. We also define the following Lion-Maganese space:

$$H_{00}^{1/2}(\Gamma_i) = \left\{ u \in H^{1/2}(\Gamma_i) : \ d(x, \partial\Gamma_i)^{-1/2} u \in L^2(\Gamma_i) \right\} \ ,$$

equipped with the norm: $\|u\|^2_{H_{00}^{1/2}(\Gamma_i)} = \|u\|^2_{H^{1/2}(\Gamma_i)} + \left\|d^{-1/2}u\right\|^2_{L^2(\Gamma_i)}$. For a smooth function $u \in \mathcal{D}(\overline{\Omega})$ we denote $\gamma_j(u)$,the corresponding trace mappings (i.e):

$$\gamma_j(u) : u \to u|_{\Gamma_j} \quad . \tag{2.38}$$

An important question is when does the trace of a function in $u \in H^{1/2}(\Omega)$ belong to $H_{00}^{1/2}(\Gamma_j)$. In order to address this, we define σ as the distance along Γ, commencing at S_i, and assign $x_i(\sigma)$ to represent the point on Γ that is σ distance away

from S_j. As such, given that $|\sigma|$ is adequately small, say $|\sigma| \leq \delta_j$, we find that $x_j(\sigma)$ belongs to Γ_i when $\sigma < 0$ and $x_j(\sigma)$ is part of Γ_{j+1} when $\sigma > 0$. Utilizing the previously defined notation, we refer back to [40, Theorem 1.5.2.3].

Theorem 2.4.1 (P. Grisvard)**.** *Let Ω be a bounded open subset of $\mathbb{R}^2$ whose boundary Γ is a curvilinear polygon of class C^1. Then the mapping $u \mapsto \{f_i\}_{j=1}^N$, where $f_j = \gamma_j u$, is a linear continuous mapping from $W_p^1(\Omega)$ onto the subspace $\prod_{j=1}^N W_p^{1-1/p}(\Gamma_j)$ defined by:*

(a) No extra condition when $1 < p < 2$.

(b) $f_j(S_j) = f_{j+1}(S_\mathrm{i})$, $1 \leq j \leq N$ when $2 < p < \infty$.

(c) $\int_0^{\delta_1} \frac{|f_{i+1}(x_j(\sigma)) - f_i(x_i(-\sigma))|^2}{\sigma} \mathrm{d}\sigma < \infty$, $1 \leq j \leq N$ when $p = 2$.

In the derivation of Theorem 2.4.1, it's worth noting that condition (c) is limited by the $K\|u\|_{W_p^1(\Omega)}$, where K is a positive constant. Hence, the following theorems can be proposed:

Theorem 2.4.2. *Let Ω be a bounded open subset of $\mathbb{R}^2$ whose boundary is a curvilinear polygon of class at least C^1. Let $u \in H^1(\Omega)$ such that:*

$$\gamma_{j-1}(u) = \gamma_{j+1}(u) = 0 \quad ,$$

then the mapping define by :

$$u \to \gamma_j(u) \quad ,$$

is a linear continuous mapping from $H^1(\Omega) \to H_{00}^{1/2}(\Gamma_j)$.

Proof. To start, recall that the norm $H^{1/2}(\Gamma)$ is described as:

$$\|u\|_{H^{1/2}(\Gamma)}^2 = \int_\Gamma u^2 d\sigma + \iint_{\Gamma\times\Gamma} \frac{|u(x) - u(y)|^2}{|x - y|^2} d\sigma(x) d\sigma(y) \tag{2.39}$$

Here, $d\sigma$ symbolizes the standard hypersurface measure on Γ. As $u \in H^1(\Omega)$, the norm of γu in $H^{1/2}(\Gamma)$ is bounded by $\|u\|_{H^1(\Omega)}$. Let's denote $f_i = \gamma_i(u)$, thus from the previously mentioned equation and by dividing the integration domain $\Gamma \times \Gamma$ into $\bigcup_{l,k} \Gamma_l \times \Gamma_k$, we obtain:

$$\begin{aligned} &\sum_{i=1}^{2M} \iint_{\Gamma_i\times\Gamma_i} \frac{|f_i(x) - f_i(y)|^2}{|x - y|^2} \, \mathrm{d}\sigma(x)\mathrm{d}\sigma(y) \\ &+ 2\sum_{l\neq k} \iint_{\Gamma_l\times\Gamma_k} \frac{|f_l(x) - f_k(y)|^2}{|x - y|^2} \, \mathrm{d}\sigma(x)\mathrm{d}\sigma(y) \leq K\|u\|_{H^1(\Omega)}^2. \end{aligned} \tag{2.40}$$

As a result, it can be seen that $f_j = \gamma_j u \in H^{1/2}(\Gamma)$ because:

$$\iint_{\Gamma_j \times \Gamma_j} \frac{|\gamma_j u(x) - \gamma_j u(y)|^2}{|x-y|^2} \, \mathrm{d}\sigma(x)\mathrm{d}\sigma(y) \leq K\|u\|^2_{H^1(\Omega)}$$

Now, since $\gamma_{j-1}(u) = \gamma_{j+1}(u) = 0$, we obtain:

$$\int_{\Gamma_j}\int_{\Gamma_{j+1}} \frac{|f_j(x)|^2}{|x-y|^2} \, \mathrm{d}\sigma(\mathrm{x})\mathrm{d}\sigma(\mathrm{y}) + \int_{\Gamma_{j-1}}\int_{\Gamma_j} \frac{|f_j(y)|^2}{|x-y|^2} \, \mathrm{d}\sigma(\mathrm{x})\mathrm{d}\sigma(\mathrm{y}) \leq K\|u\|^2_{H^1(\Omega)}$$

Following [40, Theorem 1.5.2.3], it can be observed that as $\Gamma_{j+1}, \Gamma_{j-1}$ are C^1 curves, the functions:

$$\int_{\Gamma_{j+1}} \frac{\mathrm{d}\sigma(y)}{|x-y|^2}, \int_{\Gamma_{j-1}} \frac{\mathrm{d}\sigma(x)}{|x-y|^2}$$

are equivalent to $d(x,\Gamma_{j+1})^{-1}, d(y,\Gamma_{j-1})^{-1}$ respectively. Therefore:

$$\int_{\Gamma_j} \frac{|f_j(x)|^2}{d(x,\Gamma_{j+1})} \, \mathrm{d}\sigma(\mathrm{x}) + \int_{\Gamma_j} \frac{|f_j(y)|^2}{d(y,\Gamma_{j-1})} \, \mathrm{d}\sigma(\mathrm{y}) \leq K'\|u\|^2_{H^1(\Omega)}$$

Hence, we can conclude:

$$\|f_j\|_{H^{1/2}_{00}(\Omega)} \leq K''\|u\|_{H^1(\Omega)}$$

□

Theorem 2.4.3. *Let Ω be a bounded open subset of $\mathbb{R}^2$ whose boundary is a curvilinear polygon of class at least C^1. Let $f_j \in H^{1/2}_{00}(\Gamma_j)$, and define $\widetilde{f}$ as the extension by zero en Γ (i.e):*

$$\widetilde{f}(x) = \begin{cases} f_j(x) & x \in \Gamma_j \\ 0 & x \notin \Gamma_j \end{cases} ,$$

then $\widetilde{f} \in H^{1/2}(\Gamma)$ and there exist a constant $C > 0$ such that:

$$\left\|\widetilde{f}\right\|_{H^{1/2}(\Gamma)} \leq C\|f_j\|_{H^{1/2}_{00}(\Gamma_j)} \quad .$$

Proof. Given f_j exists in $H^{1/2}_{00}(\Gamma_j)$, it's known that $f_j \in L^2(\Gamma_j)$. From equation (2.39) and separating the domain of integration $\Gamma \times \Gamma$ in $\bigcup_{j,k} \Gamma_j \times \Gamma_k$, we obtain:

$$\left\|\widetilde{f}\right\|^2_{H^{1/2}(\Gamma)} = \|f_j\|^2_{L^2(\Gamma_j)} + 2\sum_k \int_{\Gamma_j}\int_{\Gamma_k} \frac{|f_j(x) - f_k(y)|^2}{|x-y|^2} \, \mathrm{d}\sigma(x)\mathrm{d}\sigma(y) \qquad (2.41)$$

Note that the second term of equation (2.41) is bounded by $\|f_j\|_{L^2(\Omega)}$ when $k \neq j-1, j, j+1$ as the distance from Γ_j to Γ_k is strictly positive, i.e:

$$\begin{aligned}\int_{\Gamma_j}\int_{\Gamma_k}\frac{|f_j(x)|^2}{|x-y|^2}\,\mathrm{d}\sigma(x)\mathrm{d}\sigma(y) &= \int_{\Gamma_j}|f_j(x)|^2\left[\int_{\Gamma_k}\frac{\mathrm{d}\sigma(y)}{|x-y|^2}\right]\,\mathrm{d}\sigma(x)\\ &\leq \|f_j\|^2_{L^2(\Omega)}\sup_{x\in\Gamma_j}\left[\int_{\Gamma_k}\frac{\mathrm{d}\sigma(y)}{|x-y|^2}\right]\\ &\leq K\|f_j\|^2_{L^2(\Omega)}\\ &\leq K\|f_j\|^2_{H_{00}^{1/2}(\Gamma_j)}\end{aligned} \tag{2.42}$$

If $k = j$, the second term is bounded since $f_j \in H_{00}^{1/2}(\Gamma_j)$:

$$\int_{\Gamma_j}\int_{\Gamma_k}\frac{|f_j(x)-f_j(y)|^2}{|x-y|^2}\,\mathrm{d}\sigma(\mathrm{x})\mathrm{d}\sigma(\mathrm{y}) \leq \|f_j\|^2_{H_{00}^{1/2}(\Gamma_j)}$$

The only case left to consider is when $k = j-1$ or $k = j+1$. As in [40, Theorem 1.5.2.3], it is important to note that $\Gamma_{j+1}, \Gamma_{j-1}$ are C^1 curves. Therefore, the functions:

$$\int_{\Gamma_{j+1}}\frac{\mathrm{d}\sigma(y)}{|x-y|^2}, \int_{\Gamma_{j-1}}\frac{\mathrm{d}\sigma(x)}{|x-y|^2}$$

are equivalent to $d(x,\Gamma_{j+1})^{-1}, d(y,\Gamma_{j-1})^{-1}$ respectively therefore:

$$\begin{aligned}&\int_{\Gamma_j}\int_{\Gamma_{j+1}}\frac{|f_j(x)|^2}{|x-y|^2}\,\mathrm{d}\sigma(x)\mathrm{d}\sigma(y) + \int_{\Gamma_j}\int_{\Gamma_{j-1}}\frac{|f_j(y)|^2}{|x-y|^2}\,\mathrm{d}\sigma(x)\mathrm{d}\sigma(y)\\ &\leq K'\left[\int_{\Gamma_j}\frac{|f_j(x)|^2}{d(x,\Gamma_{j+1})}\,\mathrm{d}\sigma(\mathrm{x}) + \int_{\Gamma_j}\frac{|f_j(y)|^2}{d(y,\Gamma_{j-1})}\,\mathrm{d}\sigma(\mathrm{y})\right]\\ &\leq K''\|f_j\|^2_{H_{00}^{1/2}(\Gamma_j)}\end{aligned} \tag{2.43}$$

Therefore, from Equations (2.41), (2.42), and (2.43), we deduce that:

$$\left\|\widetilde{f}\right\|_{H^{1/2}(\Gamma)} \leq C\|f_j\|_{H_{00}^{1/2}(\Gamma_j)}$$

□

By employing similar reasoning as in [40, Theorem 1.5.3.10] and a proof analogous to [10, Lemma 2.4], we can state the subsequent theorem:

Theorem 2.4.4. *Let Ω be a bounded open subset of $\mathbb{R}^2$ whose boundary is a curvilinear polygon of class at least C^1. Let $\boldsymbol{E}(\Omega) = \{\boldsymbol{u} \in \boldsymbol{H}^1(\Omega) :\ \Delta\boldsymbol{u} \in \boldsymbol{H}_0(\mathrm{div},\Omega)'\}$, then the mapping:*

$$\boldsymbol{u} \to 2[\boldsymbol{D}(\boldsymbol{u})\boldsymbol{n}]_{tg}|_{\Gamma_j} \quad ,$$

which is defined on $\mathcal{D}(\overline{\Omega})$ has a unique continuous extension as an operator from:

$$\boldsymbol{E}(\Omega) \to \left(\boldsymbol{H}_{00}^{1/2}(\Gamma_j)\right)'$$

Proof. Consider $\boldsymbol{v}$ belonging to $\boldsymbol{D}(\overline{\Omega})$ and $\boldsymbol{\varphi}$ as an element of $\boldsymbol{H}^1(\Omega)$ satisfying $\boldsymbol{\varphi} \cdot \boldsymbol{n} = 0$ on Γ. Remembering the relation $\Delta \boldsymbol{v} = 2\,\mathrm{div}\,\mathbf{D}(\boldsymbol{v}) - \nabla(\mathrm{div}(\boldsymbol{v}))$, we can then proceed with an integration by parts to yield:

$$-\langle \Delta \boldsymbol{v}, \boldsymbol{\varphi} \rangle_\Omega = 2\int_\Omega \mathbf{D}(v) : \nabla \boldsymbol{\varphi} dx - \int_\Gamma 2[\mathbf{D}(\mathbf{v})\mathbf{n}]_{tg} \cdot \boldsymbol{\varphi}_{tg}\, ds - \int_\Omega div(\boldsymbol{v}) div(\boldsymbol{\varphi}) dx.$$

Hence, for every $\boldsymbol{v}$ in $\boldsymbol{D}(\overline{\Omega})$ and for each $\boldsymbol{\varphi}$ within $\boldsymbol{V}(\Omega)$, it can be stated that:

$$-\langle \Delta \boldsymbol{v}, \boldsymbol{\varphi} \rangle_\Omega = 2\int_\Omega \mathbf{D}(\mathbf{v}) : \mathbf{D}(\varphi) dx - \sum_i \int_{\Gamma_i} 2[\mathbf{D}(\mathbf{v})\mathbf{n}]_{tg} \cdot \boldsymbol{\varphi}_{tg}\, ds. \tag{2.44}$$

Consider $\boldsymbol{f_j}$ as an arbitrary member of $\boldsymbol{H}_{00}^{1/2}(\Gamma_j)$. We proceed by defining:

$$\widetilde{\boldsymbol{f}} = \begin{cases} \boldsymbol{f_j}(\boldsymbol{x}) & \boldsymbol{x} \in \Gamma_j \\ 0 & \boldsymbol{x} \notin \Gamma_j \end{cases}.$$

Consequently, by referring to Theorem 2.4.3, we have $\widetilde{\boldsymbol{f}} \in \boldsymbol{H}^{1/2}(\Gamma)$. Now, similarly to [10, Lemma 2.4], we consider φ in $\boldsymbol{H}^1(\Omega)$ to be the solution of:

$$\begin{cases} div(\boldsymbol{\varphi}) = 0 & \Omega \\ \boldsymbol{\varphi} = \widetilde{\boldsymbol{f}}_{tg} & \Gamma \end{cases},$$

satisfying $\|\boldsymbol{\varphi}\|_{\boldsymbol{H}^1(\Omega)} \leq C\|\widetilde{\boldsymbol{f}}_{tg}\|_{\boldsymbol{H}^{1/2}(\Gamma)} \leq C\|\widetilde{\boldsymbol{f}}\|_{\boldsymbol{H}^{1/2}(\Gamma)}$. Thus, using Theorem 2.4.3, it can be deduced that:

$$\|\boldsymbol{\varphi}\|_{\boldsymbol{H}^1(\Omega)} \leq C\|\boldsymbol{f_j}\|_{\boldsymbol{H}_{00}^{1/2}(\Omega)}. \tag{2.45}$$

Now notice that:

$$\begin{aligned} \left|\int_{\Gamma_j} 2[\mathbf{D}(\mathbf{v})\mathbf{n}]_{tg} \cdot \boldsymbol{f_j}\, ds\right| &= \left|\sum_i \int_{\Gamma_i} 2[\mathbf{D}(\mathbf{v})\mathbf{n}]_{tg} \cdot \widetilde{\boldsymbol{f}}_{tg}\, ds\right| \\ &= \left|\int_\Gamma 2[\mathbf{D}(\mathbf{v})\mathbf{n}]_{tg} \cdot \boldsymbol{\varphi}\, ds\right| \\ &= \left|\langle \Delta \boldsymbol{v}, \boldsymbol{\varphi} \rangle_\Omega + 2\int_\Omega \mathbf{D}(\mathbf{v}) : \mathbf{D}(\varphi) dx\right| \\ &\leq \|\Delta \boldsymbol{v}\|_{(\boldsymbol{H}_0(div,\Omega))'} \|\boldsymbol{\varphi}\|_{\boldsymbol{H}_0(div,\Omega)} + 2\|\mathbf{D}(\boldsymbol{v})\|_{\boldsymbol{L}^2(\Omega)} \|\mathbf{D}(\boldsymbol{\varphi})\|_{\boldsymbol{L}^2(\Omega)} \end{aligned}$$

Hence:

$$\left|\langle 2[\mathbf{D}(\boldsymbol{v})\boldsymbol{n}]_{tg}, \boldsymbol{f_j}\rangle_{\Gamma_j}\right| \leq \left(\|\Delta \boldsymbol{v}\|^2_{[\boldsymbol{H}_0(\mathrm{div},\Omega)]'} + 2\|\mathbf{D}(\boldsymbol{v})\|^2_{L^2(\Omega)}\right)^{\frac{1}{2}} \times \left(\|\boldsymbol{\varphi}\|^2_{L^2(\Omega)} + 2\|\mathbf{D}(\varphi)\|^2_{L^2(\Omega)}\right)^{\frac{1}{2}}$$

Recalling that $\|\boldsymbol{v}\|_{\boldsymbol{E}^p(\Omega)} = \|\boldsymbol{v}\|_{W^{1,p}(\Omega)} + \|\Delta \boldsymbol{v}\|_{[H_0(div,\Omega)]'}$, it follows that from Korn's inequality that:

$$\left|\langle [\mathbf{D}(\boldsymbol{v})\boldsymbol{n}]_{tg}, \boldsymbol{f_j}\rangle_{\Gamma_j}\right| \leq C_p \|\boldsymbol{v}\|_{\boldsymbol{E}^p(\Omega)} \|\boldsymbol{\varphi}\|_{\boldsymbol{H}^1(\Omega)}.$$

Therefore, employing equation (2.45), we can infer that:

$$\|[\mathbf{D}(\boldsymbol{v})\boldsymbol{n}]_{tg}\|_{H_{00}^{1/2}(\Gamma_j)'} \leq C\|\boldsymbol{v}\|_{\boldsymbol{E}^p(\Omega)}.$$

Hence, the linear mapping $\Theta : \boldsymbol{v} \to [\mathbf{D}(\boldsymbol{v})\boldsymbol{n}]_{tg|\Gamma_j}$ defined on $\boldsymbol{D}(\overline{\Omega})$ is continuous for the norm of $\boldsymbol{E}(\Omega)$. Since $\boldsymbol{\mathcal{D}}(\overline{\Omega})$ is dense in $\boldsymbol{E}(\Omega), \Theta$ can be extended by continuity to a mapping still called $\Theta \in \mathcal{L}\left(\boldsymbol{E}(\Omega), \boldsymbol{H}_{00}^{1/2}(\Gamma_j)\right)$. □

We are now ready to prove our green identity

Proof of theorem 2.0.1. Notice that for every $\boldsymbol{u} \in \boldsymbol{D}(\overline{\Omega})$ and $\varphi \in \{\boldsymbol{u} \in \boldsymbol{H}^1(\Omega) : \mathrm{div}(\boldsymbol{u}) = 0\}$ we have the following Green's identity:

$$\langle \Delta \boldsymbol{u}, \boldsymbol{\varphi}\rangle_\Omega = \int_\Omega 2\boldsymbol{D}(\boldsymbol{u}) : \boldsymbol{D}(\boldsymbol{\varphi})\, dx - \sum_{j=1}^{2M} \langle 2[\boldsymbol{D}(\boldsymbol{u})\boldsymbol{n}]_{tg}, \gamma_j(\boldsymbol{\varphi})\rangle_{\Gamma_j} \tag{2.46}$$

Thus, assuming that $\gamma_j(\boldsymbol{u}) \in \prod_{j=1}^{2M} \boldsymbol{H}_{00}^{1/2}(\Gamma_j)$ and using the Korn inequality, we can see that all terms of (2.46) are continuous in $\boldsymbol{u}$ for the norm of $\boldsymbol{E}(\Omega)$. Therefore, the result follows from the density of $\boldsymbol{D}(\overline{\Omega})$ in $\boldsymbol{E}(\Omega)$. □

3 Numerical perspective for the direct problem

3.1 Direct problem and experimental setup

To solve the evolutionary Stokes equations with Navier-slip boundary conditions relevant to these problems, we chose to utilize radial divergence-free kernels. This decision was based on the fact that these methods are mesh-free, enabling us to work with more complex geometries in the future, and possess spectral convergence properties, as well as ease of implementation of boundary conditions such as Navier-slip. However, a drawback of these methods is that the resulting matrix can exhibit high condition numbers and the appearance of spurious eigenvalues. To address this issue, we employed the recently introduced divergence-free hybrid kernels, as described in the works [51] and [17]. These kernels, in their scalar version, are a linear combination of Gaussian and Polyharmonic splines. The Gaussian component contributes to exponential convergence, while the polyharmonic part controls the stability of the scheme. For further details, see [17].

Let $\Omega \subset \mathbb{R}^N$, $\boldsymbol{L}_i(\boldsymbol{u}, p) = -\mu\Delta u_i + \frac{\partial p}{\partial x_i}$ and consider the system:

$$\begin{cases} \frac{\partial u_i}{\partial t} + \boldsymbol{L}_i(\boldsymbol{u}, p) = f_i & \text{in } \Omega \times (0,T), \\ \operatorname{div}(\boldsymbol{u}) = 0 & \text{in } \Omega \times (0,T), \\ \boldsymbol{B}_i(\boldsymbol{u}, p) = g_i & \text{on } \partial\Omega, \\ \boldsymbol{u}(\cdot, 0) = \boldsymbol{u}_0(\cdot) & \text{in } \Omega, \end{cases} \qquad i \in \{1, ..., N\}$$

where $\boldsymbol{B} = (\boldsymbol{B}_1, ..., \boldsymbol{B}_N)$ is a given boundary operator. In order to solve the systems, we first define a matrix-valued kernel in the following form:

$$\boldsymbol{\Phi} = \begin{bmatrix} \boldsymbol{\Phi}_{Div} & 0 \\ 0 & \psi \end{bmatrix} : \mathbb{R}^N \to \mathbb{R}^{(N+1)\times(N+1)},$$

We then propose a solution using the method of lines in combination with the general interpolation theorem [65, Proposition 3.11]:

$$
\begin{aligned}
(\hat{\boldsymbol{u}}, \hat{p})(\boldsymbol{x}, t) = &\sum_{i=1}^{N} \sum_{j=1}^{N_b} \boldsymbol{B}_i^{\xi} \boldsymbol{\Phi}(\boldsymbol{x} - \boldsymbol{\xi_j}) \alpha_{[(i-1)N_b + j]}(t) \\
&+ \sum_{i=1}^{N} \sum_{j=1}^{N_{in}} \boldsymbol{L}_i^{\xi} \boldsymbol{\Phi}(\boldsymbol{x} - \boldsymbol{\xi_{N_{in}+j}}) \alpha_{[NN_b + (i-1)N_{in} + j]}(t),
\end{aligned}
\tag{3.1}
$$

The ansatz in equation (3.1) expresses $(\hat{\boldsymbol{u}}, \hat{p})(\boldsymbol{x}, t)$ as a linear combination of vector-valued functions from $\mathbb{R}^N$ to $\mathbb{R}^{N+1}$ defined by the application of the operators $\boldsymbol{B}_i$ and $\boldsymbol{L}_i$ to each row of the kernel $\boldsymbol{\Phi}(\cdot - \boldsymbol{\xi}_i)$, (i.e, $\boldsymbol{B}_i^{\xi}\boldsymbol{\Phi}$, $\boldsymbol{L}_i^{\xi}\boldsymbol{\Phi}$). Here, $\boldsymbol{\xi}_j$ are the center nodes located both inside and on the boundary of the domain Ω, and the vector $\boldsymbol{\alpha}(t)$ are the time-varying coefficients of the ansatz. The parameters N_b and N_{in} represent the total number of boundary and interior center nodes, respectively.

In 2D, the combined Div-free velocity-pressure kernel, denoted by $\boldsymbol{\Phi}$, is given by equation (3.2):

$$
\boldsymbol{\Phi}(\mathbf{x}) = \begin{pmatrix} \boldsymbol{\Phi}_{Div}(\mathbf{x}) & 0 \\ 0 & \mathrm{e}^{-c_2\, r} + \gamma_2\, r^{2m+1} \end{pmatrix}. \tag{3.2}
$$

where $r = \|\mathbf{x}\|$, γ_2 is a positive real number related to the hybrid kernel for the pressure, and $\boldsymbol{\Phi}_{Div}$ is the divergence-free hybrid kernel given by:

$$
\boldsymbol{\Phi}_{Div}(\boldsymbol{x}) = \{-\Delta I + \nabla\nabla^T\}(\psi_1(\boldsymbol{x}) + \gamma_1 \psi_2(\boldsymbol{x})).
$$

with $\psi_1(\boldsymbol{x}) = \exp(-c_1, r^2)$, $\psi_2(\boldsymbol{x}) = r^{2n+1}$, and γ_1 is a positive real number. By direct computation, we obtain the following expression for $\boldsymbol{\Phi}_{Div}(\boldsymbol{x})$:

$$
\begin{aligned}
\boldsymbol{\Phi}_{\mathrm{Div}}(\mathbf{x}) =& 4c_1 e^{-r^2 c_1} \begin{pmatrix} -c_1 x_2^2 + \frac{1}{2} & c_1 x_1 x_2 \\ c_1 x_1 x_2 & -c_1 x_1^2 + \frac{1}{2} \end{pmatrix} \\
&+ \gamma_1 r^{2n-3}(4n^2 - 1) \begin{pmatrix} \frac{-r^2}{(2n-1)} - x_2^2 & x_1 x_2 \\ x_1 x_2 & \frac{-r^2}{(2n-1)} - x_1^2 \end{pmatrix}.
\end{aligned}
$$

By substituting the ansatz (3.1) into the Stokes system, we can derive the following system of ordinary differential equations:

$$
\begin{aligned}
M_\phi \frac{\overline{\boldsymbol{\alpha}}(t)}{dt} + M_{L\phi} \overline{\boldsymbol{\alpha}}(t) &= \mathbf{f}\ , \\
M_{B_\phi} \overline{\boldsymbol{\alpha}}(t) &= \mathbf{g}\ ,
\end{aligned}
\tag{3.3}
$$

where $M_\phi, M_{L_\phi} \in \mathbb{R}^{2N_{in}\times(2N_b+2N_{in})}$ and $M_{B_\phi} \in \mathbb{R}^{2n_b\times(2n_b+2n_{in})}$. The solution to the system of ordinary differential-algebraic equations (odea) in (3.3) provides us with the time-varying coefficients of the ansatz, $\boldsymbol{\alpha}(t)$. The system is numerically solved using a technique known as backward differentiation formulas (BDF). According to numerical simulations reported in [17], all of the eigenvalues of the Gram matrix associated with this system are found in the negative half of the complex plane. Hence, the use of BDFs ensures the stability of the numerical method.

3.2 Numerical results for the direct problem

To demonstrate the effectiveness of the hybrid divergence-free kernel method, we present numerical results for the problem (1.2)–(1.3). The computational domain for the fluid is defined as $\Omega\backslash\mathcal{O} = ([0,8]\times[0,1])\backslash\mathcal{O}$, where the obstruction $\mathcal{O}$ is parameterized as follows:

$$\partial\mathcal{O} = \begin{cases} x(s) = \theta_1 + s & s \in [0,\theta_2], \\ y(s) = \frac{\theta_3}{2}\left(1.0 - cos(\frac{2\pi s}{\theta_2})\right) & s \in [0,\theta_2]. \end{cases} \tag{3.4}$$

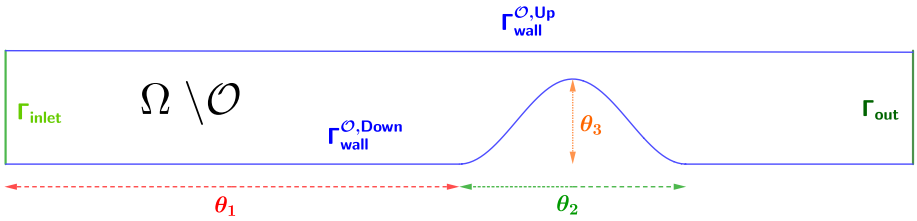

Figure 3.1: Parametric representation of the domain $\Omega\backslash\mathcal{O}$

The obstruction parameters used for this simulation are $\theta_1 = 4$, $\theta_2 = 1$, and $\theta_3 = 0.5$, which represent the position, size, and percentage depth of the obstruction, respectively. The computational domain for the wave is set to $S = [0,8]\times[1,5]$.

Since the couple problem (1.2)–(1.3) is indeed only in one direction, for simplicity, we decide to solve (1.2) with hybrid RBF and store the normal component of the stress tensor to later simulate the wave equation using the finite element method due to its simple geometry domain. We note that in all of our examples, the finite element method achieved a similar order of precision as the hybrid RBF technique.

For the numerical simulation (1.2) we use a mesh of 1119 Halton points, a BDF2 scheme to solve the odea system (3.3) with a time step of $\Delta t = \frac{1}{200}$ in the interval

$[0, 5]$, a fixed viscosity constant $\mu = 0.1$. It is important to note that for this simulation, we define $g_{in}(x,t) = g_{out}(x,t) = (cos(2\pi t + \pi) + 1)$.

For the numerical simulation of the wave equation (1.3) we use the element P1 with a mesh of 5963 points and a fixed propagation speed $c = 1$.

It should be noted that our choice of the RBF hybrid parameters, $c_1 = c_2 = 0.5$, $\gamma_1 = 10^{-4}$, and $\gamma_2 = 10^{-4}$, resulted in a reasonable condition number of 10^{14} for the associated ODE matrix system (3.3) and a high degree of accuracy, with a difference of 10^{-4} for the velocity field and 10^{-3} for the pressure field when compared to an analytical solution.

Figures 3.2 and 3.3 are snapshots of the simulations obtained from the velocity field, the pressure, and the acoustic wave:

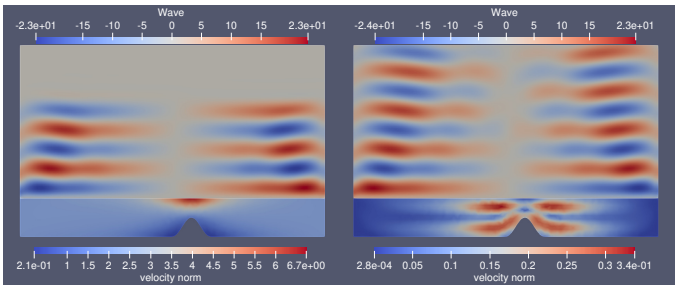

(a) **(b)**

Figure 3.2: Norm of the velocity and the wave at $t = 2.5$ (a), $t = 5$ (b)

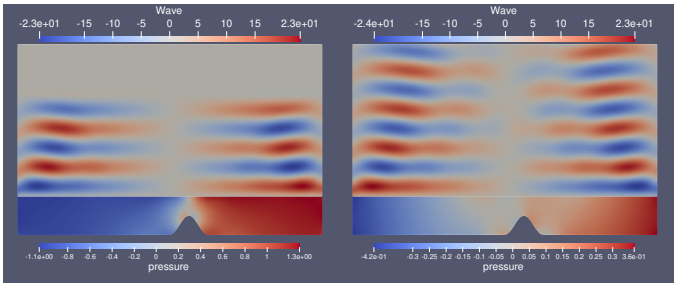

(a) **(b)**

Figure 3.3: Norm of the pressure and the wave at $t = 2.5$ (a), $t = 5$ (b)

4 An optimization process for the inverse problem

As a first step towards understanding the problem, we consider a specific class of obstacles that allow us to determine the location, depth, and size of the obstruction. To do this, we use the measurements of the acoustic wave and fluid flow.

Let $\mathcal{O} = \mathcal{O}(\theta_1, \theta_2, \theta_3)$ be the obstruction we want to identify. The measurements of the sound waves generated by the Cauchy tensor resulting from the Stokes flow is represented by $w_m(.) = w\left(.; \mathcal{O}(\theta_1, \theta_2, \theta_3^*)\right)$, as defined in the systems (1.2) –(1.3). Our goal is to reconstruct the obstruction $\mathcal{O}$ by using measurements of the acoustic wave w in the observable set $S_m = [k_1, k_2] \times H \subset \partial S$ and measurements of the tangential velocity in Γ_m, a relative open set of the fluid domain border, as shown in Figure 4.1.

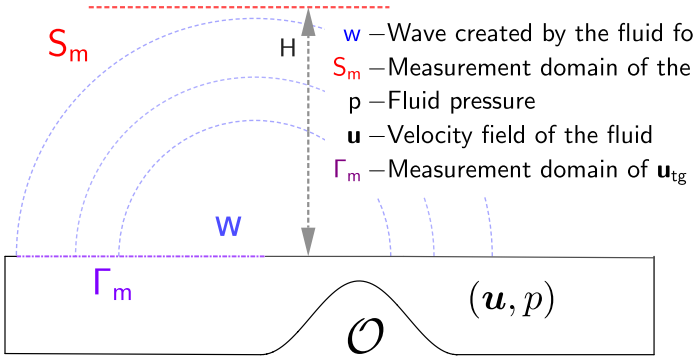

Figure 4.1: Illustration of measurement domains for the numerical inverse problems.

The obstruction in our problem is defined by a parameterized boundary, given by:

$$\partial\mathcal{O} = \begin{cases} x(s) = \theta_1 + s & s \in [0, \theta_2], \\ y(s) = \frac{\theta_3}{2}\left(1.0 - cos(\frac{2\pi s}{\theta_2})\right) & s \in [0, \theta_2]. \end{cases}$$

This parameterization allows us to understand the identification problem as one of recovering the parameters $\theta_1, \theta_2, \theta_3$ that define the obstruction $\mathcal{O}$. Furthermore, as the obstruction does not affect the domain S of the wave equation, we can decompose the inverse problem into two separate inverse problems.

4.1 Inverse problem for the wave equation

Recalling the assumption that the obstruction does not intersect with the upper wall boundary, represented by Γ^{up}_{wall}. From equation (1.3), we can see that the measurements obtained at the set S_m are dependent on the unknown values of the boundary term defined on $\Gamma^{up}_{wall} \times (0, T)$. In order to estimate these unknown boundary values, we propose to minimize the following functional:

$$J_1(f) = \int_{S_m \times (0,T)} \|w(\cdot; f) - w_m\|_2^2 \, dS \, dt, \tag{4.1}$$

where $\|.\|_2$ is the Euclidean norm and w_m are the wave measurements (see Figure 1.2) and $w(.; f) \in C([0, T], H^1(S))$ is the solution to:

$$\begin{cases} w_{tt} - c^2\Delta w = 0 & \text{in } S \times (0, T), \\ w = f & \text{on } ([0, L]\times\{D\}) \times (0, T) = \Gamma^{up}_{wall} \times (0, T), \\ \frac{\partial w}{\partial t} + c\frac{\partial w}{\partial n} = 0 & \text{on } (\partial S \setminus ([0, L]\times\{D\})) \times (0, T), \\ w_t(\boldsymbol{x}, 0) = 0 & \text{in } S, \\ w(\boldsymbol{x}, 0) = 0 & \text{in } S. \end{cases}$$

Our goal in minimizing the functional given by equation (4.1) is to obtain an estimation of the unknown boundary values on $\Gamma^{up}_{\text{wall}} \times (0, T)$. This functional quantifies the difference between the solution of the wave equation with the unknown boundary values (represented by f) and the measured wave values (w_m). By minimizing this difference, we can obtain an estimate of the unknown boundary values and, consequently, reconstruct the Cauchy tensor.

It is important to note that the wave equation has a finite propagation speed, which means that we can only recover the unknown boundary datum within the time interval $(0, T - t_c)$, where t_c represents the travel time of the wave between

the boundary datum site and the measurement site. In our specific case, given the simplicity of the geometry, we can characterize the constant t_c using the following formula:

$$t_c = \frac{\sup_{x \in \Gamma_{wall}^{up}} d(x, S_m)}{c} \ , \tag{4.2}$$

where $d(\boldsymbol{x}, S_m) := inf\{d \in \mathbb{R}^+ : \ d = \|\boldsymbol{x} - \boldsymbol{y}\|_2, y \in \Gamma_{wall}^{up}\}$ and c is the propagation speed.

In summary, the first inverse problem corresponds to:

$$\text{Find } \hat{f} \in F_{ad} \text{ such that: } J_1(\hat{f}) = \min_{f \in F_{ad}} J_1(f) \ , \tag{4.3}$$

where $F_{ad} = \{L^2\left(\Gamma_{wall}^{up} \times (0,T)\right) : \ f = 0 \ \text{ on } \ (\Gamma_{wall}^{up} \times (T - T_c, T))\}$ is the admissible space of the boundary data.

4.2 Obstacle inverse problem

Using the solution $\hat{f}$ of the first inverse problem (4.3), we can now estimate the unknown parameters of the obstruction $\mathcal{O}$. Recalling that the functional (4.1) is a quadratic form and therefore convex, it is not unreasonable to assume that $\hat{f}$ is an estimation of the normal component of the Cauchy tensor $\sigma(\boldsymbol{u}, p)\boldsymbol{n} \cdot \boldsymbol{n}$ on $\Gamma_{wall}^{up} \times (0,T)$. Additionally, we also have measurements of the tangential component of the fluid velocity, denoted as $\boldsymbol{v_{m,\tau}}$, in a set $\Gamma_m \times (0,T) \subset \Gamma_{wall}^{up} \times (0,T)$. Thus, we aim to minimize the following functional:

$$\begin{aligned} J_2(\theta) = &\int_{\Gamma_{wall}^{up} \times (0, T - t_c)} \left\| \left(\sigma\left(\boldsymbol{u}(.;\boldsymbol{\theta}), p(.;\boldsymbol{\theta})\right)\boldsymbol{n}\right) \cdot \boldsymbol{n} - \hat{f} \right\|_2^2 \, dS \, dt \\ &+ \int_{\Gamma_m \times (0,T)} \|\boldsymbol{v_{m,\tau}} - \boldsymbol{u}(.;\boldsymbol{\theta}) \cdot \boldsymbol{\tau}\|_2^2 \, dS \, dt \ , \end{aligned} \tag{4.4}$$

where $\theta \in \Theta \subset \mathbb{R}^3$ is the set of possible parameters that represent an obstruction, $\Omega_{\mathcal{O}(\theta)} = \Omega \backslash \mathcal{O}(\theta)$ and $\boldsymbol{u}(.;\Omega_{\mathcal{O}(\theta)}), p(.;\Omega_{\mathcal{O}(\theta)}) \in H^1(\Omega_{\mathcal{O}(\theta)}) \times L^2(\Omega_{\mathcal{O}(\theta)})$ are solutions

to:

$$\begin{cases} \boldsymbol{u}_t - \operatorname{div}(\sigma(u,p)) = 0 & \text{in } \Omega\backslash\mathcal{O}(\theta)\times(0,T), \\ \operatorname{div}(\boldsymbol{u}) = 0 & \text{in } \Omega\backslash\mathcal{O}(\theta)\times(0,T), \\ \boldsymbol{u} = \boldsymbol{g}_{in} & \text{on } \Gamma_{inlet}\times(0,T), \\ \boldsymbol{u} = \boldsymbol{g}_{out} & \text{on } \Gamma_{out}\times(0,T), \\ \boldsymbol{u}\cdot\boldsymbol{n} = 0,\ (\sigma(\boldsymbol{u},p)\boldsymbol{n})_{tg} = 0 & \text{on } \Gamma_{wall}^{\mathcal{O}(\theta)}\times(0,T), \\ \boldsymbol{u}(.,0) = \boldsymbol{u}_0 & \text{in } \Omega\backslash\mathcal{O}(\theta)\ . \end{cases}$$

It is important to note that the use of tangential velocity in functional (4.4) is necessary due to Theorem 2.3.4. This may seem contradictory to our initial goal, as the wave equation does not convey information about tangential velocity. However, as we will show in the following section, reasonable results can still be obtained without it (see experiment 4 in Table 4.1).

4.3 Numerical results

The optimization task outlined in the preceding section requires solving equations (1.2)-(1.3). This process is detailed in subsections (3.1)-(3.2). Importantly, for both the Stokes equation and the acoustic wave propagation equation, the same numerical time step is employed, specifically $\Delta t = 1/500$. In an effort to reduce computational cost, we define $\Omega = [0,8]\times[0,1]$, $S = [0,8]\times[1,3]$, and the terminal time $T = 1$. We also set the wave propagation speed as $c = \sqrt{30}$. To further align the simulated flow with that of blood, we assign the fluid viscosity as $\mu = 1/500$.

In order to investigate the robustness of the optimization procedure we decide to perform 8 numerical experiments, with different obstructions geometries and different observable domains of the wave S_m and of the tangential component of the velocity at the boundary Γ_m, see tables 4.1-4.3 for a summary.

For the first 6 numerical experiments we generate synthetic data using obstructions $\mathcal{O}$ defined by the parameters $(\theta_1,\theta_2,\theta_3)$ (see equation (3.4) and Figure 3.1) and for experiments 7-8 we generated the data using a different class of obstruction, defined by a cubic spline (see figure 4.4). In order to avoid the inverse crime we add a random error relative to the method order, given by a normal distribution of variance $\sigma = 10^{-5}$ and mean $\mu = 0$.

To compute an approximation of the normal component of the Cauchy tensor on the upper wall of the fluid domain, we minimize the functional described in equation (4.1). Since the functional J_1 is convex, we employ the gradient method

as the optimization technique.

The results of reconstructing the boundary data using the gradient descent method are shown in Figure 4.2. It is worth noting that our reconstruction does not provide a complete representation of the boundary data. This limitation arises from the time delay of the wave in reaching the measurement site, as explained earlier.

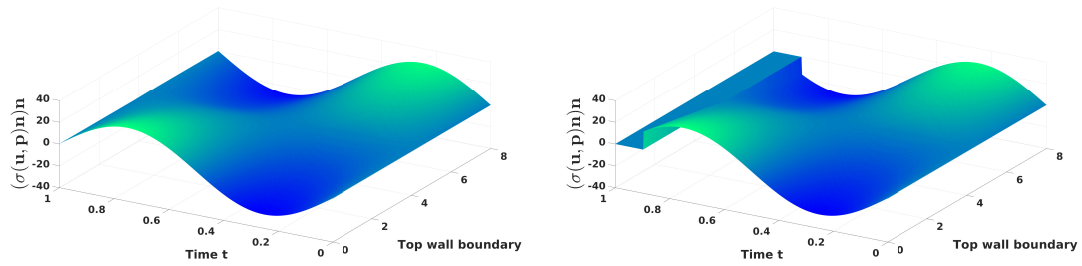

(a) **(b)**

Figure 4.2: a) Original wave boundary datum, b) Reconstructed boundary datum.

To determine the geometry of the obstruction, we utilized a Markov Chain Monte Carlo (MCMC) method to minimize the functional (4.4). This choice was motivated by several advantages that MCMC offers over other methods, such as gradient descent. The functional (4.4) has an unknown nature and may exhibit a non-convex shape, making it suitable for MCMC methods. Additionally, MCMC methods excel in exploring limited parameter spaces and can be easily parallelized, leveraging multiple CPU cores efficiently. Furthermore, MCMC methods provide an uncertainty range for the estimated parameters, which is valuable in practical applications. Considering these benefits and the lack of prior studies using MCMC in this context, we deemed it the most suitable method for our obstruction reconstruction problem. For all numerical experiments, we initialized the MCMC algorithm with $\theta_1 = 3, \theta_2 = 0.6, \theta_3 = 0.1$ as the starting point, as depicted in Figure 4.3. While gradient descent methods have shown success in articles such as [8] and [68], we believe that MCMC provides the optimal solution for our specific problem.

In our MCMC method, we employed the DRAM (Dynamically Adaptive Metropolis) algorithm. This algorithm dynamically adapts the proposal distribution during the simulation, allowing for efficient exploration of the parameter space. The

DRAM method has been demonstrated to converge faster and achieve higher acceptance rates compared to traditional MCMC methods. This, in turn, leads to more accurate results and a better estimation of the uncertainty range for the estimated parameters. The utilization of the DRAM method in this study enhances the robustness of the results and provides a more precise depiction of the obstruction's geometry. For a deeper understanding of these methods, interested readers can refer to [34].

The results of the Markov Chain Monte Carlo (MCMC) algorithm are summarized in tables 4.1 to 4.3. The data suggests that the majority of experiments produce satisfactory outcomes, with the initial parameters remaining within the mean's standard deviation. It is noteworthy that including tangential velocity information reduces the standard deviation of the estimated parameters, as shown in Experiment 4.

The probability density functions of the parameters $\theta_1, \theta_2, \theta_3$ for each experiment are shown in Figures 4.5-4.7. The majority of distributions are Gaussian in shape, centered around the original parameters, with the exception of θ_2 (obstacle size). When the tangential velocity measurement site is above or on the right side of the obstacle, the standard deviation for θ_1 (obstacle position) and θ_3 (obstruction blockage percentage) decreases, as the obstacle information is transmitted in the flow direction.

Regarding the obstacle size θ_2, most distributions are uniform, but the best results are obtained when the tangential velocity is available, as demonstrated in experiments 2,5, and 6. This highlights the importance of tangential velocity information in determining the correct size of the obstacle.

A comparison of the original and reconstructed domains for each of the eight numerical experiments is shown in Figure 4.8(a-h). The best results are obtained with the most complete information about the tangential velocity vector, as seen in Figure 4.8(b). In all cases, acceptable values for the depth and size of the obstruction are obtained, which are the most critical parameters in determining the danger level of a stenosis.

Notice also that figure 4.8(g-h) shows that even if the obstruction is outside the class of obstruction defined by $(\theta_1, \theta_2, \theta_3)$, we can still obtain some information with our low-parameter model. The approximation error in this scenario is calculated using the L^2 norm.

It is important to note that the location of the wave measurement domain has no significant impact on parameter estimation. This is because in each case, the fluid tensor $\sigma(\boldsymbol{u}, p)\boldsymbol{n}$ on the upper wall of the fluid domain is recovered, with the

only variation being the length of the time interval for the tensor estimation. The details of this estimation can be found in Subsection 4.1.

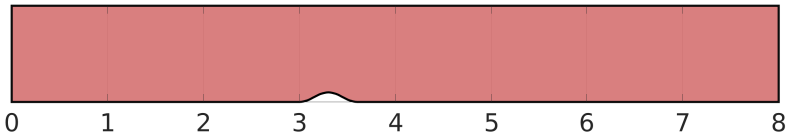

Figure 4.3: Initial guess shape for the MCMC method

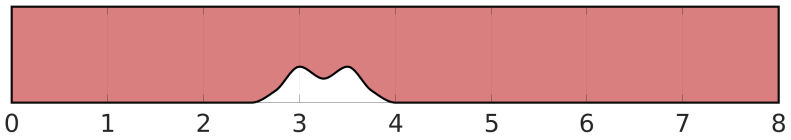

Figure 4.4: Original domain for experiments 7-8

Table 4.1: Experiment 1-4 parameter summary and numerical result.

	Experiment 1		Experiment 2		Experiment 3		Experiment 4	
S_m	$[0,3]\times\{3\}$		$[0,8]\times\{3\}$		$[5,8]\times\{3\}$		$[0,8]\times\{3\}$	
Γ_m	$[0,2]\times\{1\}$		$[0,8]\times\{1\}$		$[6,8]\times\{1\}$		$\emptyset$	
Original	Mean	S.D	Mean	S.D	Mean	S.D	Mean	S.D
$\theta_1 = 4.0$	3.8929	0.4871	3.9652	0.3207	3.8983	0.4698	3.9191	0.4722
$\theta_2 = 1.0$	1.0854	0.2653	1.0879	0.2567	1.0667	0.2834	1.0599	0.2731
$\theta_3 = 0.5$	0.4788	0.0636	0.4841	0.0593	0.4961	0.0669	0.5009	0.0639
$\|\boldsymbol{\theta} - \boldsymbol{\theta}^*\|_2$	0.1386		0.0959		0.1217		0.1007	

Table 4.2: Experiment 5-6 parameter summary and numerical result.

$S_m = [0,8] \times \{3\}$					
$\Gamma_m = [0,8] \times \{1\}$					
Experiment 5			Experiment 6		
Original	Mean	S.D	Original	Mean	S.D
$\theta_1 = 2.5$	2.5692	0.2872	$\theta_1 = 5.5$	5.3433	0.3564
$\theta_2 = 1.0$	1.0955	0.2623	$\theta_2 = 1.0$	1.0433	0.2871
$\theta_3 = 0.5$	0.4566	0.0667	$\theta_3 = 0.5$	0.4353	0.0894
$\|\boldsymbol{\theta} - \boldsymbol{\theta}^*\|_2 = 0.1257$			$\|\boldsymbol{\theta} - \boldsymbol{\theta}^*\|_2 = 0.1749$		

Table 4.3: Experiment 7-8 parameter summary and numerical result.

Experiment 7			Experiment 8		
$S_m = [0,8] \times \{3\}$ $\Gamma_m = [0,8] \times \{1\}$			$S_m = [0,8] \times \{3\}$ $\Gamma_m = \emptyset$		
Parameter	Mean	S.D	Parameter	Mean	S.D
θ_1	2.7139	0.4047	θ_1	2.9135	0.6575
θ_2	1.3822	0.5430	θ_2	1.5646	0.5698
θ_3	0.3868	0.0799	θ_3	0.3629	0.0886
$\|f - f(\theta^*)\|_{L_2} = 0.1251$			$\|f - f(\theta^*)\|_{L^2} = 0.2958$		

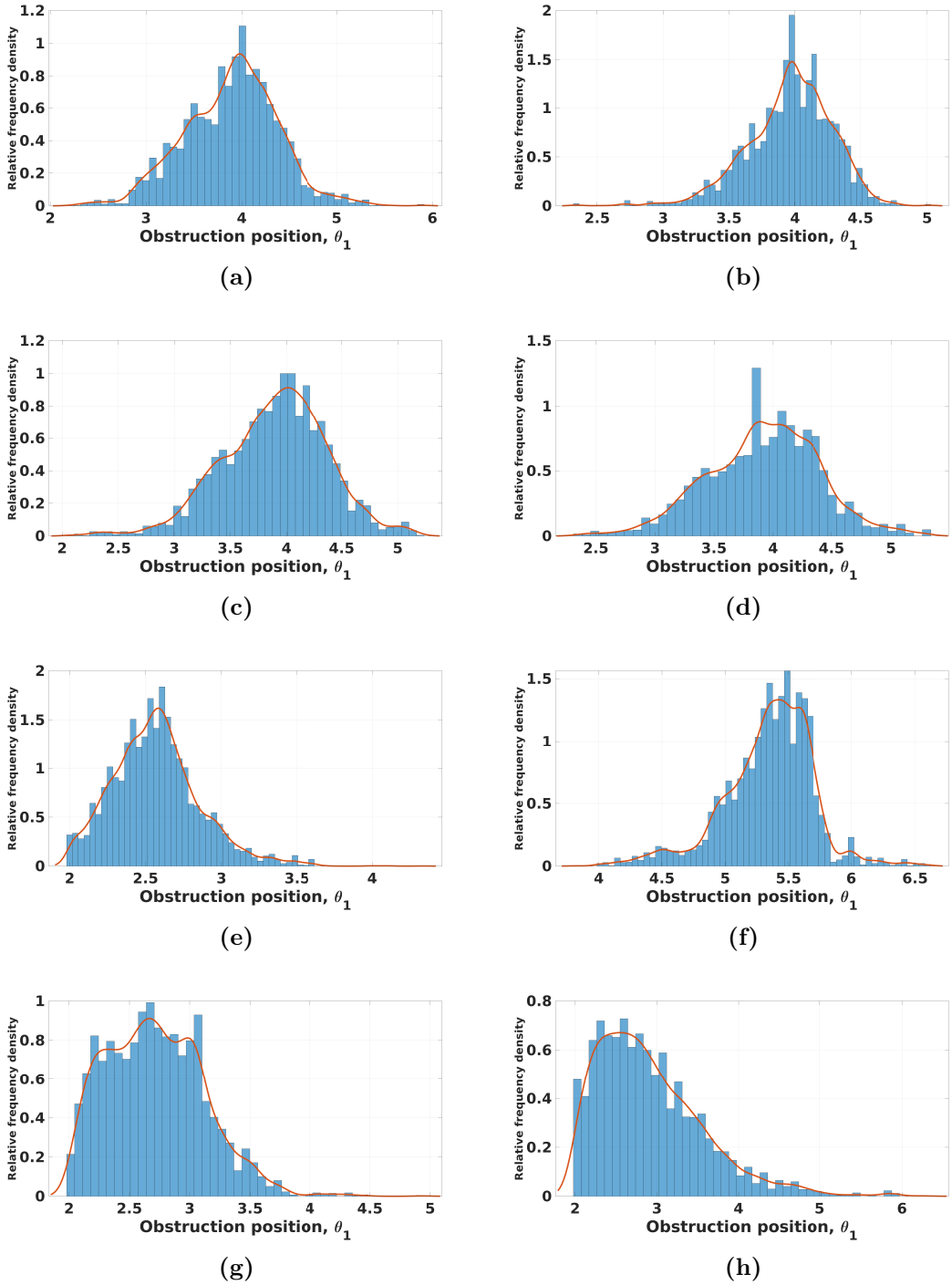

Figure 4.5: Probability density function estimate of θ_1 (Obstruction position) of experiments 1-8 (a-h)

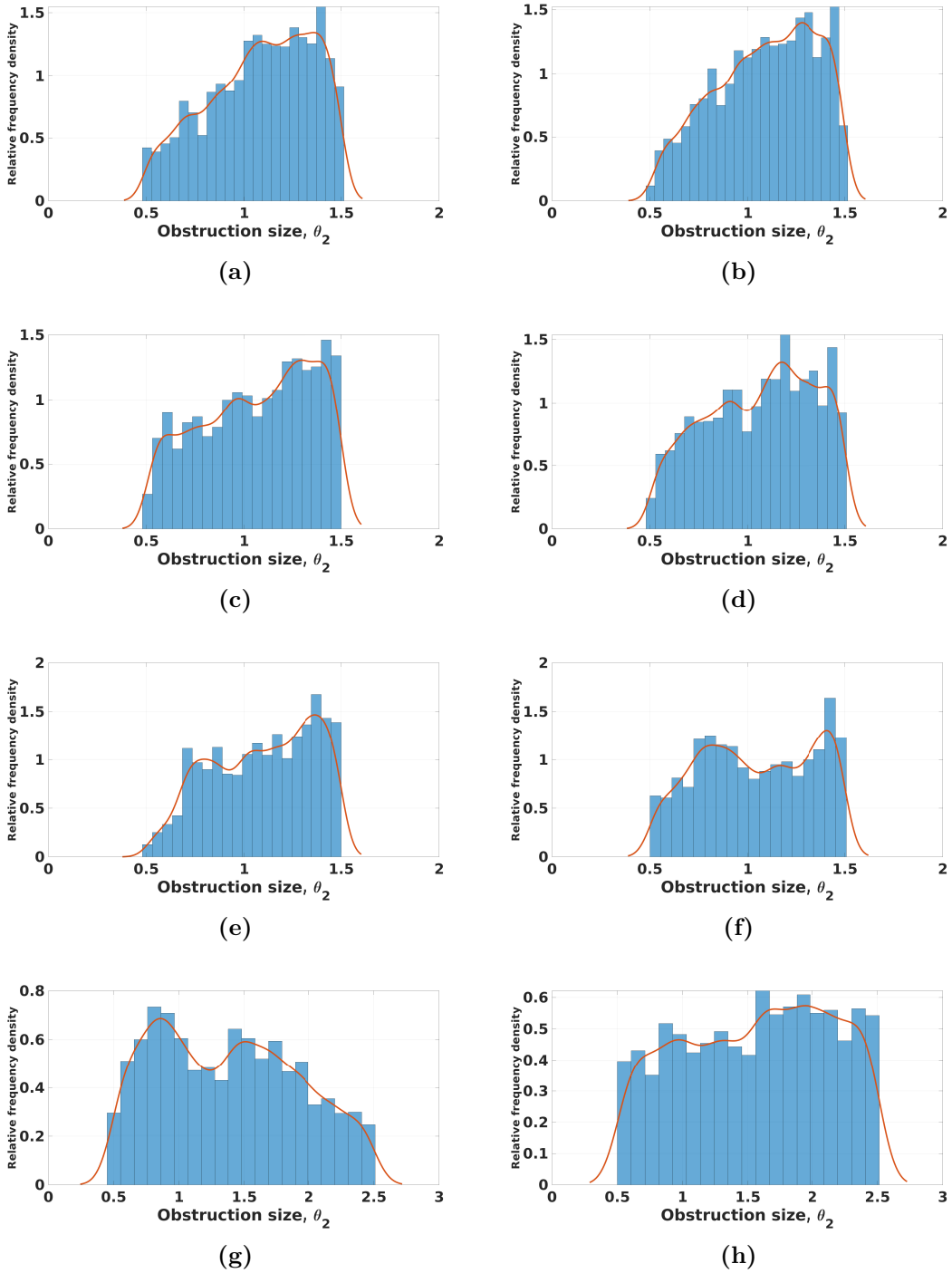

Figure 4.6: Probability density function estimate of θ_2 (Obstruction size) of experiments 1-8 (a-h)

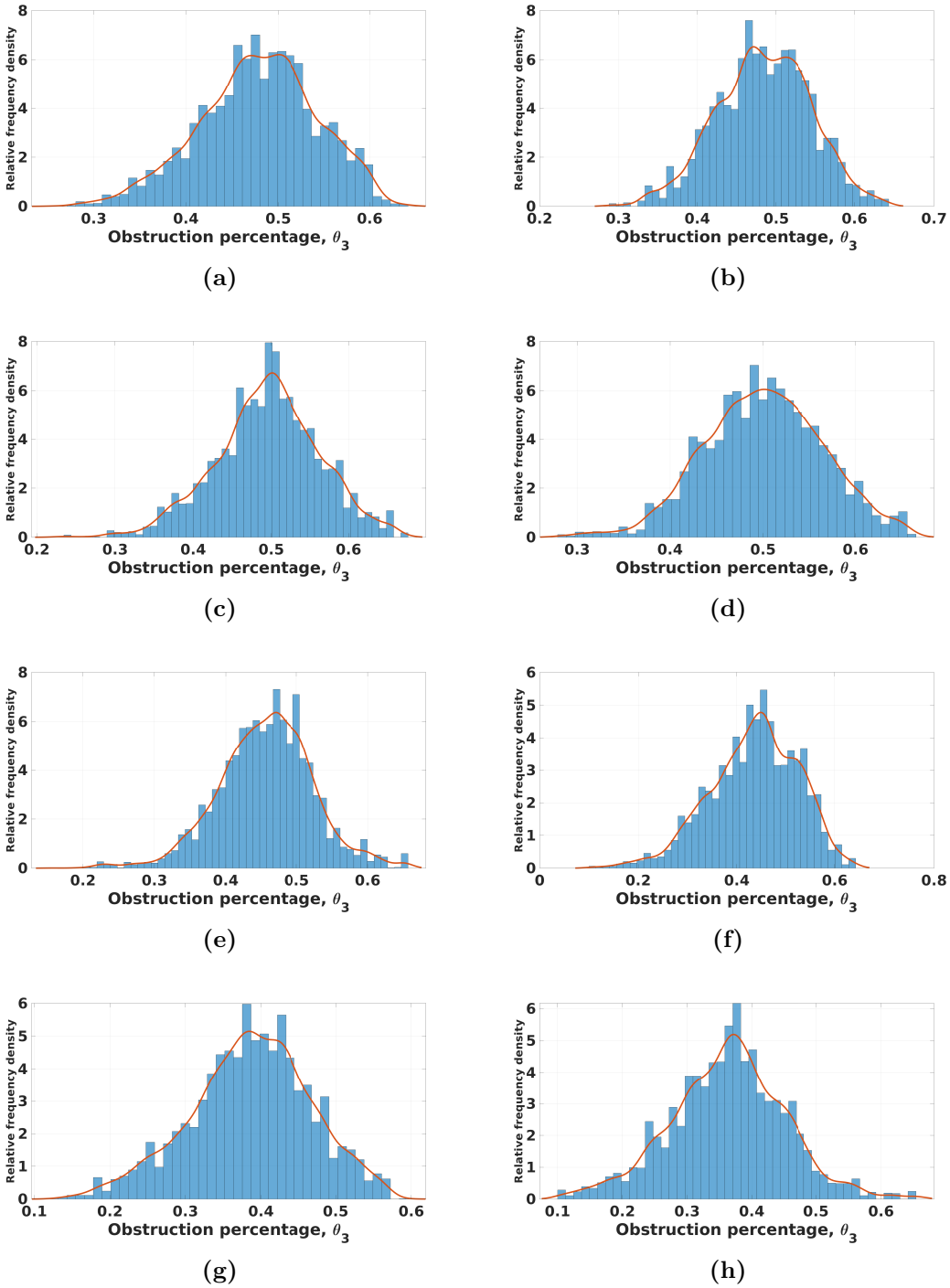

Figure 4.7: Probability density function estimate of θ_3 (Obstruction percentage) of experiments 1-8 (a-h)

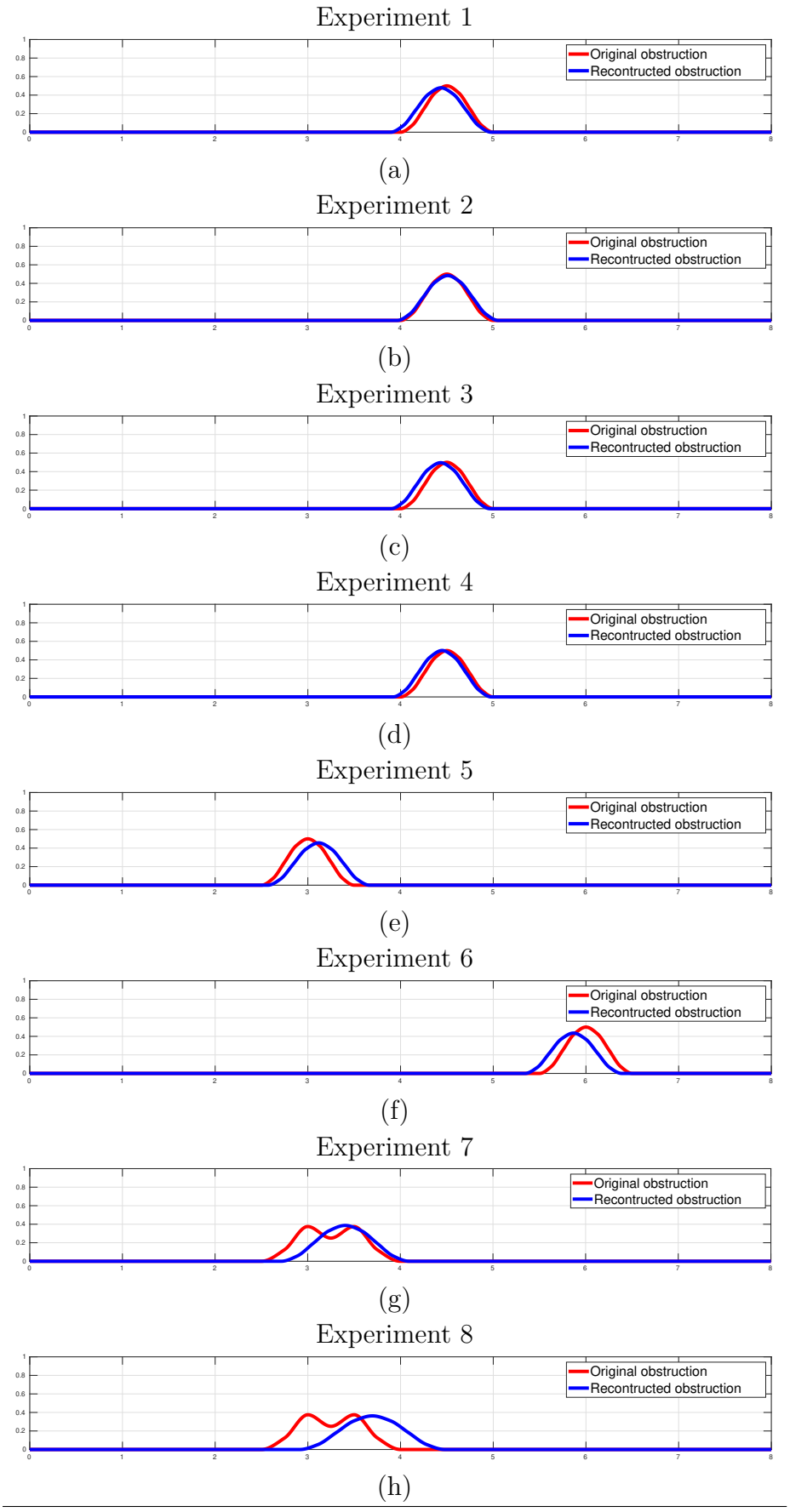

Figure 4.8: Original domain shape vs. reconstructed shape of experiments 1-8 (a-h)

5 Continuity with respect to the domain

5.1 Introduction

In this chapter, our focus is on exploring the continuity of solutions to the Stokes problem subject to domain variations. To this end, we consider a sequence of domains $\{\Omega_k\}_{k=1}^{\infty} \subset \mathbb{R}^d$, converging diffeomorphically to a domain $\Omega \subset \mathbb{R}^d$. Thus we shall analyze a sequence of solutions $(\boldsymbol{u}_k, p_k) \in L^2(0,T;\boldsymbol{V}(\Omega_k)) \times L^2_0(0,T;L^2(\Omega_k))$ corresponding to the Stokes problem given by:

$$\begin{cases} \boldsymbol{u}_t - \operatorname{div}(\sigma(\boldsymbol{u},p)) = \boldsymbol{f}_k & \Omega_k \times (0,T), \\ \operatorname{div}(\boldsymbol{u}) = 0 & \Omega_k \times (0,T), \\ \boldsymbol{u}\cdot\boldsymbol{n} = 0 & \Gamma_N^k \times (0,T), \\ [2D(\boldsymbol{u})\boldsymbol{n}]_{t_g} = \boldsymbol{h_k} & \Gamma_N^k \times (0,T), \\ \boldsymbol{u} = 0 & \Gamma_D \times (0,T), \\ \boldsymbol{u}(0,x) = 0 & \Omega_k. \end{cases} \tag{5.1}$$

From this point onward, the notation $\boldsymbol{n}$ will be used to represent the normal unit vector of the corresponding domain. The term "converge diffeomorphically" is defined as follows:

Definition 5.1.1. A sequence of open subsets $\{\Omega_k\}_{k=1}^{\infty}$ in $\mathbb{R}^d$ is said to *converge diffeomorphically* to a set $\Omega \subset \mathbb{R}^d$ if and only if there exists a sequence of diffeomorphisms $\{\psi_k\}_{k=1}^{\infty}$, with $\psi_k, \psi_k^{-1} \in \boldsymbol{W}^{1,\infty}(\mathbb{R}^d,\mathbb{R}^d)$, such that $\psi_k(\overline{\Omega}) = \overline{\Omega}_k$ and:

$$\lim_{k\to\infty} \|\psi_k - \mathrm{Id}\|_{1,\infty} = \lim_{k\to\infty} \|\psi_k^{-1} - \mathrm{Id}\|_{1,\infty} = 0,$$

where the norm $\|f\|_{1,\infty}$ is defined by

$$\|f\|_{1,\infty} = \sup_{x\in\mathbb{R}^d} |f(x)|_{\mathbb{R}^d} + \sup_{x\in\mathbb{R}^d} |\nabla f(x)|_{\mathbb{R}^{d\times d}},$$

and Id denotes the identity map.

For the sake of clarity let us revisit the spaces defined in Chapter 2 :

$$\begin{aligned}
\boldsymbol{V}(\Omega) &= \{\boldsymbol{u} \in \boldsymbol{H}^1(\Omega) :\ \mathrm{div}(\boldsymbol{u}) = 0, \boldsymbol{u}|_{\Gamma_D} = 0, \boldsymbol{u} \cdot \boldsymbol{n} = 0 \text{ on } \partial\Omega\},\\
\boldsymbol{H}_{0,\Gamma_D}(\Omega) &= \{\boldsymbol{u} \in \boldsymbol{H}^1(\Omega) :\ \boldsymbol{u}|_{\Gamma_D} = 0\},\\
L^2_0(\Omega) &= \{p \in L^2(\Omega) :\ \int_\Omega p\, dx = 0\},\\
\boldsymbol{H}(\Omega) &= \{\boldsymbol{u} \in \boldsymbol{L}^2(\Omega)\ :\ \mathrm{div}(\boldsymbol{u}) = 0\},
\end{aligned}$$

where $\boldsymbol{V}(\Omega), \boldsymbol{H}_{0,\Gamma_D}(\Omega)$ are equipped with the $\boldsymbol{H}^1(\Omega)$ norm, and $L^2_0(\Omega)$ and $\boldsymbol{H}(\Omega)$ are equipped with the standard $L^2(\Omega)$ norm.

Remark 5.1.2. We wish to recall that the Poincaré inequality still holds when only a part of the boundary is equal to zero, (refer to [5, Theorem 5.3.4] for more details). Thus the semi-norm of $\boldsymbol{H}^1_0(\Omega)$ is a norm in $\boldsymbol{V}(\Omega), \boldsymbol{H}_{0,\Gamma_D}(\Omega)$.

In the context of non-stationary scenarios, we adopt the following notation for simplicity. Given a Banach space X, we represent $L^\alpha(X) = L^\alpha(0,T;X)$ as the space of all Bochner measurable functions $u : [0,T] \to X$ that possess a finite corresponding norm:

$$\|u\|_{L^\alpha(X)} = \left(\int_0^T \|u(t)\|_X^\alpha dt)\right)^{1/\alpha}.$$

This becomes a Hilbert space if X is a Hilbert space and $\alpha = 2$. Similarly, we define $C^\alpha(X) = C(0,T;X)$ as the space of $\alpha-$continuous functions $u : [0,T] \to X$, equipped with the corresponding supremum norm. It is noteworthy, as given by Lemma 11.45 in [24], that for a Banach space Y and a continuous linear operator $A : X \to Y$, the following holds true:

$$A\int_0^T u(t)dt = \int_0^T (Au)(t)dt\,.$$

For additional simplification in our notation, when given a Banach space X, we use the following conventions:

- $x_n \to x$ if $\{x_n\} \in X$ converges to $x \in X$ in the strong topology, i.e $\|x_n - x\|_X \to 0$,
- $x_n \rightharpoonup x$ if $x_n \in X$ converges to $x \in X$ in the weak topology, i.e $\lim_{n\to\infty} \langle y, x_n\rangle_{X',X} = \langle x, y\rangle_{X',X} \quad \forall y \in X'$,
- $x_n \overset{*}{\rightharpoonup} x$ if $x_n \in X'$ converges to $x \in X'$ in the weak-start topology, i.e $\lim_{n\to\infty} \langle x_n, y\rangle_{X',X} = \langle x, y\rangle_{X',X} \quad \forall y \in X$.

Now we present the main result of this Chapter which is encapsulated in the following theorem:

Theorem 5.1.3. *Let $(\boldsymbol{u}_k, p_k) \in L^2(\boldsymbol{V}(\Omega_k)) \times L^2_0(L^2(\Omega_k))$ be a sequence the solution of the Stokes 5.1 problem and define $\boldsymbol{w}_k = \boldsymbol{u}_k \circ \psi_k$, $q_k = p_k \circ \psi_k$ Suppose following assumption hold:*

1. $\psi_k(\Gamma_N^k) = \Gamma_N$,
2. $\boldsymbol{f_k} \in L^2\left(\boldsymbol{L}^2(\Omega_k)\right)$ *such that* $\boldsymbol{f}_k \circ \psi_k \to \boldsymbol{f} \in L^2\left(\boldsymbol{L}^2(\Omega)\right)$,
3. $\boldsymbol{h_k} \in L^2\left(\boldsymbol{L}^2(\Gamma_N^k)\right)$ *such that* $\boldsymbol{h}_k \circ \psi_k \to \boldsymbol{h} \in L^2\left(\boldsymbol{L}^2(\Gamma_N)\right)$.

Then $\boldsymbol{w}_k$ converge strongly to $\boldsymbol{u}_\Omega$ in $L^2(\boldsymbol{V}(\Omega))$ solution of:

$$\begin{cases} \boldsymbol{u}_t - \operatorname{div}(\sigma(\boldsymbol{u}, p)) = \boldsymbol{f} & \Omega \times (0,T), \\ \operatorname{div}(\boldsymbol{u}) = 0 & \Omega \times (0,T), \\ \boldsymbol{u} \cdot \boldsymbol{n} = 0 & \Gamma_N \times (0,T), \\ [2D(\boldsymbol{u})\boldsymbol{n}]_{t_g} = \boldsymbol{h} & \Gamma_N \times (0,T), \\ \boldsymbol{u} = 0 & \Gamma_D \times (0,T), \\ \boldsymbol{u}(0,x) = 0 & \Omega_k. \end{cases}$$

We're also going to establish a convergence of a lesser degree for the pressure, as discussed in Theorem 5.4.2.

Remark 5.1.4. We emphasize that our primary problem of interest in this work is the convergence of $(\boldsymbol{u}_k, p_k) \in L^2(\boldsymbol{V}(\Omega_k)) \times L^2_0(L^2(\Omega_k))$ corresponding to the Stokes problem given by (5.2):

$$\begin{cases} \boldsymbol{u}_t - \operatorname{div}(\sigma(\boldsymbol{u}, p)) = \boldsymbol{f}_k & \Omega_k \times (0,T), \\ \operatorname{div}(\boldsymbol{u}) = 0 & \Omega_k \times (0,T), \\ \boldsymbol{u} \cdot \boldsymbol{n} = 0 & \Gamma_N^k \times (0,T), \\ [2D(\boldsymbol{u})\boldsymbol{n}]_{t_g} = 0 & \Gamma_N^k \times (0,T), \\ \boldsymbol{u} = \boldsymbol{g} & \Gamma_D \times (0,T), \\ \boldsymbol{u}(0,x) = 0 & \Omega_k. \end{cases} \tag{5.2}$$

However, from the proof of Theorem 2.2.1, we understand that this problem can be divided into two subproblems: one with mixed boundary conditions, i.e., problem (5.1), and one with non-homogeneous Dirichlet boundary conditions, i.e.:

$$\begin{cases} \boldsymbol{u}_t - \operatorname{div}(\sigma(\boldsymbol{u}, p)) = \boldsymbol{f}_k & \Omega_k \times (0,T), \\ \operatorname{div}(\boldsymbol{u}) = 0 & \Omega_k \times (0,T), \\ \boldsymbol{u} = 0 & \Gamma_N^k \times (0,T), \\ \boldsymbol{u} = \boldsymbol{g} & \Gamma_D \times (0,T), \\ \boldsymbol{u}(0,x) = 0 & \Omega_k. \end{cases} \tag{5.3}$$

The latter problem has already been studied in [7] using a different methodology. In this chapter, we will apply the same methodology as developed in [62].

5.2 Preliminary result

In this section, we will introduce some preliminary results that will be useful in proving the continuity of the Stokes problem with respect to its domain. These results will provide us with tools to study the behavior of the solution as the domain changes, and they will form the basis of our analysis.

5.2.1 Estimates for unsteady Stokes system with mixed boundary conditions

In this subsection, we provide an estimate for problem (5.1). It is important to note that we consider the case where the dimension, denoted as d, is set to 2. This choice is made because in the preceding chapter, we have only presented results specifically for this dimension. Generalizations to higher dimensions will be the subject of future work and investigation.

The following theorem establishes the Poincaré inequality for the spaces $\boldsymbol{V}(\Omega)$ and $\boldsymbol{H}_{0,\Gamma_D}(\Omega)$, and can be found in [5]. In simple terms, this theorem confirms that the well-known Poincaré inequality still holds in the Sobolev space where only a portion of the trace operator is equal to zero.

Theorem 5.2.1. *Let Ω be open, bounded and Liptchiz domain. Consider Γ_0 a open subset of $\partial\Omega$ and $X = \{u \in H^1(\Omega) | u = 0 \text{ on } \Gamma_0 \subset \partial\Omega\}$ then exist a constant $C > 0$ that depends only on Ω such that:*

$$\|u\|_{H^1(\Omega)} \leq C \|\nabla u\|_{L^2(\Omega)}.$$

We are now ready to prove our estimates.

Theorem 5.2.2. *Let Ω be as defined in Theorem (2.2.1). Consider $\boldsymbol{f} \in L^2\left(\boldsymbol{L}^2(\Omega)\right)$ and $\boldsymbol{h} \in L^2\left(\boldsymbol{L}^2(\Gamma_N)\right)$, where $\boldsymbol{h}\cdot\boldsymbol{n} = 0$. Then, there exists a unique solution $(\boldsymbol{u}, p)$ to the following problem:*

$$\begin{cases} \boldsymbol{u}_t - div(\sigma(\boldsymbol{u}, p)) = \boldsymbol{f} & \Omega \times (0,T), \\ \operatorname{div}(\boldsymbol{u}) = 0 & \Omega \times (0,T), \\ \boldsymbol{u}\cdot\boldsymbol{n} = 0 & \Gamma_N \times (0,T), \\ [2D(\boldsymbol{u})\boldsymbol{n}]_{t_g} = \boldsymbol{h} & \Gamma_N \times (0,T), \\ \boldsymbol{u} = 0 & \Gamma_D \times (0,T), \\ \boldsymbol{u}(0,x) = 0 & \Omega_k. \end{cases}$$

where $\boldsymbol{u} \in L^2(\boldsymbol{V}(\Omega)) \bigcap C(\boldsymbol{H}(\Omega))$ and $p \in L^2(L_0^2(\Omega))$. Furthermore we have the following estimates:

$$\left\| \frac{d}{dt}\boldsymbol{u} \right\|_{L^2(\boldsymbol{V}(\Omega)')} + \|\boldsymbol{u}\|_{L^2(\boldsymbol{V}(\Omega))} + \|p\|_{L^2(\Omega)} \leq C\left(\|\boldsymbol{f}\|_{L^2(\boldsymbol{L^2}(\Omega))} + \|\boldsymbol{h}\|_{L^2(\boldsymbol{L^2}(\Gamma_N))} \right).$$

where $C > 0$ is a constant that depends only on Ω.

Proof. The existence of the solution deduce from Theorem (2.2.1), since $L^2\left(\boldsymbol{L}^2(\Omega)\right)$ and $L^2\left(\boldsymbol{L}^2(\Gamma_N)\right)$ are continuously embedded in $L^2\left(\boldsymbol{H}_0(\operatorname{div},\Omega)'\right)$, $L^2\left(\boldsymbol{H}_0(\operatorname{div},\Omega)'\right)$ respectively.

In the process of establishing the estimates, we refer to [61, Chap 3 Lemma 1.2], which asserts that $\boldsymbol{u}$ can be used as a test function, even when $\boldsymbol{u}$ is an element of $L(\boldsymbol{V}(\Omega))$. This is feasible because the equation (5.1) can be understood as an operator equation in the form $u' + Au = f$, with all terms belonging to $L(\boldsymbol{V}(\Omega)')$. Moreover, the dual space of $L(\boldsymbol{V}(\Omega)')$ is equal to $L(\boldsymbol{V}(\Omega))'$, thus, we deduce that:

$$\frac{d}{dt}\int_\Omega |\boldsymbol{u}(t)|^2\, dx + 2\int_\Omega |\nabla \boldsymbol{u}(t)|^2\, dx = 2\int_\Omega \boldsymbol{f}\cdot\boldsymbol{u} dx + 2\int_{\Gamma_N} \boldsymbol{h}\cdot\boldsymbol{u} ds.$$

Therefore integrating from 0 to t_s and since $\boldsymbol{u}(0) = 0$ we obtain:

$$\int_\Omega |\boldsymbol{u}(t_s)|^2\, dx + 2\int_0^{t_s}\int_\Omega |\nabla \boldsymbol{u}(t)|^2\, dxdt = 2\int_0^{t_s}\int_\Omega \boldsymbol{f}\cdot\boldsymbol{u} dxdt + 2\int_0^{t_s}\int_{\Gamma_N} \boldsymbol{h}\cdot\boldsymbol{u} ds. \quad (5.4)$$

Notice that $\int_\Omega |\boldsymbol{u}(x,t_s)|^2\, dx$ is well define since $\boldsymbol{u} \in C(\boldsymbol{H}(\Omega))$, thus setting $t_s = T$ in equation (5.4)we obtain:

$$\int_0^T \int_\Omega |\nabla \boldsymbol{u}(t)|^2 \, dxdt \leq \left| \int_0^T \int_\Omega \boldsymbol{f} \cdot \boldsymbol{u} \, dxdt \right| + \left| \int_0^T \int_{\Gamma_N} \boldsymbol{h} \cdot \boldsymbol{u} \, dsdt \right|. \tag{5.5}$$

Using the Poincaré inequality , and using fact that the trace operator is continuous, there a constant $C > 0$ such that:

$$\|\boldsymbol{u}\|_{L^2(\boldsymbol{V}(\Omega))} \leq C \left(\|\boldsymbol{f}\|_{L^2(\boldsymbol{L^2}(\Omega))} + \|\boldsymbol{h}\|_{L^2(\boldsymbol{L^2}(\Gamma_N))} \right). \tag{5.6}$$

Now to bound $\frac{d}{dt}\boldsymbol{u}$ in $L^2(\boldsymbol{V}(\Omega)')$. Let $\boldsymbol{v} \in L^2(\boldsymbol{V}(\Omega)')$ and notice that:

$$\int_0^T \int_\Omega \frac{d}{dt}\boldsymbol{u} \cdot \boldsymbol{v} dxdt + \int_0^T \int_\Omega \nabla \boldsymbol{u} \cdot \nabla \boldsymbol{v} dxdt = \int_0^T \int_\Omega \boldsymbol{f} \cdot \boldsymbol{v} dx + \int_0^T \int_{\Gamma_N} \boldsymbol{h} \cdot \boldsymbol{v} ds.$$

Using again the Poincaré inequality and the fact that the trace operator is continuous we obtain:

$$\begin{aligned} \left| \int_0^T \int_\Omega \frac{d}{dt}\boldsymbol{u} \cdot \boldsymbol{v} dxdt \right| &\leq \|\nabla \boldsymbol{u}\|_{L^2(\boldsymbol{L^2}(\Omega))} \|\nabla \boldsymbol{v}\|_{L^2(\boldsymbol{L^2}(\Omega))} + \|\boldsymbol{f}\|_{L^2(\boldsymbol{L^2}(\Omega))} \|\boldsymbol{v}\|_{L^2(\boldsymbol{L^2}(\Omega))} \\ &\quad + \|\boldsymbol{h}\|_{L^2(\boldsymbol{L^2}(\Omega))} \|\boldsymbol{v}\|_{L^2(\boldsymbol{V}(\Omega))} \\ &\leq C' \left(\|\boldsymbol{f}\|_{L^2(\boldsymbol{L^2}(\Omega))} + \|\boldsymbol{h}\|_{L^2(\boldsymbol{L^2}(\Gamma_N))} \right) \|\boldsymbol{v}\|_{L^2(\boldsymbol{V}(\Omega))} \end{aligned}$$

Hence from inequality (5.6) we have:

$$\left\| \frac{d}{dt}\boldsymbol{u} \right\|_{L^2(\boldsymbol{V}(\Omega)')} \leq C' \left(\|\boldsymbol{f}\|_{L^2(\boldsymbol{L^2}(\Omega))} + \|\boldsymbol{h}\|_{L^2(\boldsymbol{L^2}(\Gamma_N))} \right). \tag{5.7}$$

Let $\boldsymbol{H}^{-1}(\Omega) = \boldsymbol{H}_0^1(\Omega)'$, analogously we have that:

$$\left\| \frac{d}{dt}\boldsymbol{u} \right\|_{L^2(\boldsymbol{H}^{-1}(\Omega))} \leq C'' \left(\|\boldsymbol{f}\|_{L^2(\boldsymbol{L^2}(\Omega))} + \|\boldsymbol{h}\|_{L^2(\boldsymbol{L^2}(\Gamma_N))} \right).$$

From the prove of (2.2.1) we know that:

$$\begin{aligned} \|\nabla p\|_{\boldsymbol{L^2}(\boldsymbol{H}^{-1}(\Omega))} &= \|\frac{d}{dt}\boldsymbol{u} - \Delta \boldsymbol{u} - \boldsymbol{f}\|_{L(H^{-1}(\Omega))} \\ &\leq \|\frac{d}{dt}\boldsymbol{u}\|_{L^2(\boldsymbol{V}(\Omega)')} + \|\boldsymbol{u}\|_{L^2(\boldsymbol{H}_0^1(\Omega))} \\ &\quad + \|\boldsymbol{f}\|_{L^2(\boldsymbol{L^2}(\Omega))}. \end{aligned} \tag{5.8}$$

Thus from equations (5.7),(5.6) and (5.8) we deduce that:

$$\|\nabla p\|_{\boldsymbol{L}^2(\boldsymbol{H}^{-1}(\Omega))} \leq C''' \left(\|\boldsymbol{f}\|_{L^2(\boldsymbol{L}^2(\Omega))} + \|\boldsymbol{h}\|_{L^2(\boldsymbol{L}^2(\Gamma_N))} \right) .$$

From the prove of (2.2.1) and from [9, Proposition 2.10] we know there is a constant $M > 0$ such that:

$$\|p\|_{L^2(L^2(\Omega)/\mathbb{R})} \leq M \|\nabla p\|_{\boldsymbol{L}^2(\boldsymbol{H}^{-1}(\Omega))} .$$

Since $p \in L^2(L^2_0(\Omega))$ and we obtain:

$$\|p\|_{L^2(L^2(\Omega))} \leq C''' M \left(\|\boldsymbol{f}\|_{L^2(\boldsymbol{L}^2(\Omega))} + \|\boldsymbol{h}\|_{L^2(\boldsymbol{L}^2(\Gamma_N))} \right) .$$

□

5.2.2 Continuity of $H^1(\Omega)$ under Diffeomorphisms

In this section, we present several important theorems and propositions that are crucial for studying the convergence of solutions with respect to diffeomorphisms. These results provide valuable insights and tools for analyzing the behavior and properties of solutions under transformations of the underlying domain. First we draw attention to two cornerstone mathematical concepts, the chain rule and the change of variables, both renowned for their significant utility in traditional spaces.

Proposition 5.2.3. *[6, Lemma 6.21] Let $\Omega_0, \Omega_1 \subset \mathbb{R}^d$ be open,. Suppose $\psi : \mathbb{R}^d \to \mathbb{R}^d$ is a diffeomorphism in $\boldsymbol{W}^{1,\infty}(\mathbb{R}^d, \mathbb{R}^d)$ such that $\psi(\Omega_0) = \Omega_1$. Let $1 \leq p \leq +\infty$ then the following holds:*

1. $u \in H^m(\Omega_1)$ if and only if $u \circ \psi \in H^m(\Omega_0)$ for $m = 0$ or $m = 1$,
2. $(\nabla u) \circ \psi = ((\nabla \psi)^{-1})^t \, \nabla(u \circ \psi)$,
3. $\int_{\Omega_1} u \, dx = \int_{\Omega_0} f \circ \psi \, |det(\nabla \psi)| dx$,
4. $\int_{\Omega_1} u \, |det(\nabla \psi^{-1})| \, dx = \int_{\Omega_0} f \circ \psi dx$.

Continuing our exploration of the chain rule, we now address a proposition concerning its application in a slightly different context - namely, the change of variables on the boundary of a domain. This proposition can be found in [6, Lemma 6.23], but the prove is given in [42, Proposion 5.4.3] .

Proposition 5.2.4. *Let $\Omega_0, \Omega_1 \subset \mathbb{R}^d$ be a open, bounded and at least of class $C^{1,1}$. Suppose $\psi : \mathbb{R}^d \to \mathbb{R}^d$ is a diffeomorphism in $\boldsymbol{W}^{1,\infty}(\mathbb{R}^d, \mathbb{R}^d) \cap C^1(\mathbb{R}^d, \mathbb{R}^d)$ such that $\psi(\Omega_0) = \Omega_1$. Let $u \in L^1(\partial\Omega_1)$, then $u \circ \psi \in L^1(\partial\Omega_0)$, and we have*

$$\int_{\partial\Omega_1} u\, ds = \int_{\partial\Omega_0} u \circ \psi |det(\nabla\psi)| \left| \left((\nabla\psi)^{-1} \right)^t \boldsymbol{n} \right|_{\mathbb{R}^N} ds,$$

where n is the external normal to $\partial\Omega_0$.

We now introduce a theorem about the transformative behavior of the Sobolev spaces under a diffeomorphism. Specifically, this theorem determines that the linear operator $\widetilde{\psi}(u) = u \circ \psi$ establishes an isomorphism between two associated Sobolev spaces. Furthermore, when the diffeomorphism approximates the identity, the associated spaces become nearly identical.

Theorem 5.2.5. *Let $\Omega_0, \Omega_1 \subset \mathbb{R}^d$ be open, bounded, and Lipschitz domains. Suppose $\psi, \psi^{-1} : \mathbb{R}^d \to \mathbb{R}^d$ are diffeomorphism in $\boldsymbol{W}^{1,\infty}(\mathbb{R}^d, \mathbb{R}^d)$ such that $\psi(\Omega_0) = \Omega_1$. Then for $m = 0$ or $m = 1$ the linear operator $\widetilde{\psi} : H^m(\Omega_1) \to H^m(\Omega_0)$, defined by*

$$\widetilde{\psi}(u) = u \circ \psi,$$

is an isomorphism between $H^m(\Omega_1)$ and $H^m(\Omega_0)$. Moreover, there exist constants $L(\psi), U(\psi) > 0$ such that for all $u \in H^m(\Omega_1)$, we have

$$L(\psi)\|u\|_{H^m(\Omega_1)} \leq \|\widetilde{\psi}(u)\|_{H^m(\Omega_0)} \leq U(\psi)\|u\|_{H^m(\Omega_1)}.$$

Furthermore if $\|\psi - I_d\|_{1,\infty} + \|\psi^{-1} - I_d\|_{1,\infty} \to 0$ then $L(\psi), U(\psi) \to 1$.

Proof. We first consider the case where $m = 0$. It can be observed that $\widetilde{\psi}$ is a linear function and its inverse is given by $\widetilde{\psi}^{-1}(w) = w \circ \psi^{-1}$. Therefore by the open mapping theorem we only need to see that $\widetilde{\psi}$ is continuous. Now, let's consider set $J(\psi) = |\det(\nabla\psi)|$ and the following expressions:

$$\begin{aligned} \|\widetilde{\psi}(u)\|^2_{L^2(\Omega_0)} &= \int_{\Omega_0} |u \circ \psi|^2 \, dx = \int_{\Omega_1} |u|^2 \, J(\psi^{-1})\, dx \\ &\leq \|J(\psi^{-1})\|_{L^\infty(\Omega_1)} \|u\|^2_{L^2(\Omega_1)}, \end{aligned} \tag{5.9}$$

$$\begin{aligned} \|u\|^2_{L^2(\Omega_1)} &= \int_{\Omega_1} |u|^2 \, dx = \int_{\Omega_0} |u \circ \psi|^2 \, J(\psi)\, dx \\ &\leq \|J(\psi)\|_{L^\infty(\Omega_0)} \|\widetilde{\psi}(u)\|^2_{L^2(\Omega_0)}. \end{aligned} \tag{5.10}$$

Thus the constants are defined as $U(\psi) = \|J(\psi^{-1})\|^{1/2}_{L^\infty(\Omega_1)}$ and $L(\psi) = \|J(\psi)\|^{-1/2}_{L^\infty(\Omega_0)}$. The finiteness of these constants is guaranteed by the determinant being an algebraic function. Moreover, the continuity of the determinant function ensures that if $\psi, \psi^{-1} \to I_d$ in the norm of $\boldsymbol{W}^{1,\infty}$, then $L(\psi), U(\psi) \to 1$.

For the case where $m = 1$, we need to bound the semi-norm, $\|\nabla\widetilde{\psi}(u)\|^2_{L^2(\Omega_0)}$, using the chain rule we have $\nabla(u \circ \psi) \circ \psi^{-1} = (\nabla\psi)^t \nabla u$. Therefore:

$$\begin{aligned}
\|\nabla\widetilde{\psi}(u)\|^2_{\boldsymbol{L}^2(\Omega_0)} &= \int_{\Omega_0} |\nabla(u \circ \psi)|^2 \, dx \\
&= \int_{\Omega_1} \left|(\nabla\psi)^t \nabla u\right|^2 \, J(\psi^{-1}) \, dx \\
&\leq \|J(\psi^{-1})\|_{L^\infty(\Omega_1)} \int_{\Omega_1} \left|(\nabla\psi)^t \nabla u\right|^2 dx \\
&\leq \|J(\psi^{-1})\|_{L^\infty(\Omega_1)} \int_{\Omega_1} S_\psi(x) \, |\nabla u|^2 \, dx \, . \qquad (5.11)
\end{aligned}$$

Here, $S_\psi(x) = \sup_{|u|_{\mathbb{R}^n}=1} |\nabla\psi(x)^t u|_{\mathbb{R}^n}$ is the operator norm of $\nabla\psi(x)^t$. Since every norm is equivalent in finite dimensions, there exists a constant $\gamma > 0$ such that $S_\psi(x) \leq \gamma|\nabla\psi(x)^t|_{\mathbb{R}^d \times \mathbb{R}^d}$. It follows then that:

$$\sup_{x \in \Omega_1} S_\psi(x) \leq \gamma \|\psi\|_{1,\infty},$$

which implies $S_\psi \in L^\infty(\Omega_1)$. From inequality (5.11) we have :

$$\|\nabla\widetilde{\psi}(u)\|^2_{\boldsymbol{L}^2(\Omega_0)} \leq \|J(\psi^{-1})\|_{L^\infty(\Omega_1)} \|S_\psi(x)\|_{L^\infty(\Omega_1)} \|\nabla u\|^2_{\boldsymbol{L}^2(\Omega_1)} \, .$$

An analogous procedure can be used to derive:

$$\|u\|^2_{\boldsymbol{L}^2(\Omega_1)} \leq \|J(\psi)\|_{L^\infty(\Omega_0)} \|S_{\psi^{-1}}(x)\|_{L^\infty(\Omega_0)} \|\nabla\widetilde{\psi}(u)\|^2_{\boldsymbol{L}^2(\Omega_0)} \, .$$

Lastly, using the fact that the operator norm is a norm, we have:

$$|S_\psi - 1| = |S_\psi - S_{I_d}| \leq |S_{\psi - I_d}| \leq \gamma \, |\nabla\psi - I_d|_{\mathbb{R}^{d \times d}} \, .$$

Therefore if $\psi, \psi^{-1} \to Id$ we have that $S_\psi, S_{\psi^{-1}} \to 1$. □

We now have the following corollary that is immediate from 5.2.5 since the constants $L(\psi), U(\psi)$ are time independent.

Corollary 5.2.1. *Let $\Omega_0, \Omega_1 \subset \mathbb{R}^d$ be open, bounded, and Lipschitz domains. Suppose $\psi, \psi^{-1} : \mathbb{R}^d \to \mathbb{R}^d$ are diffeomorphism in $\boldsymbol{W}^{1,\infty}(\mathbb{R}^d, \mathbb{R}^d)$ such that $\psi(\Omega_0) =$*

Ω_1. Let $T > 0$ and define $X_0^m = L(H^m(\Omega_0))$, $X_1^m = L(H^m(\Omega_1))$ Then for $m = 0$ or $m = 1$ the linear operator $\widetilde{\psi} : X_0^m \to X_1^m$, defined by

$$\widetilde{\psi}(u(t,x)) = u(t,\psi(x))\,,$$

is an isomorphism between X_0^m and X_1^m. Moreover, there exist constants $L(\psi), U(\psi) > 0$ such that for all $u \in H^m(\Omega_1)$, we have

$$L(\psi)\|u\|_{X_1^m} \leq \|\widetilde{\psi}(u)\|_{X_0^m} \leq U(\psi)\|u\|_{X_1^m}.$$

Furthermore if $\|\psi - I_d\|_{1,\infty} + \|\psi^{-1} - I_d\|_{1,\infty} \to 0$ then $L(\psi), U(\psi) \to 1$.

Building upon our prior discussions on diffeomorphisms and their influence on Sobolev spaces, we introduce a theorem that investigates the impact of a sequence of open sets converging diffeomorphically on a bounded sequence within these spaces.

Theorem 5.2.6. *Consider a sequence of open sets $\{\Omega_k\}_{k=1}^{\infty} \subseteq \mathbb{R}^d$ that converges diffeomorphically to Ω. Let $\{u_k\}_{k=1}^{\infty}$ be a bounded sequence in $H^m(\Omega_k)$ with $m = 0$ or $m = 1$, and define $w_k = u_k \circ \psi_k$. Then, the following hold:*

- $w_k \in H^m(\Omega)$,
- w_k is a bounded sequence,
- if $\|u_k\|_{H^m(\Omega_k)}$ converges, then $\|w_k\|_{H^m(\Omega)}$ also converges. Specifically, we have

$$\lim_{k\to\infty} \|w_k\|_{H^m(\Omega)} = \lim_{k\to\infty} \|u_k\|_{H^m(\Omega_k)}.$$

Proof. We first invoke Proposition 5.2.5 which guarantees that for every $w_k = u_k \circ \psi_k$, it is an element of $H^m(\Omega)$. Moreover, there exist sequences of constants, $L_k(\psi_k)$ and $U_k(\psi_k)$, each greater than zero, that satisfy:

$$L_k\|u_k\|_{H^m(\Omega_k)} \leq \|w_k\|_{H^m(\Omega)} \leq U_k\|u_k\|_{H^m(\Omega_k)}. \tag{5.12}$$

Given that $\|\psi - I_d\|_{1,\infty} + \|\psi^{-1} - I_d\|_{1,\infty} \to 0$ and applying Proposition 5.2.5, we arrive at:

$$\lim_{k\to\infty} L_k = \lim_{k\to\infty} U_k = 1\,. \tag{5.13}$$

Since u_k is bounded, it can be inferred from (5.12) that $\|w_k\|_{H^m(\Omega)}$ is bounded. If we assume that $\|u_k\|_{H^m(\Omega_k)}$ convergence, then applying the limit to Equation (5.12) and utilizing the result from equation (5.13), we have:

$$\lim_{k\to\infty} \|w_k\|_{H^m(\Omega)} = \lim_{k\to\infty} \|u_k\|_{H^m(\Omega_k)}\,.$$

□

Following the same logic as in our prior theorem, we extend our investigation to the setting of timed sequences.

Corollary 5.2.2. *Consider a sequence of open sets $\{\Omega_k\}_{k=1}^{\infty} \subseteq \mathbb{R}^d$ that converges diffeomorphically to Ω. Let $X_k^n = L(H^m(\Omega_k))$, $X = L(H^m(\Omega))$. Now let $\{u_k\}_{k=1}^{\infty}$ be a bounded sequence in X_k^m with $m = 0$ or $m = 1$, and define $w_k = u_k \circ \psi_k$. Then, the following hold:*

- $w_k \in X_k^m$,
- w_k is a bounded sequence, and
- if $\|u_k\|_{X_k^m}$ converges, then $\|w_k\|_{X^m}$ also converges. Specifically, we have

$$\lim_{k\to\infty} \|w_k\|_{X_k^m} = \lim_{k\to\infty} \|u_k\|_{X^m}.$$

Proposition 5.2.7. *Let $\Omega_0, \Omega_1 \subset \mathbb{R}^n$ open, bounded and Lipschitz sets. Let $\psi, \psi^{-1} \in \boldsymbol{W}^{1,\infty}(\mathbb{R}^d, \mathbb{R}^d))$ a diffeomorphims such that $\psi(\Omega_0) = \Omega_1$ and let $\gamma^{\Omega} \in \mathcal{L}(H^1(\Omega), H^{1/2}(\partial\Omega))$ be the trace operator. Then if $u \in H^1(\Omega_0)$ we have:*

$$\gamma^{\Omega_0}(u) \circ \psi = \gamma^{\Omega_1}(u \circ \psi)\,.$$

Proof. We will prove this proposition by density of $\mathcal{D}(\overline{\Omega}_0)$ functions in $H^1(\Omega_0)$. Let $u \in \mathcal{D}(\overline{\Omega}_0)$, and notice:

$$\begin{aligned} \gamma^{\Omega_0}(u) \circ \psi &= \gamma^{\Omega_1}(u \circ \psi) \\ &= (u \circ \psi)\,|_{\partial\Omega_1} \\ &= \gamma^{\Omega_1}(u \circ \psi), \end{aligned} \tag{5.14}$$

From equation (5.14), and from the classical trace inequality can deduce:

$$\begin{aligned} \left\|\gamma^{\Omega_0}(u) \circ \psi\right\|_{H^{1/2}(\partial\Omega_1)} &= \left\|\gamma^{\Omega_1}(u \circ \psi)\right\|_{H^{1/2}(\partial\Omega_1)} \\ &\leq \|u \circ \psi\|_{H^1(\Omega_1)} \\ &\leq C\|u\|_{H^1(\Omega_0)}\,. \end{aligned}$$

Hence by density the operator $\gamma^{\Omega_0} \circ \psi : H^1(\Omega_0) \to H^{1/2}(\partial\Omega_1)$ is continuous, and:

$$\gamma^{\Omega_0}(u) \circ \psi = \gamma^{\Omega_1}(u \circ \psi) \quad \forall u \in H^1(\Omega_0)\,.$$

□

Proposition 5.2.8. *Let $\Omega_0, \Omega_1 \subset \mathbb{R}^n$ open, bounded and Lipschitz sets. Let $\psi, \psi^{-1} \in \boldsymbol{W}^{1,\infty}(\mathbb{R}^d, \mathbb{R}^d)$ a diffeomorphims such that $\psi(\Omega_0) = \Omega_1$. Then $u \in H_0^1(\Omega_0)$ if and only if $u \circ \psi \in H_0^1(\Omega_1)$.*

Proof. This direct consequence of the proposition 5.2.7, because we have that $0 = \gamma^{\Omega_0}(u) \circ \psi = \gamma^{\Omega_1}(u \circ \psi)$. □

5.3 Continuity of the velocity vector field with respect the domain

This section is dedicated to establishing the continuity of the velocity vector field with respect to its domain. For simplicity of the statements in the following results, we will assume that D is a bounded domain and $\{\Omega_k\}_{k=1}^{\infty} \subset \mathbb{R}^d$ is a sequence of bounded and $C^{1,1}$ domains contained in D, such that $\Omega_k \subset D$ for all k, and Ω_k converges **diffeomorphically** to a bounded and $C^{1,1}$ domain $\Omega \subset D$. We will also consider the family of diffeomorphisms $\{\psi_k\}_{k=1}^{\infty} \in \boldsymbol{W}^{1,\infty}(\mathbb{R}^d, \mathbb{R}^d) \cap C^1(\mathbb{R}^d, \mathbb{R}^d)$ according to Definition 5.1.1 .

Remark 5.3.1. As we embark on our analysis, it is important to recall a few key concepts related to bounded sequences in Hilbert spaces. For a bounded sequence x_k in a Hilbert space H, the Banach–Alaoglu theorem assures the existence of a sub-sequence $\{x_{k_j}\}$ that weakly converges to an element $x^* \in H$ with finite norm. Moreover, if x^* is unique, then the entire sequence x_k weakly converges to x^*, not just the subsequence. This result can be conveniently derived by considering subsubsequences of x_k; the uniqueness of the weak limit ensures $x_k \rightharpoonup x^*$.

Another important fact is that, given $x_k \rightharpoonup x^*$ and $y_k \to y$, $\langle x_k, y_k \rangle_{H,H} \to \langle x, y \rangle_{H,H}$ holds. This follows from the Riesz representation theorem and the inequality:

$$\begin{aligned} \left| \langle x_k, y_k \rangle_{H,H} - \langle x, y \rangle_{H,H} \right| &\leq \left| \langle x_k, y_k - y \rangle_{H,H} \right| + \left| \langle x_k - x, y \rangle_{H,H} \right| \\ &\leq \|x_k\|_H \|y_k - y\|_H + \left| \langle x_k - x, y \rangle_{H,H} \right|, \end{aligned}$$

Since $\|x_k\|_H$ is bounded. Taking the limit yields:

$$\begin{aligned} \lim_{k \to \infty} \langle x_k, y_k \rangle_{H,H} &= \langle x, y \rangle_{H,H} \\ &= \lim_{k \to \infty} \langle x_k, y \rangle_{H,H} \end{aligned}$$

We now introduce a theorem that establishes the existence of a convergent sequence within the $\boldsymbol{V}(\Omega_k)$ space that converges to a function in $\boldsymbol{V}(\Omega)$ under diffemorphism. This result is fundamental to our analysis, providing a key link between the spaces associated with the deformed and original domains.

Theorem 5.3.2. *Let $\boldsymbol{v} \in \boldsymbol{V}(\Omega)$ then there is sequence $\boldsymbol{z_k} \in \boldsymbol{V}(\Omega_k)$ such that $\boldsymbol{v_k} = \boldsymbol{z}_k \circ \psi_k \to \boldsymbol{v}$ in $\boldsymbol{V}(\Omega)$.*

Proof. Let $\boldsymbol{w}_k \in \boldsymbol{H}^1(\Omega_k)$ be defined as $\boldsymbol{w}_k = \boldsymbol{v} \circ \psi_k^{-1}$ and let $q_k \in H^1(\Omega_k)$ be a solution of:

$$\begin{cases} \Delta q_k = \operatorname{div}(\boldsymbol{w}_k) & \Omega_k \,, \\ \frac{\partial q_k}{\partial n} = 0 & \partial\Omega_k \,. \end{cases} \tag{5.15}$$

Assuming Ω_k to be a $C^{1,1}$ domain, we can utilize the classical regularity theorem (refer to [9, Lemma 4.6]), which indicates that $q_k \in H^2(\Omega_k)$. Additionally, we have the subsequent estimate:

$$\|\nabla q_k\|_{\boldsymbol{H^1}(\Omega_k)} \leq \|\operatorname{div}(\boldsymbol{w}_k)\|_{L^2(\Omega_k)} \,.$$

Consequently, by defining $\boldsymbol{z}_k = \nabla q_k - \boldsymbol{w}_k$, we confirm that $\boldsymbol{z}_k \in \boldsymbol{V}(\Omega_k)$ because q_k is a solution to equation (5.15). Next, consider the following:

$$\boldsymbol{v_k} - \boldsymbol{v} = \boldsymbol{z_k} \circ \psi_k - \boldsymbol{v} = (\nabla q_k) \circ \psi_k \,.$$

As $\boldsymbol{z_k} \circ \psi_k - \boldsymbol{v} \in \boldsymbol{H^1}(\Omega)$, our only remaining task is to demonstrate that $\|\nabla q_k \circ \psi_k\|_{\boldsymbol{H^1}(\Omega)} \to 0$. Taking into account that $\psi_k \psi_k^{-1} \to Id$, by applying Theorem 5.2.5, we infer that there exists a sequence of constants $U_k \to 1$, such that :

$$\begin{aligned} \|\left(\nabla q_k\right) \circ \psi_k\|_{\boldsymbol{H^1}(\Omega)} &\leq U_k \|\operatorname{div}(\boldsymbol{w}_k)\|_{L^2(\Omega_k)} \\ &= U_k \|Tr(\nabla \psi_k^{-t} \nabla \boldsymbol{v})\|_{L^2(\Omega)} \end{aligned}$$

Given that the trace operator, Tr, is linearly continuous from $\left(L^2(\Omega)\right)^{d\times d}$ to $L^2(\Omega)$ and that $\nabla \psi_k^{-t} \nabla \boldsymbol{v} \to \nabla \boldsymbol{v}$ in $\left(L^2(\Omega)\right)^{d\times d}$, we can apply the limit to both sides to obtain:

$$\lim_{k\to\infty} \|\nabla q_k \circ \psi_k\|_{\boldsymbol{H^1}(\Omega)} \leq \|Tr(\nabla \boldsymbol{v})\|_{L^2(\Omega)} = 0$$

□

Building upon the previous theorem, our next corollary extends the continuity of the velocity vector field from the spatial to the temporal domain. Specifically, it ensures the existence of a convergent sequence in the $L^2(\boldsymbol{V}(\Omega_k))$ space under a diffeomorphism.

Corollary 5.3.1. *Let $\boldsymbol{v} \in L^2(\boldsymbol{V}(\Omega))$ then there is sequence $\boldsymbol{z_k} \in L^2(\boldsymbol{V}(\Omega_k))$ such that $\boldsymbol{v_k} = \boldsymbol{z}_k \circ \psi_k \to \boldsymbol{v}$ in $L^2(\boldsymbol{V}(\Omega))$.*

Proof. According to Theorem 5.3.2 $\boldsymbol{V}_\psi(\Omega) = \{\boldsymbol{z} \circ \psi_k | \boldsymbol{z} \in \boldsymbol{V}(\Omega_k), k \in \mathbb{N}\}$ is dense in $\boldsymbol{V}(\Omega)$. Consequently $L^2(\boldsymbol{V}_\psi(\Omega))$ is also dense $L^2(\boldsymbol{V}(\Omega))$. □

As we further examine the behavior of solutions to the Stokes variational problem, our subsequent lemma provides insights on the weak convergence of the solutions under a diffeomorphism.

Lemma 5.3.3. *Let $\{\boldsymbol{u}_k\} \in L^2(\boldsymbol{V}(\Omega_k))$ be a sequence the solution of the Stokes variational (5.1) problem and define $\boldsymbol{w}_k = \boldsymbol{u}_k \circ \psi_k$. Suppose following assumption hold:*

1. $\psi_k(\Gamma_N^k) = \Gamma_N$,
2. $\boldsymbol{f_k} \in L^2\left(\boldsymbol{L}^2(\Omega_k)\right)$ *such that* $\boldsymbol{f}_k \circ \psi_k \to \boldsymbol{f} \in L^2\left(\boldsymbol{L}^2(\Omega)\right)$,
3. $\boldsymbol{h_k} \in L^2\left(\boldsymbol{L}^2(\Gamma_N^k)\right)$ *such that* $\boldsymbol{h}_k \circ \psi_k \to \boldsymbol{h} \in L^2\left(\boldsymbol{L}^2(\Gamma_N)\right)$.

Then $\boldsymbol{w}_k$ converge weakly to $\boldsymbol{u}_\Omega \in L^2(\boldsymbol{V}(\Omega))$, and $\frac{d}{dt}\boldsymbol{w}_k$ converge weakly to $\frac{d}{dt}\boldsymbol{u}_\Omega \in L^2(\boldsymbol{V}(\Omega)')$,*

Proof. We first note that since both sequences $\boldsymbol{f}_k$ and $\boldsymbol{h}_k$ are bounded, from theorem 5.2.2 this implies that the sequence $\|\boldsymbol{u}_k\|_{L^2(\boldsymbol{V}(\Omega_k))}$ is bounded. Consequently, according to Lemma 5.2.6, the sequence $\boldsymbol{w}_k$ is bounded in $L^2(H^1_{0,\Gamma_D}(\Omega))$. Therefore by the Banach–Alaoglu theorem any subsequence of $\boldsymbol{w}_k$ possesses a further sub-subsequence that weakly converges to some $\boldsymbol{w}^*$ in $L^2(H^1_{0,\Gamma_D}(\Omega))$. For simplicity, we will denote this converging sub-subsequence also as $\boldsymbol{w}_k$.
Given that $\boldsymbol{v} \in \boldsymbol{V}(\Omega)$, we can apply Lemma (5.3.2) to obtain $\boldsymbol{z}_k \in \boldsymbol{V}(\Omega_k)$ with the property that $\boldsymbol{v}_k = \boldsymbol{z}_k \circ \psi_k$ converges to $\boldsymbol{v}$ in $\boldsymbol{V}(\Omega)$. Consequently, according to Proposition 2.2.4, we find:

$$\frac{d}{dt}\int_{\Omega_k} \boldsymbol{u}_k \cdot \boldsymbol{z}_k \, dx = -\int_{\Omega_k} \nabla \boldsymbol{u}_k : \nabla \boldsymbol{z}_k \; dx + \int_{\Omega_k} \boldsymbol{f}_k \cdot \boldsymbol{z}_k dx + \int_{\Gamma_N^k} \boldsymbol{h}_k \cdot \boldsymbol{v}_k ds \,. \quad (5.16)$$

Set $\widehat{\boldsymbol{f}_k} = \boldsymbol{f}_k \circ \psi_k$, and given $\phi \in \mathcal{D}(0,T)$, and using theorem 5.2.3, equation 5.16 is can be rewritten as:

$$\begin{aligned} -\int_0^T \int_\Omega \boldsymbol{w}_k \cdot \boldsymbol{v}_k J(\psi_k)\phi' \, dx = &-\int_0^T \int_\Omega \nabla \boldsymbol{w}_k : M_k^t M_k \nabla \boldsymbol{v}_k J(\psi_k)\phi \, dxdt \\ &+ \int_0^T \int_\Omega \widehat{\boldsymbol{f}_k} \boldsymbol{v}_k J(\psi_k)\phi \, dxdt \\ &+ \int_0^T \int_{\Gamma_N} \widehat{\boldsymbol{f}_k} \cdot \boldsymbol{v}_k J(\psi_k) \left|\nabla \psi_k^{-t} \boldsymbol{n}\right|_{\mathbb{R}^d} \phi ds dt \,, \end{aligned} \quad (5.17)$$

In the above equations, $\boldsymbol{n}$ denotes the normal vector in Γ_N, and $M_k = \nabla\psi_k^{-t}$, $J(\psi_k) = |det(\nabla\psi_k)|$. Now notice that since $\psi_k \to Id$ in $\boldsymbol{W}^{1,\infty}\left(\mathbb{R}^d, \mathbb{R}^d\right)$ we have:

$$\begin{cases} \boldsymbol{v}_k J(\psi_k)\phi'(t) \to \phi'(t)\boldsymbol{v} & \text{in } \boldsymbol{L}^2(\boldsymbol{L}^2(\Omega)) \\ M_k^t M_k \nabla \boldsymbol{v}_k J(\psi_k)\phi(t) \to \phi(t)\nabla\boldsymbol{v} & \text{in } \boldsymbol{L}^2(\boldsymbol{L}^2(\Omega)) \\ \boldsymbol{v}_k J(\psi_k)\left|\nabla\psi_k^{-t}\boldsymbol{n}\right|_{\mathbb{R}^d}\phi(t) \to \phi(t)\boldsymbol{v} & \text{in } \boldsymbol{L}^2(\boldsymbol{L}^2(\Gamma_N)) \,. \end{cases}$$

Hence, we can deduce that:

$$\int_0^T \int_\Omega \boldsymbol{w}^* \cdot \boldsymbol{v}\, \phi' dxdt = \int_0^T \int_\Omega \left[\nabla\boldsymbol{w}^* : \nabla\boldsymbol{v} - \boldsymbol{f}\cdot\boldsymbol{v}\right]\phi\, dxdt - \int_0^T \int_{\Gamma_N} \boldsymbol{h}\cdot\boldsymbol{v}\phi\, dsdt. \tag{5.18}$$

Our next task is to prove that $\boldsymbol{w}^* \in L(\boldsymbol{V}(\Omega))$. For this, let $\phi(t)\boldsymbol{h}(x) \in \mathcal{D}(0,T)\cdot \boldsymbol{H}_0^1(\Omega)$. Let $\boldsymbol{h}_k = \boldsymbol{h}\circ\psi_k^{-1}$, thereby from Proposition 5.2.8 we know that $\boldsymbol{h}_k \in \boldsymbol{H}_0^1(\Omega_k)$. Now consider:

$$\begin{aligned} 0 &= \int_0^T \phi\left[\int_{\Omega_k} div(\boldsymbol{u}_k)\boldsymbol{h}_k\, dx\right] dt \\ &= \int_0^T \phi\left[\int_\Omega \boldsymbol{w}_k \cdot M_k\nabla\boldsymbol{h} J(\psi) dx\right] dt\,. \end{aligned} \tag{5.19}$$

Since since $\psi_k \to Id$ in $\boldsymbol{W}^{1,\infty}\left(\mathbb{R}^d, \mathbb{R}^d\right)$ we know that $M_k\nabla\boldsymbol{h}J(\psi) \to \nabla\boldsymbol{h}$ in $\boldsymbol{L}^2(\Omega)$. Taking the limit in 5.19 yields:

$$\begin{aligned} 0 &= \int_0^T \phi\left[\int_\Omega \boldsymbol{w}^*\nabla\boldsymbol{h} dx\right] dt \\ 0 &= \int_0^T \phi \int_\Omega div(\boldsymbol{w}^*)\boldsymbol{h} dxdt \quad \forall\phi\boldsymbol{h} \in \mathcal{D}(0,T), \end{aligned}$$

Because $\mathcal{D}(0,T)$ and $\boldsymbol{H}_0^1(\Omega)$ are dense in $L^2(0,T)$ and $\boldsymbol{L}^2(\Omega)$ respectively, we can conclude that $\boldsymbol{w}^* \in L(\boldsymbol{V}(\Omega))$.
Now we shall see that $\boldsymbol{w}^* \in C(\boldsymbol{H}(\Omega))$, from equation (5.18) we have:

$$\frac{d}{dt}\int_\Omega \boldsymbol{w}^*.\boldsymbol{v} dxdt = -\int_\Omega \nabla\boldsymbol{w}^* : \nabla\boldsymbol{v}\, dxdt + \int_\Omega \boldsymbol{f}\cdot\boldsymbol{v} dxdt + \int_0^T\int_{\Gamma_N} \boldsymbol{h}\cdot\boldsymbol{v} dsdt\,.$$

This which implies that $\frac{d}{dt}\boldsymbol{w}^* \in L^2(\boldsymbol{V}(\Omega)')$ is bounded linear operator. Now noticing we also have that $\boldsymbol{w}^* \in L^2(\boldsymbol{V}(\Omega))$ this implies that $\boldsymbol{w}^* \in C(\boldsymbol{H}(\Omega))$ see for instance [61, Lemma 1.2] or [50, Chapter 1]. Now, from corollary 5.2.1, it can be observed that $\boldsymbol{u}_k \in C(\boldsymbol{H}(\Omega_k))$, and hence, $\boldsymbol{w_k} \in C([0,T], \boldsymbol{H}(\Omega))$, i.e:

$$\|\boldsymbol{w_k}(t_1) - \boldsymbol{w_k}(t_2)\|_{\boldsymbol{H}(\Omega)} \leq C_k \|\boldsymbol{u}_k(t_1) - \boldsymbol{u}_k(t_2)\|_{\boldsymbol{H}(\Omega_k)} \ .$$

Additionally, we have $\|\boldsymbol{w_k}(0)\|_{L^2(\Omega)} \leq C_k \|\boldsymbol{u}_k(0)\| = 0$,and therefore, $\boldsymbol{w}^*(0) = 0$. Therefore, by unicity of the stokes problem we have:

$$\boldsymbol{w}^* = \boldsymbol{u}_\Omega.$$

Now from 5.18, for we have that:

$$\begin{aligned}\lim_{k\to\infty} \int_0^T \int_\Omega \boldsymbol{w}_k \cdot \boldsymbol{v}\, \phi'(t) dxdt &= \int_0^T \int_\Omega \left[\nabla \boldsymbol{u}_\Omega : \nabla \boldsymbol{v} - \boldsymbol{f} \cdot \boldsymbol{v}\right] \phi(t)\, dxdt \\ &\quad - \int_0^T \int_{\Gamma_N} \boldsymbol{h} \cdot \boldsymbol{v} \phi(t) ds dt \\ &= \int_0^T \int_\Omega \boldsymbol{u}_\Omega \cdot \boldsymbol{v}\, \phi'(t) dxdt.\end{aligned}$$

This implies that $\frac{d}{dt}\boldsymbol{w}_k$ converge weakly* to $\frac{d}{dt}\boldsymbol{u}_\Omega \in L^2(\boldsymbol{V}(\Omega)')$. □

Theorem 5.3.4. *Let $\{\boldsymbol{u}_k\} \in L^2(\boldsymbol{V}(\Omega_k))$ be a sequence the solution of the Stokes variational 5.1 problem and define $\boldsymbol{w}_k = \boldsymbol{u}_k \circ \psi_k$. Suppose following assumption hold:*

1. $\psi_k(\Gamma_N^k) = \Gamma_N$,
2. $\boldsymbol{f_k} \in L^2\left(\boldsymbol{L}^2(\Omega_k)\right)$ *such that* $\boldsymbol{f}_k \circ \psi_k \to \boldsymbol{f} \in L^2\left(\boldsymbol{L}^2(\Omega)\right)$,
3. $\boldsymbol{h_k} \in L^2\left(\boldsymbol{L}^2(\Gamma_N^k)\right)$ *such that* $\boldsymbol{h}_k \circ \psi_k \to \boldsymbol{h} \in L^2\left(\boldsymbol{L}^2(\Gamma_N)\right)$.

Then $\boldsymbol{w}_k$ strongly to $\boldsymbol{u}_\Omega$ in $L^2\left(\boldsymbol{V}(\Omega)\right)$.

Proof. By utilizing Lemma 5.3.3, it is known that $\boldsymbol{w}_k$ converges weakly to $\boldsymbol{u_\Omega}$ and $\boldsymbol{w_k} \in C(\boldsymbol{H}(\Omega))$. To avoid heavy notation we define $\boldsymbol{X}_k = \boldsymbol{L}^2(\boldsymbol{V}(\Omega_k)) \cap C(\boldsymbol{H}(\Omega_k))$, let $t_s \in [0, T]$ and consider the following operators $E_k : \boldsymbol{X}_k \times \boldsymbol{X}_k \to \mathbb{R}$, $E : \boldsymbol{X} \times \boldsymbol{X} \to \mathbb{R}$ as:

$$\begin{aligned}E_k(\boldsymbol{u}, \boldsymbol{w}) &= \left[\int_{\Omega_k} \boldsymbol{u}(t_s) \cdot \boldsymbol{w}(t_s) dx + 2\int_0^{t_s} \int_{\Omega_k} \nabla \boldsymbol{u}(t) \cdot \nabla \boldsymbol{w}(t) dx\, dt\right], \\ E(\boldsymbol{u}, \boldsymbol{w}) &= \left[\int_{\Omega} \boldsymbol{u}(t_s) \cdot \boldsymbol{w}(t_s) dx + 2\int_0^{t_s} \int_{\Omega} \nabla \boldsymbol{u}(t) \cdot \nabla \boldsymbol{w}(t)\, dx\, dt\right].\end{aligned}$$

On the other hand as in Lemma 5.3.3 and equation (5.4) we have:

$$\begin{aligned}\lim_{k\to\infty} E_k(\boldsymbol{u}_k,\boldsymbol{u}_k) &= \lim_{k\to\infty} 2\left[\int_0^{t_s}\int_{\Omega_k} \boldsymbol{f}_k\cdot\boldsymbol{u}_k dx\,dt + \int_0^{t_s}\int_{\Omega_k}\boldsymbol{h}\cdot\boldsymbol{u}_k ds\,dt\right]\\ &= 2\left[\int_0^{t_s}\int_{\Omega}\boldsymbol{f}\cdot\boldsymbol{u}_{\boldsymbol{\Omega}} dx\,dt + \int_0^{t_s}\int_{\Gamma_N}\boldsymbol{h}\cdot\boldsymbol{u}_{\boldsymbol{\Omega}} ds\,dt\right]\\ &= \|\boldsymbol{u}_\Omega(t_s)\|^2_{L^2(\Omega)} + 2\int_0^{t_s}\|\nabla\boldsymbol{u}_\Omega(t_s)\|^2_{\boldsymbol{L}^2(\Omega)}dt\\ &= E(\boldsymbol{u}_{\boldsymbol{\Omega}},\boldsymbol{u}_{\boldsymbol{\Omega}})\,. \end{aligned} \tag{5.20}$$

Now from Theorem 5.2.2, have:

$$\begin{aligned}\lim_{k\to\infty} E_k(\boldsymbol{u}_k,\boldsymbol{u}_k) &= \lim_{k\to\infty}\left[\|\boldsymbol{u}_k(t_s)\|^2_{L^2(\Omega_k)} + 2\int_0^{t_s}\|\nabla\boldsymbol{u}_k(t_s)\|^2_{\boldsymbol{L}^2(\Omega_k)}dt\right]\\ &= \lim_{k\to\infty}\left[\|\boldsymbol{w}_k(t_s)\|^2_{L^2(\Omega)} + 2\int_0^{t_s}\|\nabla\boldsymbol{u}_k(t_s)\|^2_{\boldsymbol{L}^2(\Omega)}dt\right]\\ &= \lim_{k\to\infty} E(\boldsymbol{w}_k,\boldsymbol{w}_k)\,. \end{aligned} \tag{5.21}$$

Combining equations (5.20) and(5.21) we have:

$$\lim_{k\to\infty} E(\boldsymbol{w}_k,\boldsymbol{w}_k) = E(\boldsymbol{u}_{\boldsymbol{\Omega}},\boldsymbol{u}_{\boldsymbol{\Omega}})\,. \tag{5.22}$$

We remark that this does not allow us yet to conclude anything, since we do not know if $\|\boldsymbol{w}_k(t_s)\|^2_{L^2(\Omega)}$ convergence to $\|\boldsymbol{u}_\Omega(t_s)\|^2_{L^2(\Omega)}$. Thus we will analyses $E(\boldsymbol{w}_k-\boldsymbol{u}_{\boldsymbol{\Omega}},\boldsymbol{w}_k-\boldsymbol{u}_{\boldsymbol{\Omega}})$, in that spirit let notice that we have:

$$\begin{aligned}\int_\Omega \boldsymbol{w_k}(t_s)\boldsymbol{u}_\Omega(t_s)dx &= \int_0^T\int_\Omega \frac{d}{dt}\left(\boldsymbol{u}_\Omega(t)\cdot\boldsymbol{w}_k(t)\right)dxdt\\ &= \int_0^T\int_\Omega \frac{d}{dt}\boldsymbol{u}_\Omega(t)\cdot\boldsymbol{w}_k(t)dxdt + \int_0^T\int_\Omega \boldsymbol{u}_\Omega(t)\cdot\frac{d}{dt}\boldsymbol{w}_k(t)dxdt\end{aligned}$$

But by Lemma 5.3.3 $\frac{d}{dt}\boldsymbol{w}_k \rightharpoonup^* \frac{d}{dt}\boldsymbol{u}_\Omega$ and $\boldsymbol{w}_k \rightharpoonup \boldsymbol{w}^*$, therefore:

$$\begin{aligned}\lim_{k\to\infty}\int_\Omega \boldsymbol{w_k}(t_s)\boldsymbol{u}_\Omega(t_s)dx &= \int_0^{t_s}\int_\Omega \frac{d}{dt}\left(\boldsymbol{u}_\Omega(t)\cdot\boldsymbol{w}_k(t)\right)dxdt\\ &= \int_0^{t_s}\frac{d}{dt}\|\boldsymbol{u}_\Omega(t)\|_{L^2(\Omega)}dt\\ &= \|\boldsymbol{u}_\Omega(t_s)\|_{L^2(\Omega)}\,. \end{aligned} \tag{5.23}$$

It can be easily seen that E is a bilinear and symmetric form, therefore equation (5.22) we have :

$$\begin{aligned}\lim_{k\to\infty} E(\boldsymbol{w}_k-\boldsymbol{u}_{\boldsymbol{\Omega}},\boldsymbol{w}_k-\boldsymbol{u}_{\boldsymbol{\Omega}}) &= \lim_{k\to\infty}\left[E(\boldsymbol{w}_k,\boldsymbol{w}_k) - 2E(\boldsymbol{w}_k,\boldsymbol{u}_{\boldsymbol{\Omega}}) + E(\boldsymbol{u}_{\boldsymbol{\Omega}},\boldsymbol{u}_{\boldsymbol{\Omega}})\right]\\ &= \lim_{k\to\infty} 2\left[E(\boldsymbol{u}_{\boldsymbol{\Omega}},\boldsymbol{u}_{\boldsymbol{\Omega}}) - E(\boldsymbol{w}_k,\boldsymbol{u}_{\boldsymbol{\Omega}})\right]\,. \end{aligned} \tag{5.24}$$

From equation (5.23) and since $\boldsymbol{w}_k \rightharpoonup \boldsymbol{w}^*$ we have:

$$\begin{aligned}\lim_{k\to\infty} E(\boldsymbol{w}_k, \boldsymbol{u}_{\boldsymbol{\Omega}}) &= \lim_{k\to\infty} \left[\int_\Omega \boldsymbol{u}(t_s)\cdot \boldsymbol{u}_{\boldsymbol{\Omega}}(t_s)dx + 2\int_0^{t_s}\int_\Omega \nabla \boldsymbol{u}(t)\cdot\nabla \boldsymbol{u}_{\boldsymbol{\Omega}}(t)\,dx\,dt\right] \\ &= \|\boldsymbol{u}_\Omega(t_s)\|^2_{L^2(\Omega)} + 2\int_0^{t_s} \|\nabla \boldsymbol{u}_\Omega(t_s)\|^2_{\boldsymbol{L}^2(\Omega)}dt \\ &= E(\boldsymbol{u}_{\boldsymbol{\Omega}}, \boldsymbol{u}_{\boldsymbol{\Omega}})\,. \end{aligned} \tag{5.25}$$

It follows from equations (5.24) and (5.25) that:

$$\lim_{k\to\infty} E(\boldsymbol{w}_k - \boldsymbol{u}_{\boldsymbol{\Omega}}, \boldsymbol{w}_k - \boldsymbol{u}_{\boldsymbol{\Omega}}) = 0\,.$$

This implies that for any $t_s \in [0,T]$ we have:

$$\lim_{k\to\infty}\left[\|\boldsymbol{w}_k(t_s) - \boldsymbol{u}_{\boldsymbol{\Omega}}(t_s)\|^2_{L^2(\Omega)} + 2\int_0^{t_s}\|\nabla \boldsymbol{w}_k(t) - \nabla \boldsymbol{u}_{\boldsymbol{\Omega}}(t)\|^2_{\boldsymbol{L}^2(\Omega)}dt\right] = 0 \tag{5.26}$$

Setting $t_s = T$, and by remark 5.1.2 we know that $\|\nabla \boldsymbol{u}_\Omega\|_{L^2(\boldsymbol{L^2}(\Omega))}$ is an equivalent norm of $\|\boldsymbol{u}_\Omega\|_{L^2(\boldsymbol{V}(\Omega))}$therefore:

$$\boldsymbol{w}_k \to \boldsymbol{u}_{\boldsymbol{\Omega}} \text{ in } \boldsymbol{L}^2(\boldsymbol{V}(\Omega))$$

□

5.4 Pressure weak continuity with respect to the domain

In this section, we present the main result that establishes the strong continuity of the pressure with respect to converging sets under diffeomorphisms. The focus is on understanding how the pressure field behaves when the underlying set undergoes convergence through diffeomorphisms. By studying this continuity property, we gain valuable insights into the behavior and stability of the pressure field in fluid flow problems under varying geometries.

Remark 5.4.1. Before presenting the continuity result of the pressure, we recall that the gradient operator is an isomorphism between $L^2(\Omega)/\mathbb{R}$ and $\boldsymbol{H}^{-1}(\Omega) = \boldsymbol{H}^1_0(\Omega)'$ (refer to [61, Proposition 1.2 (ii)] or [9, Proposition 2.10]). Hence, we have the following inequality:

$$\inf_{c\in\mathbb{R}} \|p + c\|_{L^2(\Omega)} = \|p\|_{L^2(\Omega)/\mathbb{R}} \le C(\Omega)\|\nabla p\|_{H^{-1}(\Omega)}\,. \tag{5.27}$$

In particular, if $p \in L^2_0(\Omega)$, we have $\|p\|_{L^2(\Omega)} = \inf_{c\in\mathbb{R}} \|p + c\|_{L^2(\Omega)}$. Thus, for $p, q \in L^2_0(\Omega)$, using inquality (5.27), we obtain:

$$\|p - q\|_{L^2(\Omega)} \leq C(\Omega)\|\nabla p - \nabla q\|_{H^{-1}(\Omega)}\,.$$

Theorem 5.4.2. *Let $\{p_k\} \in L^2(L^2_0(\Omega_k))$ be a sequence the pressure solution of the Stokes problem and define $\boldsymbol{w}_k = \boldsymbol{u}_k \circ \psi_k$, $q_k = p_k \circ \psi_k$. Suppose following assumption hold:*

1. $\psi_k(\Gamma^k_N) = \Gamma_N$,
2. $\boldsymbol{f_k} \in L^2\left(\boldsymbol{L}^2(\Omega_k)\right)$ *such that* $\boldsymbol{f}_k \circ \psi_k \to \boldsymbol{f} \in L^2\left(\boldsymbol{L}^2(\Omega)\right)$,
3. $\boldsymbol{h_k} \in L^2\left(\boldsymbol{L}^2(\Gamma^k_N)\right)$ *such that* $\boldsymbol{h}_k \circ \psi_k \to \boldsymbol{h} \in L^2\left(\boldsymbol{L}^2(\Gamma_N)\right)$.

Then $\nabla\widehat{q_k} \rightharpoonup *\nabla p_\Omega$ with in $L^2(H^{-1}(\Omega))$.

Proof. First lets define $\widehat{q_k} = q_k - \overline{q_k}$, where $\overline{q_k} = |\Omega|^{-1}\langle q_k, 1\rangle$, therefore remark 5.4.1 we only need to prove the convergence of the operators $\nabla\widehat{q_k} \rightharpoonup^* \nabla p_\Omega$ in $L^2(H^{-1}(\Omega))$.

By theorem 5.2.2, we know p_k is a bounded sequence in $L^2(L^2_0(\Omega_k))$. Consequently, by 5.2.1, q_k is also a bounded sequence in $L^2(L^2_0(\Omega))$. Therefore by the banach–alaoglu theorem any subsequence of q_k possesses a further sub-subsequence that weakly converges to some q^* in $L^2(L^2(\Omega))$. Given that $q_k \rightharpoonup q^*$ and $J(\psi_k) \to 1$ in $L^2(\Omega)$, we can observe the following:

$$\begin{aligned}\int_\Omega q^* dx &= \lim_{k\to\infty}\int_\Omega q_k J(\psi_k) dx \\ &= \lim_{k\to\infty}\int_{\Omega_k} p_k dx \\ &= 0\,.\end{aligned}$$

Now we take $\phi(t)\boldsymbol{h}(x)$ from $\mathcal{D}(0,T)\cdot\boldsymbol{H}^1_0(\Omega)$. Then we define $\boldsymbol{h}_k$ as $\boldsymbol{h}\circ\psi_k^{-1}$. According to Proposition 5.2.8, it's clear that $\boldsymbol{h}_k$ is in $\boldsymbol{H}^1_0(\Omega_k)$. Now, if we take M_k to be $\nabla\psi_k^{-t}$, we can notice that:

$$\int_0^T \phi \int_{\Omega_k} p_k \operatorname{div}(\boldsymbol{h}_k)\, dxdt = \int_0^T \phi \int_\Omega q_k Tr(M_k \nabla \boldsymbol{h})\, dxdt\,.$$

Given that the trace operator, Tr, is linearly continuous from $(L^2(\Omega))^{d\times d}$ to $L^2(\Omega)$ and that $M_k\nabla\boldsymbol{h} \to \nabla\boldsymbol{h}$ in $(L^2(\Omega))^{d\times d}$, we can apply the limit to both sides to obtain:

$$\lim_{k\to\infty}\int_0^T \phi \int_{\Omega_k} p_k \operatorname{div}(\boldsymbol{h}_k)\, dxdt = \int_0^T \phi \int_\Omega q^* \operatorname{div}(\boldsymbol{h})\, dxdt\,. \tag{5.28}$$

Next, let's apply integration by parts to equation (5.1):

$$\begin{aligned}\int_0^T \phi \int_{\Omega_k} p_k \operatorname{div}(\boldsymbol{h}_k)\, dxdt &= \int_0^T \int_{\Omega_k} \phi' \boldsymbol{w}_k \cdot \boldsymbol{h} + \phi \nabla \boldsymbol{u_k} : \nabla \boldsymbol{h_k} dxdt \\ &\quad - \int_0^T \int_{\Omega_k} \phi \boldsymbol{f}_k \cdot \boldsymbol{h_k}\, dxdt \\ &= \int_0^T \int_{\Omega} \phi' \boldsymbol{w}_k \cdot \boldsymbol{h}\, J(\psi_k) + \phi M_k \nabla \boldsymbol{u_k} : M_k \nabla \boldsymbol{h_k} J(\psi_k) dxdt \\ &\quad - \int_0^T \int_{\Omega} \phi \widehat{\boldsymbol{f}_k} \cdot \boldsymbol{h}\, J(\psi_k) dxdt\,.\end{aligned} \tag{5.29}$$

By utilizing equation (5.28) and taking the limit in (5.29), we can deduce:

$$\begin{aligned}\int_0^T \phi \int_{\Omega} q^* \operatorname{div}(\boldsymbol{h})\, dxdt &= -\int_0^T \int_{\Omega} \phi' \boldsymbol{u}_{\Omega} \cdot \boldsymbol{h} + \phi \nabla \boldsymbol{u_\Omega} : \nabla \boldsymbol{h}\, dx - \int_0^T \phi \int_{\Omega} \boldsymbol{f} \cdot \boldsymbol{h}\, dxdt \\ &= \int_0^T \phi \int_{\Omega} p_{\Omega} \operatorname{div}(\boldsymbol{h})\, dxdt\,.\end{aligned}$$

This leads us to infer that $\nabla \widehat{q_k} \rightharpoonup * \nabla p_{\Omega}$ in the space $L^2(H^{-1}(\Omega))$.

□

6 Global divergence free–RBF methods for evolutionary Stokes problems

This chapter presents the development of a Radial Basis Function (RBF) method, specifically designed for the evolutionary Stokes problem. Drawing from the divergence-free RBF approximation framework introduced by Wendland [65], our approach integrates global Inverse Multiquadric (IMQ) RBFs into our spatial discretization strategy. We apply both Dirichlet and Navier-slip boundary conditions to a non-convex, particularly a star-shaped, domain. For all numerical exemplifications, numerical extended precision is utilized.

Additionally, a thorough stability analysis of the relevant Gram matrix is conducted. Our numerical results indicate that all real components of its eigenvalues are consistently negative. This observation supports the idea that our use of backward differentiation formulas will achieve iterative convergence, exhibiting exponential convergence in space and algebraic convergence in time. This behavior is substantiated through a suite of numerical examples.

Let $\Omega \subset \mathbb{R}^d$ be a bounded and Lipschitz domain, and we define $Q = \Omega \times (0, T)$, $\Sigma = \partial\Omega \times (0, T)$. Let $\boldsymbol{\mathcal{L}}(\boldsymbol{u}, p) = (\mathcal{L}_1(\boldsymbol{u}, p), ..., \mathcal{L}_d(\boldsymbol{u}, p))$ where $\mathcal{L}_i(\boldsymbol{u}, p) = -\mu\Delta u_i + \frac{\partial p}{\partial x_i}$, and consider the following system:

$$\begin{cases} \boldsymbol{u}_t + \boldsymbol{\mathcal{L}}(\boldsymbol{u}, p) = \boldsymbol{f} & \text{in} \quad Q, \\ \operatorname{div} \boldsymbol{u} = 0 & \text{in} \quad Q, \\ \boldsymbol{\mathcal{B}}(\boldsymbol{u}, p) = \boldsymbol{g} & \text{on} \quad \Sigma, \\ \boldsymbol{u}(\cdot, 0) = \boldsymbol{u}_0(\cdot) & \text{in} \quad Q, \end{cases} \tag{6.1}$$

Here $\boldsymbol{\mathcal{B}} = (\mathcal{B}_1, ..., \mathcal{B}_d)$ are given boundary operators. Notice that for Dirichlet boundary conditions, we have $\boldsymbol{B}_i(\boldsymbol{u}, p) = u_i$, while for the Navier-slip boundary conditions, we have:

$$\begin{cases} \mathcal{B}_i(\boldsymbol{u}, p) = u_i \cdot n_i & i = 1 \dots d-1, \\ \mathcal{B}_d \boldsymbol{u} := (\sigma(\boldsymbol{u}, p)\boldsymbol{n})_{tg}. \end{cases}$$

6.1 Collocation method and backward differentiation formula

Before delving into the specifics of our methodology, we introduce a pertinent theorem that will play a crucial role in our discussions. As we proceed, this theorem will guide us in laying out the specifics of the Radial Basis Function (RBF) ansatz and the generalized interpolation collocation method, as described in [64]:

Theorem 6.1.1. *Let's suppose that $\mathbf{\Phi} : \Omega \subseteq \mathbb{R}^d \to \mathbb{R}^{n\times n}$ is a positive definite, matrix-valued kernel. Further, consider that $\lambda_1, \ldots, \lambda_N \in \mathcal{N}\Phi(\Omega)^*$ are linearly independent and $f_1, \ldots, f_N \in \mathbb{R}$ are given. Here, $\mathcal{N}_\Phi(\Omega)$ represents the native space of the positive definite matrix-valued kernel $\mathbf{\Phi}$.*
Then, the problem of finding the solution of

$$\min\left\{\|\mathbf{s}\|_{\mathcal{N}_{\mathbf{\Phi}}(\Omega)} : \lambda_j(\mathbf{s}) = f_j, 1 \leq j \leq N\right\}$$

has a unique solution, which has the representation:

$$\mathbf{s}_\Lambda = \sum_{j=1}^{N} \alpha_j \lambda_j^{\mathbf{y}} \mathbf{\Phi}(\cdot - \mathbf{y}).$$

Here $\lambda^{\mathbf{y}}\mathbf{\Phi}(\mathbf{x}-\mathbf{y})$ is a vector-valued function, which is generated by applying λ with respect to $\mathbf{y}$ to every row of $\mathbf{\Phi}$. The coefficients α_j are determined via the interpolation conditions $\lambda_i(\mathbf{s}_\Lambda) = f_i, 1 \leq i \leq N$.

Our objective is to create a PDE operator by approximating the temporal derivative using a finite difference method while employing a divergence-free matrix value kernel for the spatial operators. To do this, we start by defining the divergence-free RBF as follows:

Definition 6.1.2. The divergence-free matrix-valued kernel is defined by:

$$\mathbf{\Phi}_{\text{Div}} = -\Delta I + \nabla\nabla^T \psi,$$

where Δ denotes the Laplace operator, I is the identity matrix, $\nabla\nabla^T$ denotes the Hessian matrix, and ψ represents a positive definite radial basis function.

The following time scheme takes inspiration from some concepts presented by Stevens et al. [60]. To elucidate this method, we utilize backward finite difference

techniques, which are aptly suited for ordinary differential-algebraic equations. The scheme at any given time step for the system (6.1) is:

$$\begin{cases} u_i^{n+s} + (\Delta t)\beta_s \boldsymbol{\mathcal{L}}_i(\boldsymbol{u}^{n+s}, p^{n+s}) = (\Delta t)\beta_s f_i^{n+s} + \sum_{k=0}^{s-1} \sigma_k u_i^{n+k} & \text{in } \Omega, \\ \operatorname{div} \boldsymbol{u}^{n+s} = 0 & \text{in } \Omega, \quad i \in \{1, ..., d\}. \\ \boldsymbol{\mathcal{B}_i}(\boldsymbol{u}^{n+s}, p^{n+s}) = g_i^{n+s} & \text{on } \partial\Omega, \end{cases} \tag{6.2}$$

where β_s, σ_k are known parameters defined by the BDF techniques. Thus, in each step we solve the following PDE:

$$\begin{cases} \overline{\boldsymbol{\mathcal{L}}}_i(\boldsymbol{u}^{n+s}, p^{n+s}) = \overline{f}_i^{n+s} & \text{in } \Omega, \\ \operatorname{div} \boldsymbol{u}^{n+s} = 0 & \text{in } \Omega, \quad i \in \{1, ..., d\} \\ \boldsymbol{\mathcal{B}}_i(\boldsymbol{u}^{n+s}, p^{n+s}) = g_i^{n+s} & \text{on } \partial\Omega. \end{cases} \tag{6.3}$$

where $\overline{\boldsymbol{\mathcal{L}}_i}$, $\overline{f}_i^{n+s}$ are defined by:

$$\begin{aligned} \overline{\boldsymbol{\mathcal{L}}}_i(\boldsymbol{u}^{n+s}, p^{n+s}) &= u^{n+s} + \Delta t\, \beta_s\, \boldsymbol{\mathcal{L}}_i(\boldsymbol{u}^{n+s}, p^{n+s}), \\ \overline{f}_i^{n+s} &= \Delta t\, \beta_s\, \boldsymbol{f}^{n+s} + \sum_{k=0}^{s-1} \sigma_k \boldsymbol{u}^{n+k}. \end{aligned}$$

To implement a collocation discretization of this equation system utilizing divergence-free kernels as in [64], we establish the following matrix-valued kernel:

$$\boldsymbol{\Phi} = \begin{bmatrix} \boldsymbol{\Phi}_{Div} & 0 \\ 0 & \psi \end{bmatrix} : \mathbb{R}^d \to \mathbb{R}^{(d+1)\times(d+1)}, \tag{6.4}$$

Subsequently, we introduce N_{int} and N_b node sets, termed as RBF centers, represented by ${\boldsymbol{\xi_j}}^{int}$ and ${\boldsymbol{\xi_j}}^{b}$ respectively. Here, ${\boldsymbol{\xi_j}}^{b} \in \partial\Omega$ and ${\boldsymbol{\xi_j}}^{int} \in \Omega$. Further, we define an array of operators from $\mathbb{R}^{d+1} \to \mathbb{R}$ as follows:

$$\begin{cases} \overline{\boldsymbol{\mathcal{L}}}_{ij} = \overline{\boldsymbol{\mathcal{L}}}_i(\boldsymbol{u}, p)|_{{\boldsymbol{\xi_j}}^{int}} & i \in \{1, \dots d\}, j \in \{1, \dots, N_{int}\} \\ \boldsymbol{\mathcal{B}}_{ij} = \boldsymbol{\mathcal{B}}_i(\boldsymbol{u}, p)|_{{\boldsymbol{\xi_j}}^{b}} & i \in \{1, \dots d\}, j \in \{1, \dots, N_b\} \end{cases} \tag{6.5}$$

Hence, utilizing Theorem 6.1.1, we derive the following ansatz:

$$\begin{aligned} (\widehat{\boldsymbol{u}}^{n+s}, \widehat{p}^{n+s})(\boldsymbol{x}) = &\sum_{i=1}^{d} \sum_{j=1}^{N_{int}} \overline{\mathcal{L}}_i^{\boldsymbol{\xi}} \boldsymbol{\Phi}(\boldsymbol{x} - \boldsymbol{\xi_j^{int}}) \alpha_{ij}^{n+s} \\ &+ \sum_{i=1}^{d} \sum_{j=1}^{N_b} \mathcal{B}_i^{\boldsymbol{\xi}} \boldsymbol{\Phi}(\boldsymbol{x} - \boldsymbol{\xi_j^b}) \beta_{ij}^{n+s} \end{aligned}. \tag{6.6}$$

Here, $\overline{\mathcal{L}}_i^{\boldsymbol{\xi}}\boldsymbol{\Phi}$ and $\mathcal{B}_i^{\boldsymbol{\xi}}\boldsymbol{\Phi}$ denote vector-valued functions mapping from $\mathbb{R}^d$ to $\mathbb{R}^{d+1}$, created by applying the operators $\overline{\mathcal{L}}_i^{\boldsymbol{\xi}}$ and $\mathcal{B}_i^{\boldsymbol{\xi}}$ to each row of the kernel $\boldsymbol{\Phi}$. This ansatz approximates our velocity-pressure solution at each time step as a linear combination of function values at the RBF centers, using the coefficients α and β, which are to be determined and correspond to the interior and boundary RBF centers, respectively.

Incorporating the ansatz (6.6) into the following system:

$$\begin{cases} \overline{\boldsymbol{\mathcal{L}}}_i(\widehat{\boldsymbol{u}}^{n+s}, \widehat{p}^{n+s})|_{{\boldsymbol{\xi}_j}^{int}} = \overline{f}_i^{n+s}({\boldsymbol{\xi}_j}^{int}) & i \in \{1, \dots d\}, j \in \{1, \dots, N_{int}\}, \\ \boldsymbol{\mathcal{B}}_i(\widehat{\boldsymbol{u}}^{n+s}, \widehat{p}^{n+s})|_{{\boldsymbol{\xi}_j}^{b}} = g_i^{n+s}({\boldsymbol{\xi}_j}^{b}) & i \in \{1, \dots d\}, j \in \{1, \dots, N_b\}. \end{cases}$$

The above system of equations can be represented in matrix form as follows:

$$H_+ \begin{pmatrix} \boldsymbol{\alpha}^{n+s} \\ \boldsymbol{\beta}^{n+s} \end{pmatrix} = \begin{pmatrix} \overline{\boldsymbol{f}}^{n+s} \\ \boldsymbol{g}^{n+s} \end{pmatrix}, \tag{6.7}$$

where the vectors $\left(\boldsymbol{\alpha}^{n+s}, \boldsymbol{\beta}^{n+s}\right)$ belong to $\mathbb{R}^{d(N_{int}+N_b)}$, indicating the stacking of the unknown coefficients corresponding to each time step. H_+ is the collocation matrix, belonging to $\mathbb{R}^{d(N_{int}+N_b)\times d(N_{int}+N_b)}$, that encodes the discretized system. Its construction is detailed as follows:

$$H_+ = \begin{bmatrix} H_{11} & H_{12} \\ H_{21} & H_{22} \end{bmatrix}, \tag{6.8}$$

where $H_{11} \in \mathbb{R}^{dN_{int}\times dN_{int}}$, $H_{12} \in \mathbb{R}^{dN_{int}\times dN_b}$, $H_{21} \in \mathbb{R}^{dN_b\times dN_{int}}$ and $H_{22} \in \mathbb{R}^{dN_b\times dN_b}$. Specifically, the ij-th block of each submatrix is given by:

$$\begin{aligned} H_{11}(i,j) &= \overline{\boldsymbol{\mathcal{L}}}_i^x \overline{\boldsymbol{\mathcal{L}}}_j^{\xi} \boldsymbol{\Phi}(\boldsymbol{\xi}^{int} - \boldsymbol{\xi}^{int}), \quad H_{12}(i,j) = \overline{\boldsymbol{\mathcal{L}}}_i^x \boldsymbol{\mathcal{B}}_j^{\xi} \boldsymbol{\Phi}(\boldsymbol{\xi}^{int} - \boldsymbol{\xi}^{b}), \\ H_{21}(i,j) &= \boldsymbol{\mathcal{B}}_i^x \overline{\boldsymbol{\mathcal{L}}}_j^{\xi} \boldsymbol{\Phi}(\boldsymbol{\xi}^{b} - \boldsymbol{\xi}^{int}), \quad H_{22}(i,j) = \boldsymbol{\mathcal{B}}^x \boldsymbol{\mathcal{B}}^{\xi} \boldsymbol{\Phi}(\boldsymbol{\xi}^{b} - \boldsymbol{\xi}^{b}). \end{aligned}$$

6.1.1 Stability analysis for BDF schemes

In the subsequent subsection, we will conduct a stability analysis for the scheme outlined previously. Our methodology employs a matrix-based method mirroring the process detailed in [25]. The aim is to devise a condition that enables the approximation of the Gram matrix's spectral radius. We designate the set of interior nodes as $(\boldsymbol{\xi}_{\boldsymbol{i}}^{\boldsymbol{int}})_{i=1}^{N_{int}}$ and the boundary nodes set as $(\boldsymbol{\xi}_{\boldsymbol{i}}^{\boldsymbol{b}})_{i=1}^{N_b}$. Furthermore, we introduce the standard canonical projection $I_i : \mathbb{R}^{d+1} \to \mathbb{R}$ to access the j-th coordinate of a vector in $\mathbb{R}^{d+1}$.

With this operator, we define the interpolation matrix $A \in \mathbb{R}^{d(N_{int}+N_b)\times d(N_{int}+N_b)}$ such that:

$$A\begin{pmatrix} \boldsymbol{\alpha}^{n+s} \\ \boldsymbol{\beta}^{n+s} \end{pmatrix} = \left(u_1^{n+s}(\boldsymbol{\xi}_1^{int}), \ldots, u_d^{n+s}(\boldsymbol{\xi}_{N_{int}}^{int}), u_1^{n+s}(\boldsymbol{\xi}_1^{b}), \ldots, u_d^{n+s}(\boldsymbol{\xi}_{N_b}^{b})\right)^T, \quad (6.9)$$

In essence, the matrix A functions as a linear operator that transforms the solution coefficients into the corresponding solution values at the prescribed nodes. This is formally given by:

$$A = \begin{bmatrix} A_{11} & A_{12} \\ A_{21} & A_{22} \end{bmatrix},$$

where $A_{11} \in \mathbb{R}^{dN_{int}\times dN_{int}}, A_{12} \in \mathbb{R}^{dN_{int}\times dN_b}, A_{21} \in \mathbb{R}^{dN_b\times dN_{int}}$ and $A_{22} \in \mathbb{R}^{dN_b\times dN_b}$. Specifically, the ij-th block of each submatrix is given by:

$$A_{11}(i,j) = I_i^x \overline{\boldsymbol{\mathcal{L}}}_j^{\xi} \boldsymbol{\Phi}(\boldsymbol{\xi}^{\boldsymbol{int}} - \boldsymbol{\xi}^{\boldsymbol{int}}), \quad A_{12}(i,j) = I_i^x \boldsymbol{\mathcal{B}}_j^{\xi} \boldsymbol{\Phi}(\boldsymbol{\xi}^{\boldsymbol{int}} - \boldsymbol{\xi}^{\boldsymbol{b}}),$$
$$A_{21}(i,j) = I_i^x \overline{\boldsymbol{\mathcal{L}}}_j^{\xi} \boldsymbol{\Phi}(\boldsymbol{\xi}^{\boldsymbol{b}} - \boldsymbol{\xi}^{\boldsymbol{int}}), \quad A_{22}(i,j) = I_i^x \boldsymbol{\mathcal{B}}_j^{\xi} \boldsymbol{\Phi}(\boldsymbol{\xi}^{\boldsymbol{b}} - \boldsymbol{\xi}^{\boldsymbol{b}}).$$

Setting $A = \begin{pmatrix} A_{int} \\ A_b \end{pmatrix}$, we define $H_- = \begin{pmatrix} A_{int} \\ 0 \end{pmatrix}$, thus from equations (6.7) and (6.2) we obtain:

$$H_+ \begin{pmatrix} \boldsymbol{\alpha}^{n+s} \\ \boldsymbol{\beta}^{n+s} \end{pmatrix} = H_- \sum_{k=0}^{s-1} \sigma_k \begin{pmatrix} \boldsymbol{\alpha}^{n+s} \\ \boldsymbol{\beta}^{n+s} \end{pmatrix} + \begin{pmatrix} \overline{\boldsymbol{f}}^{n+s} \\ \boldsymbol{g}^{n+s} \end{pmatrix}.$$

Thus, it follows that:

$$\widehat{\boldsymbol{u}}^{n+s} = AH_+^{-1}H_-A^{-1} \sum_{k=0}^{s-1} \sigma_k \boldsymbol{u}^{n+s} + AH_+^{-1} \begin{pmatrix} \overline{\boldsymbol{f}}^{n+s} \\ \boldsymbol{g}^{n+s} \end{pmatrix}.$$

Denoting by $\boldsymbol{u}^n$ the exact solution and by $\widehat{\boldsymbol{u}}^n$ the numerical solution, the error $\boldsymbol{e}^n = \boldsymbol{u}^n - \widehat{\boldsymbol{u}}^n$ satisfies the equation:

$$\boldsymbol{e}^{n+s} = K \sum_{k=0}^{s-1} \sigma_k \boldsymbol{e}^{n+k} + E_{n+s},$$

where E_{n+s} denotes the local error in the scheme as depicted in Equation (6.7) and K represents $AH_+^{-1}H_-A^{-1}$. In addition, given that E_{n+s} is small and thus can be ignored, we can explore the error analysis employing the following identity:

$$\boldsymbol{e}^{n+s} = K \sum_{k=0}^{s-1} \sigma_k \boldsymbol{e}^{n+k}. \quad (6.10)$$

By assuming that K is diagonalizable, i.e., $K = D^{-1}\Lambda D$, we can define $\boldsymbol{z}^n := D\boldsymbol{e}^n$ and therefore (6.10) is equivalent to:

$$\boldsymbol{z}^{n+s} = \Lambda \sum_{k=0}^{s-1} \sigma_k \boldsymbol{z}^{n+k}.$$

Given that Λ is a diagonal matrix, it holds for every $j = 1, \ldots, d(N_b + N_{int})$ that $z_j^{n+s} = \sum_{k=0}^{s-1} \lambda_j \sigma_k z_j^{n+k}$. The solution to this is given by $z_j^n = \sum_{k=0}^{s-1} C_k^j r_k^n$, where C_k^j are complex constants and r_k are the roots of the polynomial associated with the finite difference method.

Ultimately, as $|\boldsymbol{e}^n|$ approaches zero if and only if $|\boldsymbol{z}^n|$ does so, the stability of the method is ensured as long as the eigenvalues of K are within the stability region of:

$$\pi(r, \lambda) = r^s - \sum_{k=0}^{s-1} \lambda \sigma_k r^i. \tag{6.11}$$

As a consequence of the boundary locus technique [46], some stability regions are displayed in Figure 6.1.

By employing the boundary locus method, as presented in [46], we can visualize some stability regions, which are depicted in Fig. 1.

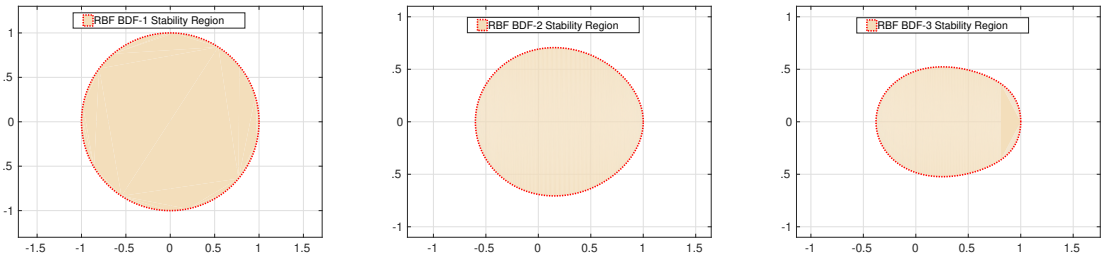

(a) One level **(b)** Two levels **(c)** Three levels

Figure 6.1: Stability regions using backward finite formula.

6.1.2 Numerical experiments

In the following subsection, we examine the precision of the BDF2-based scheme introduced earlier, taking into account either non-homogeneous Dirichlet or non-homogeneous Navier-slip boundary conditions on the system as described in (6.1).

To generate the divergence-free kernel, consistent with Definition 6.1.2, we employ the scalar inverse multiquadric (IMQ) function $\psi(\boldsymbol{r}) = \sqrt{1+cr^2}^{-1}$, setting the shape parameter $c = 1.5$. Given the ill-conditioned nature of this kernel, we leverage the high-precision computation capabilities of the ADVANPIX Matlab package, working with a precision of 50 digits. The entirety of these computations are executed in the Matlab and FreeFem++ programming environments.

We now focus on a nonconvex, star-shaped domain $\Omega \subset \mathbb{R}^2$ with its boundary defined by the parametrized curve in (6.12) (refer to Figure 6.2). The curve specification is as follows:

$$C = \Big\{(\theta, \rho(\theta)) \in \mathbb{R}^2 : \rho(\theta) = 0.8 + sin(6\theta) + sin(3\theta), \quad \theta \in [0, 2\pi)\Big\}. \tag{6.12}$$

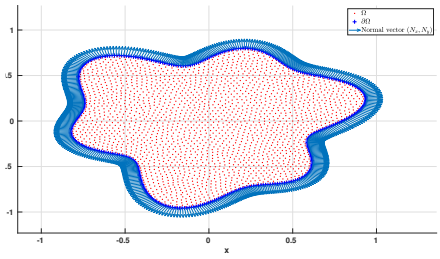

Figure 6.2: Domain $\Omega \subset \mathbb{R}^2$. The boundary is defined by the parametrization given in (6.12)

We consider the following exact solution of (6.1) for both types of boundary conditions (Dirichlet or Navier–slip):

$$\begin{aligned} u_1(x,y,t) &= -y\,\sin\Big((x^2+y^2)\sin(t^2+1)\Big)\,, \\ u_2(x,y,t) &= x\,\sin\Big((x^2+y^2)\sin(t^2+1)\Big)\,, \\ p(x,y,t) &= \sin(x-y+t). \end{aligned}$$

We evaluate the L^∞-norm error for velocity and pressure, comparing the exact solution with the numerical approximation for varying time steps, Δt. The errors are represented by $\boldsymbol{\epsilon_y} = \boldsymbol{u}_{exact} - \boldsymbol{u}_{approx}$ for velocity and $\boldsymbol{\nabla \epsilon_p} = \nabla p_{exact} - \nabla p_{approx}$ for pressure. Results for both Navier-slip and Dirichlet boundary conditions are compiled in Table 6.1 and Table 6.2, respectively.

As anticipated, it is observed that the error decreases as the number of nodes increases, consistent with expectations. Additionally, the velocity converges at

a higher rate compared to the convergence rate of the pressure gradient, which aligns with the expected behavior. The obtained results demonstrate exceptional accuracy for both Dirichlet and Navier-slip boundary conditions, irrespective of the μ value. Furthermore, it is evident that the eigenvalues of the Gram matrix lie within the stability region of the BDF schemes; otherwise, the solution would not converge. However, it has been noted from numerical experiments that this does not hold true for small values of the shape parameter, specifically $c \leq 10^{-2}$.

$\mu = 1$

$N\backslash\Delta t$	1.00e-02		5.00e-03		1.00e-03		5.00e-04		Max Cond
	$\|\|e_y\|\|_\infty$	$\|\|e_{\nabla p}\|\|_\infty$	$\|\|e_y\|\|_\infty$	$\|\|e_{\nabla p}\|\|_\infty$	$\|\|e_y\|\|_\infty$	$\|\|e_{\nabla p}\|\|_\infty$	$\|\|e_y\|\|_\infty$	$\|\|e_{\nabla p}\|\|_\infty$	
117	5.94e-03	6.32e-01	6.47e-03	6.44e-01	7.87e-03	5.52e-01	8.17e-03	4.86e-01	1.55e+21
290	1.34e-03	4.39e-01	1.38e-03	3.90e-01	2.54e-03	5.41e-01	3.38e-03	7.23e-01	1.71e+21
576	2.08e-03	5.31e-01	5.72e-04	1.45e-01	4.62e-05	2.10e-02	4.46e-05	2.06e-02	9.35e+22

$\mu = 1e-06$

$N\backslash\Delta t$	1.00e-02		5.00e-03		1.00e-03		5.00e-04		Max Cond
	$\|\|e_y\|\|_\infty$	$\|\|e_{\nabla p}\|\|_\infty$	$\|\|e_y\|\|_\infty$	$\|\|e_{\nabla p}\|\|_\infty$	$\|\|e_y\|\|_\infty$	$\|\|e_{\nabla p}\|\|_\infty$	$\|\|e_y\|\|_\infty$	$\|\|e_{\nabla p}\|\|_\infty$	
117	5.22e-02	2.96e-01	4.15e-02	2.09e-01	1.88e-02	2.16e-01	2.32e-02	3.29e-01	6.22e+28
290	2.06e-03	1.43e-02	1.49e-03	1.36e-02	9.33e-04	6.22e-03	8.68e-04	4.40e-03	8.99e+28
576	2.33e-03	1.76e-02	5.80e-04	5.45e-03	2.88e-05	2.39e-04	9.25e-06	1.54e-04	3.34e+29

Table 6.1: Global Hermite collocation–IMQ error for the Stokes system with Navier–slip boundary conditions. Here, the shape parameter is c=1.5

$\mu = 1$

$N\backslash\Delta t$	1.00e-02		5.00e-03		1.00e-03		5.00e-04		Max Cond
	$\|\|e_y\|\|_\infty$	$\|\|e_{\nabla p}\|\|_\infty$	$\|\|e_y\|\|_\infty$	$\|\|e_{\nabla p}\|\|_\infty$	$\|\|e_y\|\|_\infty$	$\|\|e_{\nabla p}\|\|_\infty$	$\|\|e_y\|\|_\infty$	$\|\|e_{\nabla p}\|\|_\infty$	
117	7.04e-03	8.31e-01	6.67e-03	7.66e-01	5.36e-03	5.26e-01	5.16e-03	5.80e-01	3.94e+19
290	9.63e-04	3.57e-01	9.83e-04	3.61e-01	9.71e-04	3.47e-01	9.29e-04	3.25e-01	3.85e+19
576	5.82e-04	1.83e-01	1.65e-04	6.26e-02	4.22e-05	1.76e-02	4.02e-05	1.67e-02	7.48e+20

$\mu = 1e-06$

$N\backslash\Delta t$	1.00e-02		5.00e-03		1.00e-03		5.00e-04		Max Cond
	$\|\|e_y\|\|_\infty$	$\|\|e_{\nabla p}\|\|_\infty$	$\|\|e_y\|\|_\infty$	$\|\|e_{\nabla p}\|\|_\infty$	$\|\|e_y\|\|_\infty$	$\|\|e_{\nabla p}\|\|_\infty$	$\|\|e_y\|\|_\infty$	$\|\|e_{\nabla p}\|\|_\infty$	
117	2.40e-02	2.34e-01	2.39e-02	1.95e-01	2.98e-02	4.12e-01	3.52e-02	5.60e-01	8.11e+19
290	1.77e-03	1.01e-02	1.05e-03	8.88e-03	7.99e-04	3.69e-03	7.84e-04	3.30e-03	1.68e+20
576	1.90e-03	1.35e-02	4.77e-04	4.00e-03	2.26e-05	1.92e-04	1.47e-05	1.31e-04	1.65e+21

Table 6.2: Global Hermite collocation–IMQ error for the Stokes system with Dirichlet boundary conditions. Here, the shape parameter is c=1.5

7 LHI divergence free–RBF methods for Stokes problems

In this chapter, we present an alternative method for the evolutionary Stokes system, which is a RBF-LHI vectorial technique. This method is a generalization of the local Hermite interpolation (LHI) scalar method, as described in [60]. Additionally, we introduce a vectorial generalization of a recent scalar method that uses hybrid kernels, which are called the RBF-Hybrid method and are discussed in [52].

The organization of this section is as follows: In subsection 7.1, we review some concepts and notation for the scalar LHI method, as described in [39]. Next, in subsection 7.2, we present the numerical algorithm for the steady Stokes system, while subsection 7.3 displays numerical examples with different types of boundary conditions. These examples demonstrate that the RBF-LHI method can handle up to 23,000 nodes and produce excellent results.

However, the eigenvalues of the matrix for Div-free IMQ kernels can have positive real eigenvalue components, which makes them unsuitable for evolutionary problems. To address this issue, we introduce vectorial Div-free hybrid kernels and formulate the evolutionary Stokes LHI method in subsection 7.4. We describe an implicit discretization scheme for temporal discretization. Finally, we present numerical experiments for evolutionary problems in subsection 7.5.

7.1 A reminder of the scalar LHI method

To provide a comprehensive understanding, we'll take a moment to recap the Local Hermite Interpolation (LHI) scalar method, as proposed by Stevens et al. [60]. A similar review is also available in [39]. This scalar method will be the basis for the generalized vector technique used later in this study to address the Stokes problem.

In the context of the LHI scalar method, the focus is on approximating the

analytic solution u for a well-posed, steady, linear partial differential problem:

$$\begin{cases} \mathcal{L}u(x) = f(x) & \text{in} \quad \Omega, \\ \mathcal{B}u(x) = g(x) & \text{on} \quad \partial\Omega, \end{cases} \tag{7.1}$$

Here, $\Omega \subset \mathbb{R}^d$ represents the spatial domain, $f : \Omega \to \mathbb{R}$ and $g : \partial\Omega \to \mathbb{R}$ stand for the prescribed right-hand sides, and $\mathcal{L}$ and $\boldsymbol{\mathcal{B}}$ denote linear partial differential operators operating in the domain Ω and on the boundary $\partial\Omega$, respectively. These operators are locally approximated as follows:

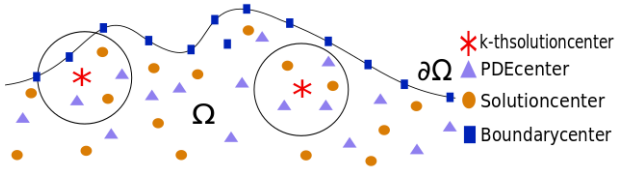

Figure 7.1: Centers and local subdomains for the LHI method

We begin by establishing a set of dispersed nodes $\Omega_n \subset \overline{\Omega}$. Subsequently, we specify three subsets of nodes as illustrated in Figure 7.1:

- Ω_{sc}: A subset of N_{sc} nodes from Ω_n, known as solution centers.
- Ω_{bc}: A subset of N_{bc} nodes from $\partial\Omega \cap \Omega_n$, referred to as boundary centers.
- Ω_{pde}: A subset of N_{pdec} nodes from $\Omega \cap \Omega_n$, termed PDE centers.

Consider D^k, a disk with a varying radius, centered at the k^{th} node in Ω_{sc}. Let's account for the set of $N^{(k)}$ fixed nodes $\Omega_n \cap D^k$, also illustrated in Figure 7.1. To carry out the local discretization, we present the following notation:

$$\begin{aligned} \Omega_{sc}^{(k)} &= \{x_j^{(k,sc)}\}_{j=1}^{N_{sc}^k} = D^k \cap \Omega_{sc}, && \text{denoting the local solution centers.} \\ \partial\Omega_{bc}^{(k)} &= \{x_j^{(k,bc)}\}_{j=1}^{N_{bc}^k} = D^k \cap \partial\Omega, && \text{representing the local boundary nodes.} \\ \Omega_{pdec}^{(k)} &= \{x_j^{(k,pdec)}\}_{j=1}^{N_{pdec}^k} = D^k \cap \Omega, && \text{indicating the local PDE nodes.} \end{aligned}$$

For each disk D^k, we define a corresponding local subsystem as follows:

$$\begin{cases} \mathcal{L}u(x_j) = f(x_j) & x_j \in \Omega_{pdec}^{(k)} \\ \mathcal{B}u(x_j) = g(x_j) & x_j \in \partial\Omega_{bc}^{(k)} \\ u(x_j) = h_j & x_j \in \Omega_{sc}^{(k)} \end{cases} \tag{7.2}$$

where h_i are the unknown values, we define the following ansatz using the symmetric collocation technique:

$$\begin{aligned}\widehat{u}^{(k)}(x) = &\sum_{\xi_j \in \Omega_{sc}^{(k)}} \beta_j^{k,sc} \phi(x-\xi_j) + \sum_{\xi_j \in \Omega_{bc}^{(k)}} \beta_j^{k,bc} \mathcal{B}^{\xi} \phi(x-\xi_j) \\ &+ \sum_{\xi_j \in \Omega_{pde}^{(k)}} \beta_j^{k,pde} \mathcal{L}^{\xi} \phi(x-\xi_j) + \sum_{j=n^k+1 \dots C_p} \beta_j^k p_j^m(x)\end{aligned} \tag{7.3}$$

In the above expression, k is the index for the local linear system, and p_j^m corresponds to the components of a multivariate polynomial of degree m in $\mathbb{R}^d$, thus $C_p = \binom{d+m}{m}$. This polynomial is an element of the null space of the linear system given by (7.2) as described in [60].
By substituting the ansatz detailed in (7.3) into (7.2), we obtain a series of local linear systems, represented by:

$$A^{(k)} \beta^{(k)} = d^{(k)}, \tag{7.4}$$

By defining the Gram matrix $A^{(k)}$ and the right-hand vector $d^{(k)}$, the local linear system in (7.4) can be formulated in vector notation as follows:

$$A^{(k)} = \begin{bmatrix} \Phi_{sc,sc} & \mathcal{B}^{\xi}\Phi_{sc,bc} & \mathcal{L}^{\xi}\Phi_{sc,pde} & P_{j,sc} \\ \mathcal{B}^{x}\Phi_{sc,sc} & \mathcal{B}^{x}\mathcal{B}^{\xi}\Phi_{sc,bc} & \mathcal{B}^{x}\mathcal{L}^{\xi}\Phi_{sc,pde} & \mathcal{B}^{x}P_{j,bc} \\ \mathcal{L}^{x}\Phi_{sc,sc} & \mathcal{L}^{x}\mathcal{B}^{\xi}\Phi_{sc,bc} & \mathcal{L}^{x}\mathcal{L}^{\xi}\Phi_{sc,pde} & \mathcal{L}^{x}P_{j,pde} \\ [P_{j,sc}]^T & [\mathcal{B}^{x}P_{j,bc}]^T & [\mathcal{L}^{x}P_{j,pde}]^T & 0 \end{bmatrix} \in \mathbb{R}^{(N^{(k)}+C_p)\times(N^{(k)}+C_p)},$$

$$\text{and} \quad d^{(k)} = \begin{bmatrix} h^{(k,sc)} \\ g^{(k,bc)} \\ f^{(k,pde)} \\ 0 \end{bmatrix}$$

Here the term $J\Phi_{A,B}$ correspond to $J\Phi(\xi_i - \xi_j)$ where $\xi_i \in A$ and $\xi_j \in B$. Similarly, $JP_{j,A}$ represents $Jp_j^m(\xi_i)$ for $\xi_i \in A$.

The Gram matrix $A^{(k)}$ is well-known to be invertible, as discussed in [64]. Therefore, we can solve for $\beta^{(k)}$ by taking the inverse of $A^{(k)}$ and multiplying it by $d^{(k)}$. Using (7.4), we can rewrite $\widehat{u}^{(k)}(x)$ as follows:

$$\widehat{u}^{(k)}(x) = H^{(k)}(x)\beta^{(k)} = H^{(k)}(x)(A^{(k)})^{-1}d^{(k)} = W^{(k)}(x)d^{(k)}, \tag{7.5}$$

In this formulation, $H^{(k)} : \mathbb{R}^d \to \mathbb{R}^{N^k + C_p}$ is expressed as:

$$H^{(k)}(x) = \left[\phi(x-\xi^{sc}) \dots \mathcal{B}^{\xi}\phi(x-\xi^{bc}) \dots \mathcal{B}^{\xi}\phi(x-\xi^{pde}) \dots p_j^m(x)\right]^T$$

The vector $W^{(k)}(x) = H^{(k)}(x)(A^{(k)})^{-1}$ represents the weights correlated with the RBF approximations at the $N^{(k)}$ nodes within the local domain, and this is typically referred to as the weight vector [64]. When an arbitrary differential operator $\mathcal{J}$ comes into play, we can express it in the following manner:

$$\mathcal{J}\widehat{u}^{(k)}(x) = \mathcal{J}H(x)(A^{(k)})^{-1}d^{(k)} = \mathcal{J}(W^{(k)})(x)d^{(k)}.$$

By employing the above interpretation, we denote the result of applying the differential operator $\mathcal{L}$ to $W^{(k)}(x)$ as $W_{\mathcal{L}}^{(k)}$. Consequently, given the system defined by equation (7.2), we can construct the subsequent system of equations:

$$f(x_1^{(k)}) = W_{\mathcal{L}}^{(k)}(x_1^{(k)})\ d^{(k)}, \quad k = 1, \ldots, N_{sc}, \tag{7.6}$$

Indeed, for each index k in the range from 1 to N_{sc}, the function f evaluated at $x_1^{(k)}$ is equivalent to the inner product of $W_{\mathcal{L}}^{(k)}(x_1^{(k)})$ and the vector $d^{(k)}$. Recall that, as defined in (7.2), we have $u_{sc}^k = h^{(k,sc)}$. Hence, in vector notation, equation (7.6) can be restated as:

$$\begin{bmatrix} W_J^{(k,sc)}(x_1^k) \\ W_J^{(k,bc)}(x_1^k) \\ W_J^{(k,pde)}(x_1^k) \\ W_J^P(x_1^k) \end{bmatrix}^T \begin{bmatrix} u_{sc}^k \\ g^{(k,bc)} \\ f^{(k,pde)} \\ 0 \end{bmatrix} = f(x_1^k) \quad k = 1 \ldots N_{sc} \tag{7.7}$$

The linear system (7.7) can be succinctly denoted as $Su_{sc} = b$. Here, u_{sc} represents the unknown values at the solution centers Ω_{sc}. The matrix S comprises rows with zero elements, except for the weights corresponding to each disc D^k. Therefore, each row contains only $N_{sc}^{(k)}$ non-zero entries. Given that N_{sc} is significantly larger than $N_{sc}^{(k)}$, it follows that the matrix S is sparse.

To efficiently construct the matrix S and compute the weights, we can solve the following equations:

$$A^{(k)}W_{\mathcal{J}}^{(k)}\left(x_1^{(k)}\right) = \mathcal{J}H^{(k)}(x_1^{(k)}), \quad k = 1, \ldots, N_{sc}. \tag{7.8}$$

Since the matrix S is sparse, standard solvers and preconditioners can be used to efficiently solve the linear system $Su_{sc} = b$. Furthermore, it is worth noting that by using the method of lines and a suitable numerical time integrator, the LHI method can be used to solve non-stationary linear PDE problems. For a comprehensive review of the LHI method, interested readers can refer to [60, 28] and related references..

7.2 Steady state problems: Div-free RBF, LHI method

In this subsection, we describe the vectorial LHI algorithm for solving the stationary Stokes problem using divergence-free RBFs. The problem involves finding the solution $u : \mathbb{R}^d \to \mathbb{R}^d$ and $p : \mathbb{R}^d \to \mathbb{R}$ of the following system of equations:

$$\begin{cases} \mathcal{L}_i(\boldsymbol{u}, p) = f_i & \text{in } \Omega, \\ \text{div}(\boldsymbol{u}) = 0 & \text{in } \Omega, \qquad i \in \{1, ..., d\} \\ \mathcal{B}_i(\boldsymbol{u}, p) = g_i & \text{on } \partial\Omega, \end{cases}$$

where $\mathcal{L}_i(\boldsymbol{u}, p) = -\mu\Delta u_i + \frac{\partial p}{\partial x_i}$, $f_i, g_i : \mathbb{R} \to \mathbb{R}$ are known functions and $\boldsymbol{\mathcal{B}} = (\mathcal{B}_1, ..., \mathcal{B}_d)$ are given boundary operators.

Notice that for Dirichlet boundary conditions, we have $\mathcal{B}_i(\boldsymbol{u}, p) = u_i$, while for the Navier-slip boundary conditions, we have:

$$\begin{cases} \mathcal{B}_i(\boldsymbol{u}, p) = u_i \cdot n_i & i = 1 \dots d-1 \\ \mathcal{B}_d\boldsymbol{u} := (\sigma(\boldsymbol{u}, p)\boldsymbol{n})_{tg} \end{cases}$$

where $\boldsymbol{n}$ is the outer normal vector of $\partial\Omega$, and $(\cdot)_{tg}$ denotes the tangential component. As discussed in subsection 7.1, for each disk D^k with center x_1^k, we need to define a local system:

$$\begin{cases} I_i(\boldsymbol{u}, p)|_{\boldsymbol{\xi_j}^{(k,sc)}} = u_i\left(\boldsymbol{\xi_j}^{(k,sc)}\right) & i \in \{1, \dots d\}, j \in \{1, \dots, N_{sc}^k\}, \\ \boldsymbol{\mathcal{B}}_i(\boldsymbol{u}, p)|_{\boldsymbol{\xi_j}^{(k,bc)}} = g_i\left(\boldsymbol{\xi_j}^{(k,bc)}\right) & i \in \{1, \dots d\}, j \in \{1, \dots, N_{bc}^k\}, \\ \boldsymbol{\mathcal{L}_i}(\boldsymbol{u}, p)|_{\boldsymbol{\xi_j}^{(k,pde)}} = f_i\left(\boldsymbol{\xi_j}^{(k,pdec)}\right) & i \in \{1, \dots d\}, j \in \{1, \dots, N_{pde}^k\}. \end{cases} \tag{7.9}$$

Here, $I_i : \mathbb{R}^{(d+1)} \to \mathbb{R}$ is the canonical projection operator that maps a vector to its j^{th} component.

The exclusion of the div operator from system (7.9) is attributed to the employment of a matrix-valued kernel, represented by $\boldsymbol{\Phi}$. This kernel comprises a divergence-free positive definite kernel $\boldsymbol{\Phi}_{Div}$ and a global C^∞ positive definite scalar radial basis function (RBF) ψ. The kernel is expressed as:

$$\boldsymbol{\Phi} = \begin{bmatrix} \boldsymbol{\Phi}_{Div} & 0 \\ 0 & \psi \end{bmatrix} : \mathbb{R}^d \to \mathbb{R}^{(d+1)\times(d+1)}$$

with $\mathbf{\Phi}_{Div} : \mathbb{R}^d \to \mathbb{R}^d \times \mathbb{R}^d$ defined as: $\mathbf{\Phi}_{Div} = -\Delta I + \nabla\nabla^T\psi$. In this context, Δ denotes the Laplace operator, I signifies the identity matrix, and $\nabla\nabla^T$ represents the Hessian matrix. Although the pressure is not incorporated as an unknown variable in the local system (7.9), we will describe the method to calculate it.

Now, using the generalized interpolation Theorem 6.1.1 as in section 6.1 the ansatz for the Stokes equation is given by:

$$\begin{aligned}(\widehat{\boldsymbol{u}}^{(k)}, \widehat{p}^{(k)})(\boldsymbol{x}) = &\sum_{i=1}^{d}\sum_{j=1}^{N_{sc}^k} I_i^{\boldsymbol{\xi}}\mathbf{\Phi}(\boldsymbol{x} - \boldsymbol{\xi}_{\boldsymbol{j}}^{\boldsymbol{sc(k)}})\alpha_{ij}^k \\ &+ \sum_{i=1}^{d}\sum_{j=1}^{N_{bc}^k} \mathcal{B}_i^{\boldsymbol{\xi}}\mathbf{\Phi}(\boldsymbol{x} - \boldsymbol{\xi}_{\boldsymbol{j}}^{\boldsymbol{bc(k)}})\beta_{ij}^k \\ &+ \sum_{i=1}^{d}\sum_{j=1}^{N_{pdec}^k} \mathcal{L}_i^{\boldsymbol{\xi}}\mathbf{\Phi}(\boldsymbol{x} - \boldsymbol{\xi}_{\boldsymbol{j}}^{\boldsymbol{pdec(k)}})\gamma_{ij}^k,\end{aligned} \tag{7.10}$$

Here, (α, β, γ) denotes a vector in $\mathbb{R}^{d\times N_{tot}^k}$, where N_{tot}^k represents the sum of N_{sc}^k, N_{bc}^k, and N_{pdec}^k. These quantities individually account for the total numbers of local solution centers, boundary centers, and PDE centers, respectively. The terms $I_i^{\boldsymbol{\xi}}\mathbf{\Phi}$, $\mathcal{B}_i^{\boldsymbol{\xi}}\mathbf{\Phi}$, $\mathcal{L}_i^{\boldsymbol{\xi}}\mathbf{\Phi}$ are vector-valued functions from $\mathbb{R}^d$ to $\mathbb{R}^{d+1}$ defined by the application of the operators $I_i^{\boldsymbol{\xi}}$, $\mathcal{B}_i^{\boldsymbol{\xi}}$, $\mathcal{L}_i^{\boldsymbol{\xi}}$ to each row of the kernel $\mathbf{\Phi}$ respectively.

Substituting the ansatz (7.10) into the local Stokes system (7.9), we arrive at the following local system:

$$A^k \begin{bmatrix}\boldsymbol{\alpha}^k \\ \boldsymbol{\gamma}^k \\ \boldsymbol{\beta}^k\end{bmatrix} = \begin{bmatrix}\boldsymbol{u}^{(k,sc)} \\ \boldsymbol{g}^{(k,bc)} \\ \boldsymbol{f}^{(k,pdec)}\end{bmatrix}, \tag{7.11}$$

Where the local Gram matrix denoted here as A^k belongs to $\mathbb{R}^{d(N_{tot}^k)\times d(N_{tot}^k)}$, and can be described as the following block of matrix:

$$A^k = \begin{bmatrix}A_{11}^k & A_{12}^k & A_{13}^k \\ A_{21}^k & A_{22}^k & A_{23}^k \\ A_{31}^k & A_{32}^k & A_{33}^k\end{bmatrix},$$

where $A_{ij}^k \in \mathbb{R}^{dN_i\times dN_j}$, where $N = (N_{sc}^k, N_{bc}^k, N_{pdec}^k)$. Specifically, the ij-th block

of each submatrix is given by:

$$A_{11}(i,j) = I_i^x I_j^\xi \mathbf{\Phi}(\boldsymbol{\xi}^{(k,sc)} - \boldsymbol{\xi}^{(k,sc)}), \quad A_{12}(i,j) = I_i^x \boldsymbol{\mathcal{B}}_j^\xi \mathbf{\Phi}(\boldsymbol{\xi}^{(k,sc)} - \boldsymbol{\xi}^{(k,bc)}),$$
$$A_{21}(i,j) = \boldsymbol{\mathcal{B}}_i^x I_j^\xi \mathbf{\Phi}(\boldsymbol{\xi}^{(k,bc)} - \boldsymbol{\xi}^{(k,sc)}), \quad A_{22}(i,j) = \boldsymbol{\mathcal{B}}_i^x \boldsymbol{\mathcal{B}}_j^\xi \mathbf{\Phi}(\boldsymbol{\xi}^{(k,bc)} - \boldsymbol{\xi}^{(k,bc)}),$$
$$A_{31}(i,j) = \boldsymbol{\mathcal{L}}_i^x I_j^\xi \mathbf{\Phi}(\boldsymbol{\xi}^{(k,pdec)} - \boldsymbol{\xi}^{(k,sc)}), \quad A_{32}(i,j) = \boldsymbol{\mathcal{L}}_i^x \boldsymbol{\mathcal{B}}_j^\xi \mathbf{\Phi}(\boldsymbol{\xi}^{(k,pdec)} - \boldsymbol{\xi}^{(k,bc)}),$$

$$A_{13}(i,j) = I_i^x \boldsymbol{\mathcal{L}}_j^\xi \mathbf{\Phi}(\boldsymbol{\xi}^{(k,sc)} - \boldsymbol{\xi}^{(k,pdec)}),$$
$$A_{23}(i,j) = \boldsymbol{\mathcal{B}}_i^x \boldsymbol{\mathcal{L}}_j^\xi \mathbf{\Phi}(\boldsymbol{\xi}^{(k,bc)} - \boldsymbol{\xi}^{(k,bc)}),$$
$$A_{33}(i,j) = \boldsymbol{\mathcal{L}}_i^x \boldsymbol{\mathcal{L}}_j^\xi \mathbf{\Phi}(\boldsymbol{\xi}^{(k,pdec)} - \boldsymbol{\xi}^{(k,pdec)}).$$

This in turn let us compute the weights of the differential operator $\mathcal{L}_j$ by solving the following systems:

$$A^{(k)} W_{\mathcal{L}_j}^{(k)} \left(x_1^{sc(k)}\right) = \mathcal{L}_j H^{(k)}(x_1^{sc(k)}), \quad k = 1, ..., N_{sc}, \tag{7.12}$$

where $H^k(x)$ is given by

$$H^{(k)}(x) = \left(I_1^{\boldsymbol{\xi}} \mathbf{\Phi}(\|\boldsymbol{x} - \boldsymbol{\xi}^{\boldsymbol{sc(k)}}\|) \dots \mathcal{B}_1^{\boldsymbol{\xi}} \mathbf{\Phi}(\|\boldsymbol{x} - \boldsymbol{\xi}^{\boldsymbol{bc(k)}}\|) \dots \mathcal{L}_d^{\boldsymbol{\xi}} \mathbf{\Phi}(\|\boldsymbol{x} - \boldsymbol{\xi}^{\boldsymbol{pdec(k)}}\|)\right)^T. \tag{7.13}$$

Once the weights are known, we can build the sparse global matrix from the following equations

$$W_{\mathcal{L}_j}^{(k)} \left(x_1^{sc(k)}\right) d^{(k)} = F_j(x_1^{sc(k)}) \quad k = 1, .., N_{sc}, \quad j = 1, ..., d, \tag{7.14}$$

where

$$d^{(k)} = \left(u_1(x^{sc(k)}), ..., u_d(x^{sc(k)}), g_1(x^{bc(k)}), ..., g_d(x^{bc(k)}), f_1(x^{pdec(k)}), ..., f_d(x^{pdec(k)})\right)^T.$$

Defining the unknown values of the vector field as

$$\boldsymbol{u}(x^{sc}) = \left(u_1(x_1^{sc}), ..., u_1(x_{N_{sc}}^{sc}), ..., u_d(x_{N_{sc}}^{sc})\right)^T$$

and the known values as $\boldsymbol{g}(x^{bc}) \in \mathbb{R}^{dN_{bc}}$, $\boldsymbol{f}(x^{pde}) \in \mathbb{R}^{dN_{pde}}$ respectively.

The global system induced by (7.14) can be expressed in matrix form as follows:

$$\begin{pmatrix} W_L^y & W_L^B & W_L^L \end{pmatrix} \begin{bmatrix} \boldsymbol{u}(x^{sc}) \\ \boldsymbol{g}(x^{bc}) \\ \boldsymbol{f}(x^{pde}) \end{bmatrix} = [\boldsymbol{f}(x^{sc})], \tag{7.15}$$

where $W_L^{\boldsymbol{u}} \in \mathbb{R}^{dN_{sc}\times dN_{sc}}$, $W_L^B \in \mathbb{R}^{dN_{sc}\times dN_{bc}}$,$W_L^B \in \mathbb{R}^{dN_{sc}\times dN_{pde}}$.

Therefore, in order to compute the velocity field, we must solve the following linear system

$$W_L^y \boldsymbol{u}(x^{sc}) = \boldsymbol{f}(x^{sc}) - W_L^B \boldsymbol{g}(x^{bc}) \; - W_L^L \boldsymbol{f}(x^{pde}). \tag{7.16}$$

To compute the pressure gradient we need to obtain the weights linked to the partial derivatives of the pressure component of the local Anzats. In other words, we need to compute the weight of the operators

$$LP_i(\boldsymbol{u}, p) \equiv \frac{\partial\, I_{d+1}(\boldsymbol{u}, p)}{\partial x_i}, \quad i = 1, 2. \tag{7.17}$$

Again, this is performed in solving the following local systems:

$$A^{(k)} W_{LP_i}^{(k)} \left(x_1^{sc(k)}\right) = LP_i H^{(k)}(x_1^{sc(k)}), \quad k = 1, ..., N_{sc}. \tag{7.18}$$

Once these weights are obtained and assuming that $\boldsymbol{u}(x^{sc})$ have been computed via (7.16), we just have to do the following matrix multiplication

$$W_{LP} \begin{bmatrix} \boldsymbol{u}(x^{sc}) \\ \boldsymbol{g}(x^{bc}) \\ \boldsymbol{f}(x^{pde}) \end{bmatrix} = \left[\nabla p(x^{sc})\right]. \tag{7.19}$$

Remark 7.2.1. It is important to highlight that in order to avoid singularity of the sparse system, we need that $x_1^{sc(k)} \notin \Omega_{pdec}^k$ (see [60]).

7.3 Numerical results: stationary problem

Using the LHI Div–free IMQ RBFs technique, we present numerical results concerning to the convergence order for Dirichlet and Navier–slip boundary condition. Also we verify that the errors, even for small number of support centers and different values of the diffusion parameter μ are excellent.

We consider the non–convex domain whose boundary was defined in (6.12) and the following exact solution :

$$\boldsymbol{u}(\boldsymbol{x}) = \left(-\pi y sin(\frac{\pi}{2}(x^2+y^2)), \pi x sin(\frac{\pi}{2}(x^2+y^2)\right), \quad p(\boldsymbol{x}) = sin(x-y).$$

Here, the non–dimensional shape parameter is $c = 0.1$. Tables 7.1 , 7.2 contains the approximation orders in the L^2 and L^∞ norms of the velocity field and pressure.

$\mu = 1$

Total nodes	Local nodes	$\|\|e_y\|\|_{L_2}$	$\|\|e_y\|\|_\infty$	$\|\|e_{\nabla p}\|\|_{L_2}$	$\|\|e_{\nabla p}\|\|_\infty$	local cond	Sparse cond
1010	15	3.14e-06	4.96e-06	4.45e-04	2.00e-03	4.74e+21	5.05e+07
1010	20	1.49e-06	2.21e-06	3.65e-04	1.15e-03	1.24e+25	4.02e+08
1010	30	3.63e-09	1.12e-08	1.32e-06	8.83e-06	7.37e+30	1.44e+08
1010	40	4.11e-10	1.22e-09	1.66e-07	8.51e-07	1.55e+35	1.04e+09
2177	15	3.83e-06	5.91e-06	4.52e-04	3.26e-03	8.01e+23	5.57e+08
2177	20	5.40e-08	9.89e-08	1.11e-05	4.84e-05	2.96e+27	6.53e+08
2177	30	2.08e-10	9.06e-10	9.14e-08	6.22e-07	1.24e+34	1.14e+09
2177	40	2.97e-12	1.14e-11	1.25e-09	4.14e-09	1.16e+39	2.23e+09
5924	15	2.36e-06	4.99e-06	2.81e-04	1.81e-03	3.24e+26	3.49e+10
5924	20	8.23e-09	1.10e-08	1.85e-06	3.04e-05	4.29e+30	1.45e+10
5924	30	1.08e-12	3.43e-12	7.17e-10	4.19e-09	1.62e+38	1.27e+10
5924	40	5.38e-14	2.52e-13	5.74e-11	3.36e-10	1.16e+44	5.82e+10
15051	15	1.64e-07	3.12e-07	3.06e-05	2.11e-04	9.63e+28	1.76e+11
15051	20	1.83e-09	2.81e-09	7.45e-07	5.29e-06	4.45e+33	4.65e+11
15051	30	3.87e-14	9.73e-14	4.27e-11	5.27e-10	9.63e+41	2.17e+11
15051	40	1.18e-16	6.70e-16	1.41e-13	9.34e-13	3.63e+48	1.64e+11
23461	15	3.31e-07	5.92e-07	3.53e-05	1.67e-04	2.57e+30	1.67e+12
23461	20	3.67e-10	5.58e-10	2.12e-07	2.82e-06	1.02e+35	9.00e+11
23461	30	4.11e-14	6.82e-14	3.15e-11	6.81e-10	5.47e+43	2.01e+12
23461	40	1.45e-17	4.05e-17	1.44e-14	2.33e-13	2.97e+50	1.87e+12

$\mu = 1e-03$

Total nodes	Local nodes	$\|\|e_y\|\|_{L_2}$	$\|\|e_y\|\|_\infty$	$\|\|e_{\nabla p}\|\|_{L_2}$	$\|\|e_{\nabla p}\|\|_\infty$	local cond	Sparse cond
1010	15	4.29e-05	7.65e-05	1.50e-05	1.16e-04	2.89e+19	5.84e+07
1010	20	1.88e-06	3.65e-06	7.90e-07	5.53e-06	1.85e+23	9.80e+07
1010	30	7.07e-08	1.68e-07	2.41e-08	1.06e-07	3.89e+28	2.85e+08
1010	40	1.37e-09	4.56e-09	5.59e-10	3.52e-09	1.18e+33	1.43e+10
2177	15	6.58e-06	1.50e-05	2.39e-06	1.87e-05	3.32e+21	1.82e+09
2177	20	1.19e-06	2.04e-06	2.57e-07	1.29e-06	5.13e+25	1.92e+09
2177	30	1.28e-09	5.39e-09	5.96e-10	6.09e-09	7.92e+31	1.94e+09
2177	40	9.12e-12	3.16e-11	6.13e-12	3.87e-11	5.37e+36	2.31e+09
5924	15	1.62e-04	2.96e-04	1.43e-05	7.55e-05	9.33e+23	3.29e+11
5924	20	1.66e-07	3.51e-07	6.17e-08	5.75e-07	1.17e+29	6.66e+10
5924	30	6.13e-12	1.81e-11	5.59e-12	4.52e-11	5.00e+35	5.76e+09
5924	40	2.16e-13	7.80e-13	1.83e-13	2.03e-12	3.30e+41	5.50e+10
15051	15	7.24e-07	1.19e-06	1.08e-07	1.08e-06	2.94e+26	2.81e+11
15051	20	4.59e-08	6.95e-08	7.24e-09	1.46e-07	1.09e+32	1.89e+12
15051	30	3.23e-13	6.31e-13	4.48e-13	5.31e-12	5.36e+39	8.10e+10
15051	40	8.62e-15	3.07e-14	2.17e-14	1.94e-13	1.45e+46	8.37e+11
23461	15	4.99e-07	8.47e-07	1.11e-07	1.16e-06	2.86e+27	7.96e+11
23461	20	8.39e-10	1.28e-09	3.62e-10	7.71e-09	1.94e+33	1.80e+12
23461	30	6.43e-14	9.86e-14	9.15e-14	1.22e-12	2.70e+41	2.23e+11
23461	40	2.21e-16	9.69e-16	5.04e-16	7.49e-15	1.40e+48	9.00e+11

Table 7.1: Div free IMQ LHI Error table for stationary case with Dirichlet boundary condition and shape parameter c=1.0

$\mu = 1$

Total nodes	Local nodes	$\|\|e_y\|\|_{L_2}$	$\|\|e_y\|\|_\infty$	$\|\|e_{\nabla p}\|\|_{L_2}$	$\|\|e_{\nabla p}\|\|_\infty$	local cond	Sparse cond
1010	15	2.02e-05	3.88e-05	1.93e-03	6.68e-03	4.32e+21	4.57e+07
1010	20	3.18e-06	8.24e-06	5.00e-04	2.64e-03	9.56e+24	2.03e+08
1010	30	5.26e-08	2.12e-07	9.79e-06	4.59e-05	6.36e+30	1.50e+09
1010	40	4.19e-10	2.44e-09	1.38e-07	8.23e-07	1.45e+35	2.30e+09
2177	15	4.35e-06	9.47e-06	6.66e-04	2.69e-03	7.60e+23	4.21e+08
2177	20	1.63e-07	5.19e-07	2.02e-05	7.65e-05	2.69e+27	2.56e+09
2177	30	1.67e-09	4.79e-09	3.12e-07	8.17e-07	1.11e+34	5.76e+09
2177	40	4.13e-11	9.94e-11	7.59e-09	3.10e-08	1.31e+39	1.95e+10
5924	15	4.93e-07	9.11e-07	7.28e-05	7.66e-04	2.33e+26	4.79e+09
5924	20	1.55e-07	3.43e-07	2.20e-05	7.93e-05	4.97e+30	2.36e+11
5924	30	8.96e-11	2.20e-10	1.53e-08	1.08e-07	1.71e+38	3.33e+11
5924	40	2.37e-11	7.26e-11	7.61e-09	4.73e-08	1.17e+44	3.60e+13
15051	15	1.14e-07	1.86e-07	1.73e-05	1.26e-04	8.48e+28	2.78e+11
15051	20	2.07e-08	3.39e-08	2.22e-06	2.02e-05	3.86e+33	2.40e+13
15051	30	6.89e-11	2.32e-10	7.58e-09	4.71e-08	1.00e+42	2.62e+14
15051	40	1.98e-13	6.70e-13	2.05e-11	1.15e-10	2.69e+48	4.42e+14
23461	15	4.30e-06	8.38e-06	3.06e-04	3.47e-03	8.51e+29	7.42e+12
23461	20	6.57e-10	1.49e-09	1.57e-07	2.00e-06	7.12e+34	5.83e+12
23461	30	1.20e-10	5.91e-10	3.11e-08	4.24e-07	4.55e+43	2.69e+15
23461	40	6.94e-15	2.92e-14	2.12e-12	1.21e-11	2.73e+50	9.49e+14

$\mu = 1e-03$

Total nodes	Local nodes	$\|\|e_y\|\|_{L_2}$	$\|\|e_y\|\|_\infty$	$\|\|e_{\nabla p}\|\|_{L_2}$	$\|\|e_{\nabla p}\|\|_\infty$	local cond	Sparse cond
1010	15	3.29e-05	6.80e-05	6.31e-06	2.51e-05	5.09e+19	3.27e+08
1010	20	4.36e-06	1.82e-05	5.66e-07	1.98e-06	2.25e+23	7.47e+07
1010	30	6.21e-07	1.72e-06	1.48e-07	7.93e-07	6.28e+28	1.37e+09
1010	40	2.32e-09	6.91e-09	5.46e-10	2.30e-09	1.30e+33	4.40e+09
2177	15	3.66e-05	6.08e-05	4.95e-06	2.34e-05	4.33e+21	1.86e+09
2177	20	7.75e-07	2.24e-06	7.93e-08	4.06e-07	5.67e+25	1.56e+09
2177	30	5.59e-09	1.63e-08	1.25e-09	5.67e-09	7.95e+31	1.05e+10
2177	40	4.17e-10	1.53e-09	7.60e-11	4.10e-10	5.71e+36	1.08e+11
5924	15	1.15e-05	4.14e-05	2.53e-06	3.76e-05	6.94e+23	1.56e+10
5924	20	2.89e-06	6.13e-06	1.99e-07	1.04e-06	1.59e+29	3.70e+11
5924	30	1.56e-10	4.61e-10	3.07e-11	1.60e-10	9.54e+35	1.16e+12
5924	40	2.11e-12	6.49e-12	2.31e-13	1.05e-12	3.57e+41	2.15e+12
15051	15	3.18e-04	4.62e-04	3.10e-05	4.15e-04	2.16e+26	4.50e+13
15051	20	6.38e-08	1.31e-07	8.65e-09	1.03e-07	1.25e+32	1.63e+12
15051	30	1.86e-11	6.80e-11	2.26e-12	1.40e-11	4.32e+39	2.81e+12
15051	40	2.23e-14	5.64e-14	2.93e-15	2.04e-14	1.44e+46	1.46e+13
23461	15	2.13e-05	3.02e-05	1.47e-06	1.19e-05	2.54e+27	3.02e+13
23461	20	1.20e-08	2.20e-08	1.54e-09	3.37e-08	1.79e+33	6.92e+12
23461	30	1.30e-12	3.48e-12	2.09e-13	2.63e-12	2.71e+41	4.62e+12
23461	40	2.25e-15	5.92e-15	4.75e-16	3.00e-15	1.95e+48	1.62e+13

Table 7.2: Div free IMQ LHI Error table for stationary case with Navier–slip boundary condition and shape parameter c=1.0

We denote such an errors by $e_u := \boldsymbol{u}_{exact} - \boldsymbol{u}_{aprox}$ and $e_{\nabla p} := \boldsymbol{\nabla p}_{exact} - \boldsymbol{\nabla p}_{aprox}$. In all experiments, we have used extended precision via the mpfr++ library in c++ in order to overcome the ill condition Gram matrix.

From Tables 7.1 and 7.2, it can be appreciated that we obtain spectral order of convergence as the number of local nodes increases or equivalently if the fill distance decreases. Also the results are excellent both for $\mu = 1$ and $\mu = 10^{-3}$, and the error consistently decreases as the number of local nodes increases. The main point to be noted from this tables is that we can use up to $24,000$ total number of nodes in the computations. This can not be done with global collocation methods due to the high value of the condition number of the Gram matrix.

7.4 LHI method and BDF scheme for the non-stacionary Stokes equations

In this subsection we formulate a RBF–LHI vectorial technique for the evolutionary Stokes problem

$$\begin{cases} \boldsymbol{u}_t + \boldsymbol{\mathcal{L}}(\boldsymbol{u}, p) = \boldsymbol{f} & \text{in} \quad Q, \\ \operatorname{div} \boldsymbol{u} = 0 & \text{in} \quad Q, \\ \boldsymbol{\mathcal{B}u} = \boldsymbol{g} & \text{on} \quad \Sigma, \\ \boldsymbol{u}(\cdot, 0) = \boldsymbol{u}_0(\cdot) & \text{in} \quad Q, \end{cases} \tag{7.20}$$

where $\boldsymbol{\mathcal{L}}(\boldsymbol{u}, p) = -\mu \Delta \boldsymbol{u} + \nabla p$.

Observe that, for every $t \in (0, T)$, (7.20) can be seen as a stationary Stokes equation

$$\begin{cases} \boldsymbol{\mathcal{L}}(\boldsymbol{u}, p) = \boldsymbol{f} & \text{in} \quad \Omega, \\ \operatorname{div} \boldsymbol{u} = 0 & \text{in} \quad \Omega, \\ \boldsymbol{\mathcal{B}u} = \boldsymbol{g} & \text{on} \quad \partial\Omega, \end{cases} \tag{7.21}$$

where $\boldsymbol{f} = \boldsymbol{f} - \boldsymbol{u}_t$.

This implies that we can use the weight of the stationary system (see equation (7.12)) to approximate (7.21). Thus, by using (7.14) we have

$$\begin{pmatrix} W_L^y & W_L^B & W_L^L \end{pmatrix} \begin{bmatrix} \boldsymbol{u}(t; x^{sc}) \\ \boldsymbol{g}(t; x^{bc}) \\ \boldsymbol{f}(t; x^{pde}) \end{bmatrix} = [\boldsymbol{f}(t; x^{sc})] \tag{7.22}$$

Now, assuming that $x^{sc} = x^{pde}$, we get the following ODE system

$$(I - W_L^L)\,\boldsymbol{u}_t(t; x^{sc}) = -W_L^y\,\boldsymbol{u}(t; x^{sc}) - W_L^B \boldsymbol{g}(t; x^{bc}) + (I - W_L^L)\boldsymbol{F}(\boldsymbol{t}; \boldsymbol{x}^{\boldsymbol{sc}}), \quad (7.23)$$

where the boundary condition have been imposed in the LHI weights.

To solve the above system, we use a BDF2 scheme. Thus, in each time step we shall solve the system

$$\left(I - W_L^L + \frac{2\Delta t}{3} W_L^y\right) \boldsymbol{u}_{n+2} = \left(I - W_L^L\right) \left(\frac{2\Delta t}{3} \boldsymbol{F_{n+2}} + \frac{4}{3}\boldsymbol{u}_{n+1} - \frac{1}{3}\boldsymbol{u}_n\right) - \frac{2\Delta t}{3} W_L^B \boldsymbol{g}_{n+2}. \quad (7.24)$$

7.5 Numerical results: evolutionary problem

In this subsection we use the theoretical description of the RBF–LHI method presented in 7.4, to solve the unsteady Stokes system. We also introduce the concept of Divergence free hybrid radial basis function, a generalization of the scalar hybrid RBF (see [52]), which allows us to build a global LHI matrix whose eigenvalues have negative real parts. We present numerical results for different benchmark problems. use IMQ kernels since in this case we obtain that always some of the eigenvalues have positive real components for all the shape parameters.

We stress that, in some cases and according to extensive numerical experimentation, no matter which parameters c, μ or h we select, it is not possible to obtain eigenvalues with negative real parts for the IMQ kernel, thus the discrete system is unstable.

On the other hand, for hybrid kernels, the eigenvalues can always be obtained to be negative depending on the parameters we choose, thus providing the stability condition for ODE's solvers. We first define the concept of Div–free hybrid kernel.

Definition 7.5.1. Let $\boldsymbol{r} = \|\boldsymbol{x}\|$, $\psi_1(\boldsymbol{r}) = \exp^{-c\boldsymbol{r}^2}$ and $\psi_2(\boldsymbol{r}) = \boldsymbol{r}^{2n+1}$. The divergence free hybrid kernel $\boldsymbol{\Phi}_{Div} : \mathbb{R}^d \to \mathbb{R}^{d+1}$ is defined by

$$\boldsymbol{\Phi}_{Div}(\boldsymbol{x}) = \{-\Delta I + \nabla\nabla^T\}(\psi_1(\boldsymbol{x}) + \gamma_1\psi_2(\boldsymbol{x})).$$

where Δ denotes the Laplace operator, I signifies the identity matrix, and $\nabla\nabla^T$ represents the Hessian matrix.

By direct computation we obtain

$$\begin{aligned}\mathbf{\Phi}_{\mathrm{Div}}(\mathbf{x}) =& 4c_1 e^{-r^2 c_1}\begin{bmatrix} -c_1 x_2^2 + \frac{1}{2} & c_1 x_1 x_2 \\ c_1 x_1 x_2 & -c_1 x_1^2 + \frac{1}{2}\end{bmatrix} \\ &+ \gamma_1 r^{2n-3}(4n^2-1)\begin{bmatrix} \frac{-r^2}{(2n-1)} - x_2^2 & x_1 x_2 \\ x_1 x_2 & \frac{-r^2}{(2n-1)} - x_1^2\end{bmatrix}.\end{aligned}$$

and the combined velocity–pressure kernel is given by

$$\mathbf{\Phi}(\boldsymbol{x}) = \begin{pmatrix} \mathbf{\Phi}_{Div}(\boldsymbol{x}) & 0 \\ 0 & \mathrm{e}^{-c_2 r} + \gamma_2 r^{2m+1}\end{pmatrix}. \tag{7.25}$$

Here γ_2 is corresponding weight relative to the hybrid kernel related to the pressure.

In the following experiments and for stability reasons, we use a weight parameter γ_1, a shape parameter c_1 for the velocity and the corresponding values γ_2; c_2 for the pressure. Also we shall use the values $n = 3$ and $m = 1$ in equation (7.25), ie. r^7 for the $\mathbf{\Phi}_{Div}$ vector component and r^3 for the scalar component.

We note that the condition numbers of the local and global Gram matrices are considerable lower than for the non hybrid, IMQ RBF. This is in agreement with a recently, a new approach to reduce the ill-conditioning problem in RBF approximations by using a hybrid Gaussian-cubic kernel was proposed [52]. The basic idea behind such a hybridization is to obtain a kernel which utilizes the merits of two different kernels while compensating for the limitations of each and keeping the formulation as a standard RBF method.

The numerical results of tables(7.3)–(7.6) were obtained by using divergence-free hybrid kernels and considering the following analytical solution to (7.20)

$$\begin{aligned} u_1(x,y,t) &= -\pi\, y\, \sin\left(\frac{\pi}{2}(tx^2+y^2)\right)\sin(20\pi t), \\ u_2(x,y,t) &= -\pi\, y\, \sin\left(\frac{\pi}{2}(tx^2+y^2)\right)\sin(20\pi t)t, \\ p(x,y,t) &= \sin(x-y+t). \end{aligned}$$

The total number of nodes for tables (7.3)–(7.6) is 1010. To better appreciate the convergence of the method as the fill distance decrease we scale the domain by factor α ranging from 1 to 10^{-5}.

As in section 6.1.2, we compare the velocity error in the L^2–norm between the exact and numerical solutions, i.e., $\boldsymbol{\epsilon_y} = \boldsymbol{u}_{exact} - \boldsymbol{u}_{aprox}$.

Δt				2.00e-02	1.00e-02	1.00e-03	1.00e-04	1.00e-05
Fill distance	Local nodes	Velocity $-\gamma_1$	Max local cond	$\|\|e_y\|\|_{L_2}$	$\|\|e_y\|\|_{L_2}$	$\|\|e_y\|\|_{L_2}$	$\|\|e_y\|\|_{L_2}$	$\|\|e_y\|\|_{L_2}$
5.00e-02	15	2.00e-01	4.20e+11	3.89631e-01	1.37393e-01	2.28270e-02	2.26144e-02	2.26158e-02
5.00e-02	20	1.00e-01	1.62e+12	3.27511e-01	1.14382e-01	1.16019e-02	1.12192e-02	1.12195e-02
5.00e-02	30	1.00e-01	3.00e+12	3.17346e-01	1.10879e-01	1.03071e-02	9.88475e-03	9.88514e-03
5.00e-03	15	1.00e-01	1.12e+17	2.37872e-02	8.84353e-03	2.85082e-04	2.36036e-05	2.18281e-05
5.00e-03	20	1.00e-01	1.96e+17	2.37824e-02	8.84254e-03	2.84566e-04	1.62663e-05	1.35604e-05
5.00e-03	30	1.00e-01	3.98e+17	2.37821e-02	8.84248e-03	2.84493e-04	1.49392e-05	1.19358e-05
5.00e-04	15	1.00e-01	1.15e+22	2.37205e-03	8.81808e-04	2.83446e-05	8.96755e-07	3.59745e-08
5.00e-04	20	1.00e-01	1.99e+22	2.37205e-03	8.81808e-04	2.83446e-05	8.96564e-07	3.08596e-08
5.00e-04	30	1.00e-01	4.08e+22	2.37205e-03	8.81808e-04	2.83446e-05	8.96543e-07	3.02459e-08
5.00e-05	15	1.00e-01	1.15e+27	2.37201e-04	8.81791e-05	2.83440e-06	8.96463e-08	2.83496e-09
5.00e-05	20	1.00e-01	2.01e+27	2.37201e-04	8.81791e-05	2.83440e-06	8.96463e-08	2.83490e-09
5.00e-05	30	1.00e-01	4.28e+27	2.37201e-04	8.81791e-05	2.83440e-06	8.96463e-08	2.83490e-09

Table 7.3: Error table for Stokes-unsteady, Dirichlet boundary condition with BDF2 LHI-semidiscret method $\mu = 1$, Pressure $\gamma_2 = 1e-06$, Velocity $c_1 = 0.5$, Pressure $c_2 = 5e-04$

Δt				2.00e-02	1.00e-02	1.00e-03	1.00e-04	1.00e-05
Fill distance	Local nodes	Velocity $-\gamma_1$	Max local cond	$\|\|e_y\|\|_{L_2}$	$\|\|e_y\|\|_{L_2}$	$\|\|e_y\|\|_{L_2}$	$\|\|e_y\|\|_{L_2}$	$\|\|e_y\|\|_{L_2}$
5.00e-02	15	1.00e+00	1.20e+09	1.51164e+00	9.95465e-01	8.52428e-01	8.52643e-01	8.52750e-01
5.00e-02	20	1.00e-01	1.63e+10	8.20890e-01	4.66209e-01	3.80483e-01	3.80544e-01	3.80584e-01
5.00e-02	30	1.00e-01	3.26e+10	6.43212e-01	2.95525e-01	2.08385e-01	2.08408e-01	2.08428e-01
5.00e-03	15	1.00e-01	9.62e+14	2.42604e-02	8.98489e-03	7.02252e-04	6.42266e-04	6.42253e-04
5.00e-03	20	1.00e-01	1.67e+15	2.38317e-02	8.85552e-03	3.26210e-04	1.60253e-04	1.60013e-04
5.00e-03	30	1.00e-01	3.22e+15	2.37950e-02	8.84617e-03	3.05968e-04	1.13596e-04	1.13247e-04
5.00e-04	15	1.00e-01	9.51e+19	2.37205e-03	8.81808e-04	2.83447e-05	9.00079e-07	8.52535e-08
5.00e-04	20	1.00e-01	1.51e+20	2.37205e-03	8.81808e-04	2.83446e-05	8.97570e-07	5.25082e-08
5.00e-04	30	1.00e-01	3.41e+20	2.37205e-03	8.81808e-04	2.83446e-05	8.96529e-07	2.98050e-08
5.00e-05	15	1.00e-01	9.68e+24	2.37201e-04	8.81791e-05	2.83440e-06	8.96463e-08	2.83489e-09
5.00e-05	20	1.00e-01	1.54e+25	2.37201e-04	8.81791e-05	2.83440e-06	8.96463e-08	2.83487e-09
5.00e-05	30	1.00e-01	3.48e+25	2.37201e-04	8.81791e-05	2.83440e-06	8.96463e-08	2.83487e-09

Table 7.4: Error table for Stokes-unsteady, Dirichlet boundary condition with BDF2 LHI-semidiscret method $\mu = 1e-03$, Pressure $\gamma_2 = 1e-06$, Velocity $c_1 = 0.5$, Pressure $c_2 = 5e-04$

Δt				2.00e-02	1.00e-02	1.00e-03	1.00e-04	1.00e-05
Fill distance	Local nodes	Velocity $-\gamma_1$	Max local cond	$\|\|e_y\|\|_{L_2}$	$\|\|e_y\|\|_{L_2}$	$\|\|e_y\|\|_{L_2}$	$\|\|e_y\|\|_{L_2}$	$\|\|e_y\|\|_{L_2}$
5.00e-02	15	2.00e-01	4.20e+11	5.34629e-01	2.03483e-01	8.57445e-02	8.56851e-02	8.56904e-02
5.00e-02	20	1.00e-01	1.62e+12	4.59891e-01	1.65007e-01	3.61239e-02	3.60060e-02	3.60083e-02
5.00e-02	30	1.00e-01	3.00e+12	4.83596e-01	1.75874e-01	4.08739e-02	4.07419e-02	4.07447e-02
5.00e-03	15	1.00e-01	1.12e+17	2.38759e-02	8.86207e-03	2.92628e-04	6.98930e-05	6.93184e-05
5.00e-03	20	1.00e-01	1.96e+17	2.38063e-02	8.84747e-03	2.86525e-04	3.70751e-05	3.59725e-05
5.00e-03	30	1.00e-01	3.98e+17	2.38141e-02	8.84912e-03	2.88693e-04	5.11912e-05	5.04004e-05
5.00e-04	15	1.00e-01	1.15e+22	2.37205e-03	8.81808e-04	2.83447e-05	8.99279e-07	7.63437e-08
5.00e-04	20	1.00e-01	2.10e+22	2.37205e-03	8.81808e-04	2.83446e-05	8.97295e-07	4.75745e-08
5.00e-04	30	1.00e-01	4.08e+22	2.37205e-03	8.81808e-04	2.83446e-05	8.97518e-07	5.16150e-08
5.00e-05	15	1.00e-01	1.15e+27	2.37201e-04	8.81791e-05	2.83440e-06	8.96463e-08	2.83576e-09
5.00e-05	20	1.00e-01	2.01e+27	2.37201e-04	8.81791e-05	2.83440e-06	8.96463e-08	2.83511e-09
5.00e-05	30	1.00e-01	4.28e+27	2.37201e-04	8.81791e-05	2.83440e-06	8.96463e-08	2.83526e-09

Table 7.5: Error table for Stokes-unsteady, Navier–slip boundary condition with BDF2 LHI–semidiscret method $\mu = 1$, Pressure $\gamma_2 = 1e-06$, Velocity $c_1 = 1.0$,Pressure $c_2 = 5e-06$

Δt				2.00e-02	1.00e-02	1.00e-03	1.00e-04	1.00e-05
Fill distance	Local nodes	Velocity $-\gamma_1$	Max local cond	$\|\|e_y\|\|_{L_2}$	$\|\|e_y\|\|_{L_2}$	$\|\|e_y\|\|_{L_2}$	$\|\|e_y\|\|_{L_2}$	$\|\|e_y\|\|_{L_2}$
5.00e-02	15	1.00e-01	2.30e+11	1.67563e+00	1.10142e+00	9.45213e-01	9.45553e-01	9.45679e-01
5.00e-02	20	1.00e-01	2.01e+11	1.51242e+00	9.90276e-01	8.43845e-01	8.44026e-01	8.44133e-01
5.00e-02	30	1.00e-01	3.50e+11	1.45439e+00	9.47934e-01	8.06837e-01	8.06999e-01	8.07101e-01
5.00e-03	15	8.00e-01	1.58e+14	2.29486e-01	1.18803e-01	1.10860e-01	1.11219e-01	1.11242e-01
5.00e-03	20	1.00e-01	2.19e+15	3.66377e-02	1.41194e-02	5.86116e-03	5.85250e-03	5.85300e-03
5.00e-03	30	1.00e-01	4.17e+15	5.24203e-02	2.30795e-02	1.97011e-02	1.97778e-02	1.97812e-02
5.00e-04	15	5.12e+01	2.70e+17	2.88384e-03	1.01449e-03	8.02069e-05	7.48608e-05	7.48610e-05
5.00e-04	20	1.00e-01	2.08e+20	2.37255e-03	8.81927e-04	2.84960e-05	3.06396e-06	2.93023e-06
5.00e-04	30	1.00e-01	3.72e+20	2.49592e-03	9.14376e-04	5.79928e-05	5.05434e-05	5.05393e-05
5.00e-05	15	4.10e+02	3.33e+21	2.37209e-04	8.81807e-05	2.83544e-06	1.17900e-07	7.66347e-08
5.00e-05	20	1.00e-01	1.79e+25	2.37201e-04	8.81791e-05	2.83440e-06	8.96478e-08	2.88258e-09
5.00e-05	30	8.00e-01	5.21e+24	2.37201e-04	8.81791e-05	2.83440e-06	8.97063e-08	4.33499e-09

Table 7.6: Error table for Stokes-unsteady, Navier–slip boundary condition with BDF2 LHI–semidiscret method $\mu = 1e-03$, Pressure $\gamma_2 = 1e-06$, Velocity $c_1 = 1.0$, Pressure $c_2 = 5e-06$

From the tables presented in this subsection, we conclude that the local condition number for hybrid kernels are several orders of magnitude smaller than the values of tables presented in subsection (7.3), which corresponds to the condition number for inverse multi quadrics. We stress however, that the error is greater for hybrids kernels than for IMQ. The values of the shape parameters were obtained by direct trial and error computation. Of course, up to now, there is no theory that tells us how to obtain these values. It is important to note that in order to obtain a good condition number, we only need to decrease the value γ_1 and decrease the shape parameter of the pressure for a fixed γ_2. Here, γ_1 is the parameter of the convex combination of the hybrid kernel related to the velocity, and γ_2 the parameter related to the pressure. This means that the algorithm is relatively stable with respect to the variation of the parameters.

8 Application to a control problem of the LHI-div free

In this chapter, we address the numerical solution for the approximate controllability problem in the context of a two-dimensional Stokes system, subject to a limited number of scalar controls. Both Dirichlet and Navier-slip boundary conditions are incorporated in our analysis. Our numerical implementation builds upon the previously developed Radial Basis Function - Local Hermite Interpolation (RBF-LHI) technique. For validation and comparison, the outcomes derived from the RBF-LHI approach are benchmarked against results obtained from the Finite Element Method (FEM) under similar conditions, i.e., considering both Dirichlet and Navier-slip boundary conditions

Following the methodology outlined in [37], we implement the Conjugate Gradient Method (CGM) to solve the dual system as defined in equations (8.2) and (8.7). We adopt a stopping criterion of $\epsilon = 10^{-8}$. Furthermore, the considered domain Ω is a subset of $\mathbb{R}^2$ and is shaped as a star, with its boundary being parametrized by a specific curve:

$$C = \Big\{(\theta, \rho(\theta)) \in \mathbb{R}^2 \mid \rho(\theta) = 0.8 + sin(6\theta) + sin(3\theta),\ \theta \in [0, 2\pi)\Big\}. \tag{8.1}$$

The set of observations, denoted by ω, is defined as $\omega = (x, y) \in \mathbb{R}^2 : \frac{x^2}{2.5e^{-3}} + \frac{y^2}{4e^{-4}} < 1.0$. The time period under consideration, T, is set to 1.0. We deploy a uniform mesh comprising 1010 points, constructed using FreeFem++. The chosen time step size is $\Delta t = 5 \times 10^{-3}$, and the diffusion coefficient is set as $\mu = 1e - 03$. Initial conditions are defined as follows:

$$(u_1^0, u_2^0) = \left(-10^2\pi\, y\, \cos\left(\frac{\pi}{2}(x^2 + y^2)\right)^2, 10^2\pi\, x\, \cos\left(\frac{\pi}{2}(x^2 + y^2)\right)^2\right).$$

In terms of the functional defined in equation (8.5), we establish the regularization parameters as $\beta_1 = 1.0e - 03$ and $\beta_2^{-1} = 0$ for controls that include both

non-zero scalar components ($\boldsymbol{v} = (v_1, v_2)$). Alternatively, we use $\beta_1^{-1} = 0$ and $\beta_2 = 1.0e{-}03$ when the controls have only one scalar component (either $\boldsymbol{v} = (v_1, 0)$ or $\boldsymbol{v} = (0, v_2)$).

For the numerical experiments, a triangular mesh is employed. This choice is motivated by two factors. First, it allows a fair comparison between the RBF-LHI and FEM methods. Second, the CGM requires calculation of integrals over the domain. While this can be accomplished using scattered nodes, efficiency is improved by employing a triangulation within the LHI-RBF framework to compute these integrals with $\mathbb{P}_1$-type elements.

8.1 A Control problem formulation

Before proceeding, let's establish some useful notations. Let Ω denote a connected, open subset of $\mathbb{R}^d$ ($d = 2$ or $d = 3$) of class C^∞. Define $T > 0$ and let ω represent a small, non-empty, open subset of Ω, corresponding to the control domain. Furthermore, we introduce $Q := \Omega \times (0, T)$ and $\Sigma := \partial\Omega \times (0, T)$. The vector $\boldsymbol{n}(x)$ is the outward unit normal vector to Ω at the point $x \in \partial\Omega$. Furthermore, we define:

$$H := \{\boldsymbol{u} \in L^2(\Omega)^d : \nabla \cdot \boldsymbol{u} = 0 \text{ in } \Omega, \;\; \boldsymbol{u} \cdot \boldsymbol{n} = 0 \text{ on } \partial\Omega\}$$

and

$$V := \{\boldsymbol{u} \in H_0^1(\Omega)^d : \nabla \cdot \boldsymbol{u} = 0 \text{ in } \Omega\}.$$

We turn our attention to the continuous approximate control problem for the Stokes system, applicable to both Dirichlet and Navier-slip boundary conditions, which is outlined as follows:

Approximate control. Starting with an initial data $\boldsymbol{u}_0$, the goal is to identify a control function $\boldsymbol{v} = \boldsymbol{v}(x, t)$, acting in the domain $\omega \times (0, T)$ with its support, $supp, \boldsymbol{v}$, confined within $\omega \times (0, T)$. This control function should result in a solution to the following problem:

$$\begin{cases} \boldsymbol{u}_t - \mu\Delta\boldsymbol{u} + \nabla p = \boldsymbol{v}1_\omega & \text{in} \quad Q, \\ \nabla \cdot \boldsymbol{u} = 0 & \text{in} \quad Q, \\ +\text{BC} & \text{on} \quad \Sigma, \\ \boldsymbol{u}(\cdot, 0) = \boldsymbol{u}_0(\cdot) & \text{in} \quad \Omega, \end{cases} \tag{8.2}$$

such that for every $\varepsilon > 0$ we have:

$$\boldsymbol{u}(\cdot, T) \leq \varepsilon \quad \text{in} \quad \Omega, \qquad \text{(approximate control to zero)} \tag{8.3}$$

In equation (8.2), $\mu > 0$ represents the viscosity coefficient and p is the pressure. Our attention is primarily directed towards two types of boundary conditions on Σ, specifically:

$$\underbrace{\boldsymbol{u} = \boldsymbol{g}}_{(a)\text{ Dirichlet}} \quad \text{or} \quad \underbrace{\boldsymbol{u}\cdot\boldsymbol{n} = 0,\ \ (\sigma(\boldsymbol{u},p)\cdot\boldsymbol{n})_{tg} = \boldsymbol{g},}_{(b)\text{ Navier–slip}} \tag{8.4}$$

In this context, $\sigma(\boldsymbol{u},p) := -pId + 2\mu D\boldsymbol{u}$ defines the stress tensor, with D representing the symmetrized gradient of $\boldsymbol{u}$. The term tg refers to the tangential component of the respective vector field, which is given by:

$$\boldsymbol{u}_{tg} = \boldsymbol{u} - (\boldsymbol{u}\cdot\boldsymbol{n})\boldsymbol{n}.$$

We now frame the control problem in terms of seeking the optimal or minimum value of a quadratic convex functional in $(L^2(Q))^2$, following the approach delineated in [33]. Specifically, for $\boldsymbol{u}_0 \in H$, our goal is to determine the control $\boldsymbol{v}$ that has one vanishing component (the jth component, where $j \in 1,2$) such that it minimizes the functional J as defined by:

$$J(\boldsymbol{v}) := \frac{1}{2}\iint\limits_{\omega\times(0,T)} |\boldsymbol{v}|^2\,dx\,dt + \frac{1}{2\beta_1}\|\boldsymbol{u}(\cdot,T)\|^2_{L^2(\Omega)}\,dx + \frac{1}{2\beta_2}\iint\limits_{\omega\times(0,T)} |v_j|^2\,dx\,dt, \tag{8.5}$$

where $\boldsymbol{u}$ represents the solution of the Stokes system as characterized by equation (8.2). The coefficients β_1 and β_2 denote arbitrary positive numbers, associated respectively with the final condition $\boldsymbol{u}(\cdot,T) \le \varepsilon$ and the control function $\boldsymbol{v}$.

The optimal control function, $\boldsymbol{v}$, can be identified by computing the Fréchet derivative of J with respect to $\boldsymbol{v}$. Verification shows that this leads to the following: expressions:

$$\frac{\partial J}{\partial \boldsymbol{v}}(\boldsymbol{v}) = v_i - w_i \text{ if } i \neq j \quad \text{and} \quad \frac{\partial J}{\partial \boldsymbol{v}}(\boldsymbol{v}) = \frac{1}{2\beta_2}v_j - w_j, \quad \text{in } \omega\times(0,T), \tag{8.6}$$

where $\boldsymbol{w} \in V$ is the solution of the adjoint system of (8.2):

$$\begin{cases} -\boldsymbol{w}_t - \mu\Delta\boldsymbol{w} + \nabla q = 0 & \text{in} \quad Q, \\ \nabla\cdot\boldsymbol{w} = 0 & \text{in} \quad Q, \\ +\text{BC} & \text{on} \quad \Sigma, \\ \boldsymbol{w}(\cdot,T) = -\dfrac{1}{\beta_1}\boldsymbol{u}(\cdot,T) & \text{in} \quad \Omega. \end{cases} \tag{8.7}$$

In [33], a unique minimal control $\boldsymbol{v}$, associated with (8.5), is confirmed for every $\beta_1 > 0$, $\beta_2 > 0$. Only Dirichlet boundary conditions are examined in this study.

For extensive research on the control theory of the Stokes system with internal controls, see [41].

Computational studies, like the one by Fernandez-Cara et al. [30], focus on numerical two-dimensional analyses of heat, Stokes, and Navier-Stokes equations with Dirichlet boundary conditions. The methodology applied, outlined in [32], uses the Fursikov-Imanuvilov formulation and a Lagrangian approximation through mixed finite elements. An alternative approximation scheme is presented in [29] for a turbulence model using Dirichlet boundary conditions.

However, no known numerical approximation for the Stokes problem employs Radial Basis Functions (RBFs) under Navier-slip boundary conditions. Subsequent sections address this and demonstrate its utility for solving the control problem for the Stokes system.

Table 8.1 shows the number of iterations to achieve the stopping criteria $\epsilon = 10^{-8}$ in the CGM.

B.C	$\mathbf{v} = (v_1, v_2)$	$\mathbf{v} = (v_1, 0)$	$\mathbf{v} = (0, v_2)$
Navier–slip	116	68	99
Dirichlet	78	208	304

Table 8.1: Number of iterations for obtaining the convergence criteria of the CGM for Hybrid-LHI-RBF.

Table 8.2 and Figures 8.1–8.2 show the L^2–norm of the velocity vector field for the approximate control problems as a function of time. The numerical control function $\boldsymbol{v}$ has all possible structures, namely, $\boldsymbol{v} = \mathbf{0}$, $\boldsymbol{v} = (v_1, v_2)$, $\boldsymbol{v} = (v_1, 0)$ and $\boldsymbol{v} = (0, v_2)$.

8.1.1 Finite element method, FEM, for the control problem

Taking as starting point the classical optimal control problem for the Stokes system [37], we can solve the optimality system given in (8.2) (8.6) and (8.7) in a similar way. In our case, the time–space discretization of the coupled system (8.2), (8.7), lies in a mixed finite element formulation in space using $\mathbb{P}_2$–type elements for the velocity and $\mathbb{P}_1$–type elements for the pressure, meanwhile finite differences are used for the time discretization (see [38, 35, 4] for a complete review). It has to be pointed that in order to solve the unsteady Stokes equation with Navier–slip boundary condition we used a penalization method given in [26].

Boundary Condition = Dirichlet

t	$\mathbf{v} = \mathbf{0}$	$\mathbf{v} = (v_1, v_2)$	$\mathbf{v} = (v_1, 0)$	$\mathbf{v} = (0, v_2)$
0.0E+00	6.103E+00	6.103E+00	6.103E+00	6.103E+00
1.0E-01	1.561E+00	1.551E+00	1.551E+00	1.550E+00
2.0E-01	7.845E-01	7.658E-01	7.651E-01	7.656E-01
3.0E-01	4.221E-01	3.988E-01	3.977E-01	3.988E-01
4.0E-01	2.318E-01	2.064E-01	2.058E-01	2.066E-01
5.0E-01	1.283E-01	1.025E-01	1.032E-01	1.028E-01
6.0E-01	7.114E-02	4.664E-02	4.943E-02	4.694E-02
7.0E-01	3.949E-02	1.797E-02	2.319E-02	1.818E-02
8.0E-01	2.193E-02	5.207E-03	1.167E-02	5.203E-03
9.0E-01	1.218E-02	1.192E-03	5.297E-03	1.118E-03
1.0E+00	6.761E-03	8.748E-05	1.093E-03	1.271E-04

Boundary Condition = Navier-Slip

t	$\mathbf{v} = \mathbf{0}$	$\mathbf{v} = (v_1, v_2)$	$\mathbf{v} = (v_1, 0)$	$\mathbf{v} = (0, v_2)$
0.0E+00	6.982E+00	6.982E+00	6.982E+00	6.982E+00
1.0E-01	3.495E+00	3.335E+00	3.385E+00	3.262E+00
2.0E-01	2.413E+00	2.112E+00	2.213E+00	2.004E+00
3.0E-01	1.713E+00	1.322E+00	1.473E+00	1.210E+00
4.0E-01	1.226E+00	7.921E-01	9.911E-01	6.993E-01
5.0E-01	8.801E-01	4.454E-01	6.824E-01	3.838E-01
6.0E-01	6.331E-01	2.313E-01	4.845E-01	2.027E-01
7.0E-01	4.559E-01	1.113E-01	3.460E-01	1.078E-01
8.0E-01	3.285E-01	5.040E-02	2.260E-01	5.858E-02
9.0E-01	2.368E-01	1.815E-02	1.146E-01	2.558E-02
1.0E+00	1.708E-01	2.149E-03	5.506E-02	6.359E-03

Table 8.2: Evolution in time of the L^2–norm for the solution of the approximate control problem with few scalar controls.(LHI–RBF with hybrid kernel) $\mu = 1.0e-03$. For Dirichlet boundary condition $\gamma_1 = 1e-01$,$\gamma_2 = 1e-05$, and for Navier–slip $\gamma_1 = 1e-03$,$\gamma_2 = 1e-08$

Table 8.3 shows the number of iterations to achieve the stopping criteria $\epsilon = 10^{-8}$ in the CGM implemented.

Table 8.4 and Figures 8.3-8.4 display the evolution in time of the L^2–norm of the velocity vector field $\boldsymbol{u} = (u_1, u_2)$, which represents the solution to the approximate

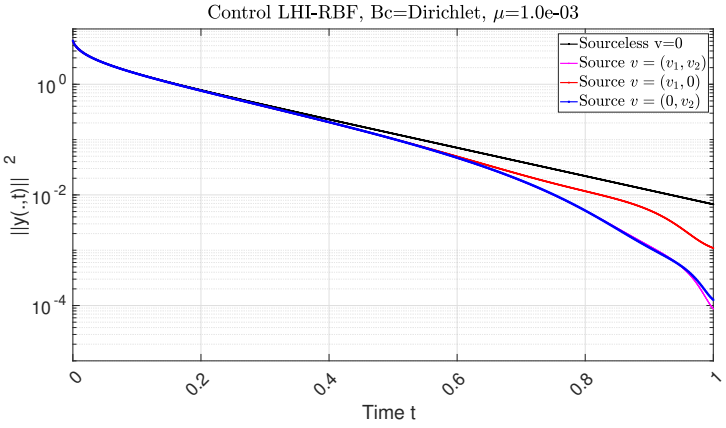

Figure 8.1: L^2–norm square solution of the velocity field (as a function of time) for the approximate control problem with controls $\boldsymbol{v} = \mathbf{0}$ (black), $\boldsymbol{v} = (v_1, v_2)$ (pink), $\boldsymbol{v} = (v_1, 0)$ (red) and $\boldsymbol{v} = (0, v_2)$ with Dirichlet boundary condition. LHI–RBF hybrid kernel, with parameters $\gamma_1 = 1e-01$,$\gamma_2 = 1.0e-5$,$c_1 = 0.5$,$c_2 = 5.e-8$

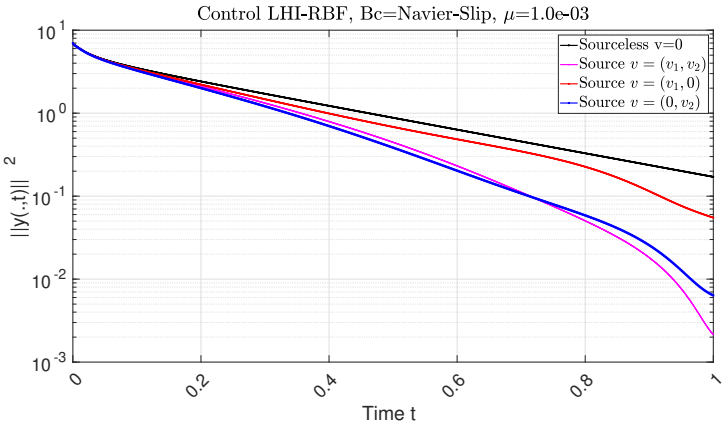

Figure 8.2: L^2–norm square solution of the velocity field (as a function of time) for the approximate control problem with controls $\boldsymbol{v} = \mathbf{0}$ (black), $\boldsymbol{v} = (v_1, v_2)$ (pink), $\boldsymbol{v} = (v_1, 0)$ (red) and $\boldsymbol{v} = (0, v_2)$ with Navier–slip boundary condition. LHI–RBF hybrid kernel, with parameters $\gamma_1 = 1e-03$,$\gamma_2 = 1e-08$,$c_1 = 1.0$,$c_2 = 5.e-10$.

control problem (8.2), and where the control function v has different structure, namely, $\boldsymbol{v} = 0$, $\boldsymbol{v} = (v_1, v_2)$, $\boldsymbol{v} = (v_1, 0)$ and $\boldsymbol{v} = (0, v_2)$.

As we can see from Tables 8.2–8.4, the RBF–LHI method or FEM are similar,

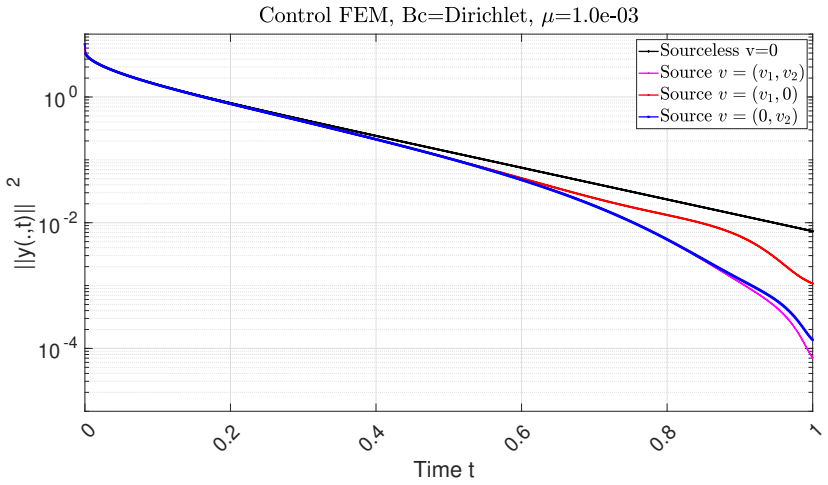

Figure 8.3: Evolution in time of the L^2–norm square for the solution of the approximate control problem with Dirichlet boundary conditions and $v = 0$ (black), $v = (v_1, v_2)$ (pink), $v = (v_1, 0)$ (red) and $v = (0, v_2)$ (blue). (FEM)

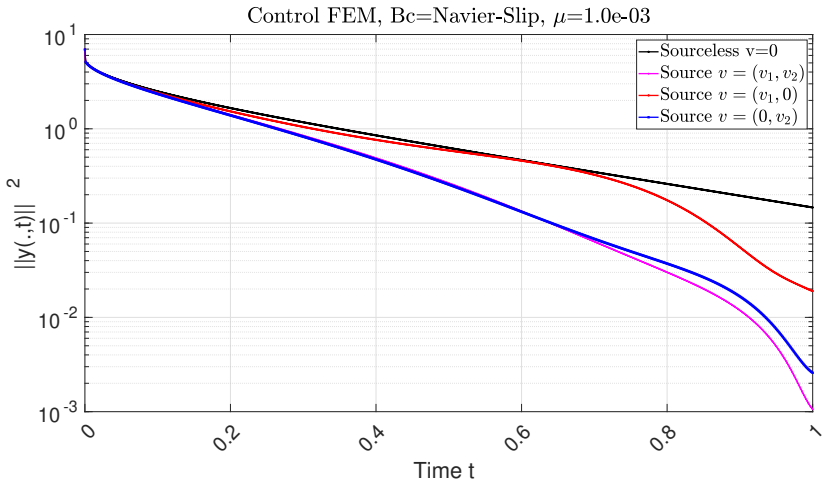

Figure 8.4: Evolution in time of the L^2–norm square for the solution of the approximate control problem with Dirichlet boundary conditions and $v = 0$ (black), $v = (v_1, v_2)$ (pink), $v = (v_1, 0)$ (red) and $v = (0, v_2)$ (blue). (FEM)

B.C	$\mathbf{v} = (v_1, v_2)$	$\mathbf{v} = (v_1, 0)$	$\mathbf{v} = (0, v_2)$
Navier–slip	73	73	65
Dirichlet	56	54	49

Table 8.3: Number of iterations for obtaining the convergence criteria of the CGM for FEM.

nevertheless, RBF–LHI method has the advantage of being mesh–less and showing more accuracy by using divergence free kernels. The number of iterations for the CGM necessary to converge is higher for the RBF–LHI method, however it should be noted that for RBF–LHI technique we use $\mathbb{P}_1$–type elements to compute the integral expressions in the CGM, while for FEM we use $\mathbb{P}_2$–type elements.

Boundary Condition = Dirichlet				
t	$\mathbf{v} = \mathbf{0}$	$\mathbf{v} = (v_1, v_2)$	$\mathbf{v} = (v_1, 0)$	$\mathbf{v} = (0, v_2)$
0.0E+00	6.103E+00	6.103E+00	6.103E+00	6.103E+00
1.0E-01	1.572E+00	1.561E+00	1.560E+00	1.560E+00
2.0E-01	8.014E-01	7.814E-01	7.788E-01	7.799E-01
3.0E-01	4.351E-01	4.101E-01	4.070E-01	4.085E-01
4.0E-01	2.409E-01	2.135E-01	2.111E-01	2.121E-01
5.0E-01	1.342E-01	1.065E-01	1.059E-01	1.055E-01
6.0E-01	7.498E-02	4.864E-02	5.097E-02	4.798E-02
7.0E-01	4.192E-02	1.879E-02	2.463E-02	1.854E-02
8.0E-01	2.344E-02	5.397E-03	1.326E-02	5.418E-03
9.0E-01	1.311E-02	1.120E-03	6.087E-03	1.256E-03
1.0E+00	7.333E-03	7.110E-05	1.076E-03	1.371E-04

Boundary Condition = Navier-Slip				
t	$\mathbf{v} = \mathbf{0}$	$\mathbf{v} = (v_1, v_2)$	$\mathbf{v} = (v_1, 0)$	$\mathbf{v} = (0, v_2)$
0.0E+00	6.934E+00	6.934E+00	6.934E+00	6.934E+00
1.0E-01	2.496E+00	2.359E+00	2.403E+00	2.345E+00
2.0E-01	1.660E+00	1.409E+00	1.531E+00	1.388E+00
3.0E-01	1.173E+00	8.462E-01	1.048E+00	8.255E-01
4.0E-01	8.519E-01	4.890E-01	7.634E-01	4.731E-01
5.0E-01	6.277E-01	2.652E-01	5.884E-01	2.563E-01
6.0E-01	4.663E-01	1.335E-01	4.587E-01	1.319E-01
7.0E-01	3.480E-01	6.361E-02	3.254E-01	6.801E-02
8.0E-01	2.604E-01	3.009E-02	1.747E-01	3.719E-02
9.0E-01	1.952E-01	1.188E-02	5.537E-02	1.668E-02
1.0E+00	1.465E-01	1.060E-03	1.904E-02	2.582E-03

Table 8.4: Evolution in time of the L^2–norm for the solution of the approximate control problem with Dirichlet boundary conditions and few scalar controls, (FEM) $\mu = 1.0e-03$

Conclusion: Achievements and Future Perspectives

In this thesis, we have addressed a simplified geometrical inverse problem related to the identification of stenosis, an obstruction, in a coronary duct by utilizing measurements of acoustic waves. A key novelty of our work is the introduction of an exterior approach. The Stokes flow, confined within an interior domain, becomes turbulent upon encountering the boundary obstruction, resulting in movement of the elastic boundary of the duct and generation of acoustic waves. The inverse problem, involving the identification of the location, extent, and height of the obstruction (lumen reduction), is formulated and solved by utilizing external wave measurements taken far enough from the duct, effectively considering them as measurements in the exterior domain. Notably, previous works in the literature assume that the obstruction is contained within the domain and that the boundary measurements are not external, meaning they are taken solely on the unique boundary of the problem.

From a theoretical standpoint, we have addressed and analyzed the problem both in continuous and numerical settings. The well-posedness of the Stokes flow with mixed boundary conditions has been proven, which is a notable contribution as previous works have mainly focused on Dirichlet boundary conditions. Additionally, we have established unique results for the obstruction when the data is given by the normal component of the Cauchy stress tensor and the tangential velocity on a subset of the boundary.

From a numerical perspective, we have successfully solved, with a reasonable degree of accuracy, the identification of a boundary obstruction immersed in a Stokes flow using measurements of acoustic waves taken on the external boundary of the problem. The inverse problem for the fluid obstruction has been addressed by employing a Monte Carlo Markov Chain (MCMC) method, which involves solving two direct problems: a direct Stokes problem solved using mesh-free hybrid radial basis function kernels, and a direct wave system solved using the finite element method.

In addition to the aforementioned contributions, this work has also introduced radial basis function (RBF) methods for approximating the solution of the non-stacionary Stokes equations. We have presented two types of RBF solvers, global and local, for the direct Stokes problems, incorporating Dirichlet or Navier-slip boundary conditions. Stability analysis demonstrates the stability of the method for backward difference formulas (BDFs) when the shape parameter is properly selected. Exponential convergence has been numerically demonstrated. Furthermore, by generalizing recently formulated scalar hybrid kernels to a vectorial setting, we have developed divergency-free matrix hybrid radial basis kernels (Div-Free-Hybrid). These kernels have significantly reduced the condition number of the local matrices and allowed for the selection of parameters that result in all negative real components of the eigenvalues, thereby allowing the convergence of the solution.

In terms of future work, several aspects can be further explored and improved upon. Firstly, it would be valuable to complete the pressure continuity analysis about the domain for mixed boundary conditions. This would provide a more comprehensive understanding of the flow behavior and enhance the accuracy of the results. Additionally, studying the regularity of the solution with mixed boundary conditions would contribute to a deeper insight into the mathematical properties of the problem and potentially lead to refined analytical results.

Furthermore, a focus on enhancing the usability of the RBF codes is essential. Making the RBF implementation more user-friendly, similar to the accessibility of software tools like FreeFem++, would greatly benefit researchers and practitioners in the field. Simplifying the coding process and providing clear documentation and examples would facilitate the adoption and utilization of RBF methods by a broader audience.

Addressing these areas of further work will contribute to the advancement and wider adoption of RBF techniques in the field of fluid dynamics and boundary obstacle problems, fostering more efficient and accurate analysis and applications in practical scenarios.

Agradecimientos

Me gustaría expresar mi más sincero agradecimiento a las personas que han sido fundamentales en el desarrollo de mi tesis.

En primer lugar, quiero agradecer a mis padres, Maria Dolores y Jean Paul, por su incondicional apoyo a lo largo de este proyecto. Su amor, aliento y comprensión han sido fundamentales para mi éxito académico.

También quiero agradecer a mi querida esposa Gabriela por su constante apoyo y motivación. Tu amor y comprensión han sido un pilar fundamental en este camino.

A mis amigos Tona, Efren y Joel, gracias por estar siempre presentes, animarme y brindarme su apoyo en los momentos difíciles. Sus palabras de aliento y amistad significan mucho para mí.

Quiero expresar mi profundo agradecimiento a mi profesor y amigo, Jesús López Estrada. Durante muchos años hemos compartido una valiosa relación de investigación, y su guía, conocimientos y experiencia han sido invaluables para mi crecimiento académico y personal.

Bibliography

[1] Paul Acevedo, Chérif Amrouche, Carlos Conca, and Amrita Ghosh. Stokes and Navier–Stokes equations with Navier boundary condition. *Comptes Rendus Mathematique*, 357(2):115–119, 2019.

[2] Hind Al Baba, Chérif Amrouche, and Ahmed Rejaiba. The time-dependent Stokes problem with Navier slip boundary conditions on L^p-spaces. *Analysis (Berlin)*, 36(4):269–285, 2016.

[3] Giovanni Alessandrini, Antonino Morassi, and Edi Rosset. Detecting an inclusion in an elastic body by boundary measurements. *SIAM review*, 46(3):477–498, 2004.

[4] Grégoire Allaire. *Analyse numérique et optimisation: une introduction à la modélisation mathématique et à la simulation numérique*. Editions Ecole Polytechnique, 2005.

[5] Grégoire Allaire. *Numerical analysis and optimization*. Numerical Mathematics and Scientific Computation. Oxford University Press, Oxford, 2007. An introduction to mathematical modelling and numerical simulation, Translated from the French by Alan Craig.

[6] Grégoire Allaire and Marc Schoenauer. *Conception optimale de structures*, volume 58. Springer, 2007.

[7] Catalina Alvarez, Carlos Conca, Luis Friz, Otared Kavian, and Jaime H Ortega. Identification of immersed obstacles via boundary measurements. *Inverse Problems*, 21(5):1531, 2005.

[8] Catalina Alvarez, Carlos Conca, Rodrigo Lecaros, and Jaime H Ortega. On the identification of a rigid body immersed in a fluid: A numerical approach. *Engineering analysis with boundary elements*, 32(11):919–925, 2008.

[9] Chérif Amrouche and Vivette Girault. Decomposition of vector spaces and application to the Stokes problem in arbitrary dimension. *Czechoslovak Mathematical Journal*, 44(1):109–140, 1994.

[10] Chérif Amrouche and Ahmed Rejaiba. Lp-theory for Stokes and Navier–Stokes equations with Navier boundary condition. *Journal of Differential Equations*, 256(4):1515–1547, 2014.

[11] Mehdi Badra, Fabien Caubet, and Marc Dambrine. Detecting an obstacle immersed in a fluid by shape optimization methods. *Mathematical Models and Methods in Applied Sciences*, 21(10):2069–2101, 2011.

[12] Harvey Thomas Banks and John R Samuels Jr. Detection of cardiac occlusions using viscoelastic wave propagation. *Advances in Applied Mathematics and Mechanics*, 1(1):1–28, 2009.

[13] Cecile Baron, Jean-François Aubry, Mickael Tanter, Stephen Meairs, and Mathias Fink. Simulation of intracranial acoustic fields in clinical trials of sonothrombolysis. *Ultrasound in medicine & biology*, 35(7):1148–1158, 2009.

[14] Alvin Bayliss and Eli Turkel. Radiation boundary conditions for wave-like equations. *Comm. Pure Appl. Math.*, 33(6):707–725, 1980.

[15] Amel Ben Abda and Faten Khayat. Reconstruction of missing boundary conditions from partially overspecified data: the Stokes system. *ARIMA Rev. Afr. Rech. Inform. Math. Appl.*, 23:79–100, 2016.

[16] Muriel Boulakia, Anne-Claire Egloffe, and Céline Grandmont. Stability estimates for a Robin coefficient in the two-dimensional Stokes system. *arXiv preprint arXiv:1202.1263*, 2012.

[17] Louis Breton, Pedro González-Casanova, and Cristhian Montoya. RBF collocation and hybrid-LHI methods for Stokes systems and its application to controllability problems. *Comput. Appl. Math.*, 40(1):15, 2021.

[18] Louis Breton, Cristhian Montoya, Pedro González-Casanova, and Jesús López Estrada. Identification of a boundary obstacle in a stokes fluid with dirichlet–navier boundary conditions: external measurements. *arXiv preprint arXiv:2210.07479*, 2022.

[19] Haim Brezis and Haim Brézis. *Functional analysis, Sobolev spaces and partial differential equations*, volume 2. Springer, 2011.

[20] R Brown, Irina Mitrea, Marius Mitrea, and M Wright. Mixed boundary value problems for the Stokes system. *Transactions of the American Mathematical Society*, 362(3):1211–1230, 2010.

[21] Fabien Caubet. Detecting an obstacle immersed in a fluid: the Stokes case. In *Eleventh International Conference Zaragoza-Pau on Applied Mathematics and Statistics*, volume 37 of *Monogr. Mat. Garc'ıa Galdeano*, pages 91–101. Prensas Univ. Zaragoza, Zaragoza, 2012.

[22] Fabien Caubet, Carlos Conca, and Mat'ıas Godoy. On the detection of several obstacles in 2D Stokes flow: topological sensitivity and combination with shape derivatives. *Inverse Problems & Imaging*, 10(2):327, 2016.

[23] Fabien Caubet, Marc Dambrine, and Helmut Harbrecht. A new method for the data completion problem and application to obstacle detection. *SIAM J. Appl. Math.*, 79(1):415–435, 2019.

[24] D Charalambos and Border Aliprantis. *Infinite Dimensional Analysis: A Hitchhiker's Guide*. Springer-Verlag Berlin and Heidelberg GmbH & Company KG, 2013.

[25] PP Chinchapatnam, K Djidjeli, and PB Nair. Unsymmetric and symmetric meshless schemes for the unsteady convection–diffusion equation. *Computer methods in applied mechanics and engineering*, 195(19-22):2432–2453, 2006.

[26] Ibrahima Dione and José M Urquiza. Penalty: finite element approximation of Stokes equations with slip boundary conditions. *Numerische Mathematik*, 129(3):587–610, 2015.

[27] C. Fabre and G. Lebeau. Prolongement unique des solutions. *Communications in Partial Differential Equations*, 21(3-4):573–596, 1996.

[28] Gregory E Fasshauer. *Meshfree Approximation Methods with Matlab:(With CD-ROM)*, volume 6. World Scientific Publishing Co Inc, 2007.

[29] Enrique Fernández-Cara, J Limaco, and SB de Menezes. Theoretical and Numerical Local Null Controllability of a Ladyzhenskaya–Smagorinsky Model of Turbulence. *Journal of Mathematical Fluid Mechanics*, 17(4):669–698, 2015.

[30] Enrique Fernández-Cara, Arnaud Münch, and Diego A Souza. On the Numerical Controllability of the Two-Dimensional Heat, Stokes and Navier–Stokes Equations. *Journal of Scientific Computing*, 70(2):819–858, 2017.

[31] Luca Formaggia, Alfio Quarteroni, and Allesandro Veneziani. *Cardiovascular Mathematics: Modeling and simulation of the circulatory system*, volume 1. Springer Science & Business Media, 2010.

[32] Andrej Vladimirovic Fursikov. *Controllability of evolution equations*. Seoul National University, 1996. number 34.

[33] Galina C Garc'ia, Cristhian Montoya, and Axel Osses. A source reconstruction algorithm for the Stokes system from incomplete velocity measurements. *Inverse Problems*, 33(10):105003, 2017.

[34] Andrew Gelman, John B. Carlin, Hal S. Stern, David B. Dunson, Aki Vehtari, and Donald B. Rubin. *Bayesian data analysis*. Texts in Statistical Science Series. CRC Press, Boca Raton, FL, third edition, 2014.

[35] Vivette Girault and Pierre-Arnaud Raviart. *Finite element methods for Navier-Stokes equations: theory and algorithms*, volume 5. Springer Science & Business Media, 2012.

[36] Dan Givoli, Thomas Hagstrom, and Igor Patlashenko. Finite element formulation with high-order absorbing boundary conditions for time-dependent waves. *Computer Methods in Applied Mechanics and Engineering*, 195(29-32):3666–3690, 2006.

[37] Roland Glowinski, Jacques-Louis Lions, and Jiwen He. *Exact and Approximate Controllability for Distributed Parameter Systems: A Numerical Approach (Encyclopedia of Mathematics and its Applications)*. Cambridge University Press, 2008.

[38] Roland Glowinski and Olivier Pironneau. Finite element methods for Navier-Stokes equations. *Annual review of fluid mechanics*, 24(1):167–204, 1992.

[39] Pedro González-Casanova, Christian Gout, and Jorge Zavaleta. Radial basis function methods for optimal control of the convection diffusion equation: A numerical study. *Engineering Analysis with Boundary Elements*, 108:201 – 209, 2019.

[40] Pierre Grisvard. *Elliptic problems in nonsmooth domains*. SIAM, 2011.

[41] Sergio Guerrero and Cristhian Montoya. Local null controllability of the N-dimensional Navier–Stokes system with nonlinear Navier-slip boundary conditions and N- 1 scalar controls. *Journal de Mathématiques Pures et Appliquées*, 113:37–69, 2018.

[42] Antoine Henrot and Michel Pierre. *Variation et optimisation de formes: une analyse géométrique*, volume 48. Springer Science & Business Media, 2006.

[43] Robert L. Higdon. Numerical absorbing boundary conditions for the wave equation. *Math. Comp.*, 49(179):65–90, 1987.

[44] Andreas Karageorghis and Daniel Lesnic. Identification of obstacles immersed in a stationary Oseen fluid via boundary measurements. *Inverse Probl. Sci. Eng.*, 28(7):950–967, 2020.

[45] R. Kosloff and D. Kosloff. Absorbing boundaries for wave propagation problems. *J. Comput. Phys.*, 63(2):363–376, 1986.

[46] John Denholm Lambert. *Numerical methods for ordinary differential systems: the initial value problem*. John Wiley & Sons, Inc., 1991.

[47] Robert S Lees and C Forbes Dewey. Phonoangiography: a new noninvasive diagnostic method for studying arterial disease. *Proceedings of the National Academy of Sciences*, 67(2):935–942, 1970.

[48] Jacques-Louis. Lions. *Quelques méthodes de résolution des problèmes aux limites non linéaires*. Dunod; Gauthier-Villars, Paris, 1969.

[49] Jacques-Louis Lions. Contrôlabilité exacte, perturbations et stabilisation de systèmes distribués. Tome 1. *RMA*, 8, 1988.

[50] Jacques Louis Lions and Enrico Magenes. *Non-homogeneous boundary value problems and applications: Vol. 1*, volume 181. Springer Science & Business Media, 2012.

[51] Pankaj K Mishra, Gregory E Fasshauer, Mrinal K Sen, and Leevan Ling. A stabilized radial basis-finite difference (RBF-FD) method with hybrid kernels. *Computers & Mathematics with Applications*, 77(9):2354–2368, 2019.

[52] P.K. Mishra, S.K. Nath, M.K. Sen, and G.E. Fasshauer. Hybrid Gaussian-cubic radial basis functions for scattered data interpolation. *Comput Geosci*, 22:1203 – 1218, 2018.

[53] Chandrasegaran Narasimhan, Richard Ward, Kara L Kruse, Murthy Guddati, and Gnanamanikam Mahinthakumar. A high resolution computer model for sound propagation in the human thorax based on the Visible Human data set. *Computers in Biology and Medicine*, 34(2):177–192, 2004.

[54] CLMH Navier. Mémoire sur les lois du mouvement des fluides. *Mémoires de l'Académie Royale des Sciences de l'Institut de France*, 6(1823):389–440, 1823.

[55] Kohei Okita, Kenji Ono, Shu Takagi, and Yoichiro Matsumoto. Development of high intensity focused ultrasound simulator for large-scale computing. *International journal for numerical methods in fluids*, 65(1-3):43–66, 2011.

[56] ALFIO Quarteroni, Andrea Manzoni, and Christian Vergara. The cardiovascular system: mathematical modelling, numerical algorithms and clinical applications. *Acta Numerica*, 26:365–590, 2017.

[57] Alfio Quarteroni, Andrea Manzoni, Christian Vergara, et al. *Mathematical modelling of the human cardiovascular system: data, numerical approximation, clinical applications*, volume 33. Cambridge University Press, 2019.

[58] Wayne Rosamond, Katherine Flegal, Gary Friday, Karen Furie, Alan Go, Kurt Greenlund, Nancy Haase, Michael Ho, Virginia Howard, Bret Kissela, et al. Heart disease and stroke statistics—2007 update: a report from the American Heart Association Statistics Committee and Stroke Statistics Subcommittee. *Circulation*, 115(5):e69–e171, 2007.

[59] Jung Hee Seo and Rajat Mittal. A coupled flow-acoustic computational study of bruits from a modeled stenosed artery. *Medical & biological engineering & computing*, 50(10):1025–1035, 2012.

[60] D Stevens, H Power, M Lees, and H Morvan. A local hermitian RBF meshless numerical method for the solution of multi-zone problems. *Numerical Methods for Partial Differential Equations*, 27(5):1201–1230, 2011.

[61] Roger Temam. *Navier-Stokes equations: theory and numerical analysis*, volume 343. American Mathematical Soc., 2001.

[62] Louis Breton Tenorio and Jesus López Estrada. Develación del dominio de un fluido de stokes estacionario. *Boletín de la Sociedad Mexicana de Computación Científica y sus Aplicaciones*, 2018.

[63] Lloyd N. Trefethen and Laurence Halpern. Well-posedness of one-way wave equations and absorbing boundary conditions. *Math. Comp.*, 47(176):421–435, 1986.

[64] Holger Wendland. *Scattered data approximation*, volume 17. Cambridge university press, 2004.

[65] Holger Wendland. Divergence-free kernel methods for approximating the Stokes problem. *SIAM Journal on Numerical Analysis*, 47(4):3158–3179, 2009.

[66] Edward J Wing and Fred J Schiffman. *Cecil Essentials of Medicine E-Book*. Elsevier Health Sciences, 2021.

[67] Masahiro Yamamoto. Stability, reconstruction formula and regularization for an inverse source hyperbolic problem by a control method. *Inverse problems*, 11(2):481, 1995.

[68] Wen-Jing Yan and Yi-Chen Ma. Shape reconstruction of an inverse Stokes problem. *Journal of Computational and Applied Mathematics*, 216(2):554–562, 2008.